UTILIZATION OF ALLOSTERIC ENZYME ACTIVATION FOR ADVANCED AMPEROMETRIC BIOSENSING

Somjai Teanphonkrang

A Thesis Submitted in Partial Fulfilment of the Requirements for the Degree of Doctor of Philosophy in Chemistry

Suranaree University of Technology

Academic Year 2018

การใช้ประโยชน์ของการกระตุ้นอัลโลสเตอริกเอนไซม์สำหรับเทคนิคแอมเพอโรเมตริกไบโอเซนซิงขั้นสูง

นางสาวสมใจ เตียนพลกรัง

วิทยานิพนธ์นี้เป็นส่วนหนึ่งของการศึกษาตามหลักสูตรปริญญาวิทยาศาสตรดุษฎีบัณฑิต
สาขาวิชาเคมี
มหาวิทยาลัยเทคโนโลยีสุรนารี
ปีการศึกษา 2561

UTILIZATION OF ALLOSTERIC ENZYME ACTIVATION FOR ADVANCED AMPEROMETRIC BIOSENSING

Suranaree University of Technology has approved this thesis submitted in partial fulfilment of the requirements for the Degree of Doctor of Philosophy.

Thesis Examining Committee

(Prof. Dr. James R. Ketudat-Cairns)

Chairperson

(Asst. Prof. Dr. Panida Khunkaewla)

Member (Thesis Advisor)

(Prof. Dr. Albert Schulte)

Member

(Prof. Dr. Wolfgang Schuhmann)

Member

(Prof. Dr. Wipa Suginta)

Member

(Asst. Prof. Dr. Jeerus Sucharitakul)

Member

(Prof. Dr. Santi Maensiri)

Vice Rector for Academic Affairs and Internationalization

(Asst. Prof. Dr. Worawat Meevasana)

Dean of Institute of Science

สมใจ เตียนพลกรัง : การใช้ประโยชน์ของการกระตุ้นอัลโลสเตอริกเอนไซม์สำหรับเทคนิคแอมเพอโรเมตริกไบโอเซนซิงขั้นสูง (UTILIZATION OF ALLOSTERIC ENZYME ACTIVATION FOR ADVANCED AMPEROMETRIC BIOSENSING). อาจารย์ที่ปรึกษา : ผู้ช่วยศาสตราจารย์ ดร.พนิดา ขันแก้วหล้า, 160 หน้า.

ไบโอเซนซิง แอมเพอโรเมทรีขั้นสูง เอนไซม์อัลโลสเตอริก พารา-ไฮดรอกซีฟีนิลอะซิเตต ส่วนประกอบ HPAH-รีดักเตส ตัวบ่งชี้ภาวะการเกิดโรค

อัลโลสเตอริกเอนไซม์แบบกระตุ้นสามารถเพิ่มอัตราการเปลี่ยนสารตั้งต้นในรูปแบบที่ขึ้นกับความเข้มข้น เป็นที่แน่ชัดว่าอัลโลสเตอริกแบบกระตุ้นนั้นน่าสนใจสำหรับงานทางเทคโนโลยีชีวภาพ เพราะสัมพันธ์กับการให้ผลิตภัณฑ์ที่เพิ่มขึ้นปริมาณมาก ซึ่งจะส่งผลให้ประสิทธิภาพของกระบวนการผลิตดีกว่า สำหรับเทคนิคแอมเพอโรเมตริกเอนไซม์ไบโอเซนซิงนั้นจะช่วยให้การขยายสัญญาณและการตรวจวัดของสารตั้งต้นหรือตัวกระตุ้นดีขึ้น ดังนั้นการทำให้เทคนิคแอมเพอโรเมตริกไบโอเซนซิงขั้นสูงเพื่อตรวจวัดสารตั้งต้นและตัวกระตุ้นเอนไซม์เกิดขึ้นได้จริง จึงเป็นวัตถุประสงค์หลักของงานในวิทยานิพนธ์เคมีเชิงวิเคราะห์ระดับปริญญาเอกนี้ สำหรับโมเลกุลที่ใช้ในการกระตุ้นนี้กำลังเป็นที่น่าสนใจ เนื่องจากเป็นตัวบ่งชี้ภาวะการเกิดโรคที่มีศักยภาพ

เอนไซม์ที่ถูกนำมาศึกษาในงานวิจัยนี้คือ เอนไซม์รีดักเทส จากแบคทีเรียชื่อ *Acinetobacter baumannii* ซึ่งส่วนประกอบรีดักเทส C1 ซึ่งพบว่าสามารถเปลี่ยนสารตั้งต้น NADH ให้เป็น NAD^+ และปฏิกิริยาเกิดได้เร็วขึ้นเมื่อมีตัวกระตุ้น พารา-ไฮดรอกซีฟีนิลอะซิเตท (*p*-HPA) ซึ่งในทางการแพทย์ *p*-HPA เป็นโมเลกุลที่สำคัญในการเป็นตัวบ่งชี้ภาวะการเกิดโรคและการเพิ่มขึ้นของโมเลกุลนี้ในปัสสาวะสามารถบ่งบอกความไม่สมดุลของแบคทีเรียในระบบย่อยอาหารและ โรคทางสมองต่าง ๆ

เนื่องจากเอนไซม์รีดักเทส C1 ต้องการวัฏจักรการเกิดปฏิกิริยารีดอกซ์อย่างมีประสิทธิภาพสำหรับวัฏจักรการเร่งปฏิกิริยาทางชีวภาพของ NADH ซึ่งโดยปกติเกิดจากการทำปฏิกิริยากับออกซิเจนที่ละลายในสารละลาย ผลิตภัณฑ์ข้างเคียงจากการทำงานอย่างต่อเนื่องของ เอนไซม์รีดักเทส C1 ที่สามารถตรวจวัดได้คือ ไฮโดรเจนเปอร์ออกไซด์ ดังนั้นไบโอเซนเซอร์แบบตรึงในตัวกลางรีดอกซ์เทียมอาจถูกนำมาใช้กับ C1 สำหรับการสร้างวัฏจักรปฏิกิริยารีดอกซ์และการตรวจวัด ซึ่งกรอบงานของวิทยานิพนธ์นี้ที่ประสบผลสำเร็จลุล่วง คือ

- C1 แอมเพอโรเมตริกไบโอเซนซิงของ NADH และ *p*-HPA โดยเอนไซม์จะทำปฏิกิริยากับ สารตั้งต้น ออกซิเจน และ ตัวกระตุ้นในสารละลาย โดยมีขั้วไฟฟ้า

แคโทรดแบบสกรีน ปริ้นท์ที่เคลือบด้วย Prussian Blue ทำหน้าที่ในการหาปริมาณไฮโดรเจนเปอร์ออกไซด์ที่เกิดจากปฏิกิริยา

- C1 แอมเพอโรเมตริกไบโอเซนซิงของ NADH และ *p*-HPA แบบตรึงเอนไซม์ภายในรีดอกซ์โพลีเมอร์ออสเมียม (Os^{3+}) เพื่อใช้หาปริมาณ NADH ทั้งในสภาวะที่มีและไม่มีการกระตุ้นแบบอัลโลสเตอริก ผ่านการถ่ายโอนอิเล็กตรอนระหว่าง Os^{2+} และ Os^{3+} ที่ขั้วไฟฟ้า
- การประยุกต์ใช้ออสเมียม C1 ไบโอเซนเซอร์ สำหรับตรวจสอบหาปริมาณของ *p*-HPA ซึ่งเป็นตัวบ่งชี้ภาวะการเกิดโรคในตัวอย่างที่ทราบค่าและในปัสสาวะเทียม

ผลสัมฤทธิ์ข้างต้นกล่าวได้ว่าเป็นพื้นฐานของการวิเคราะห์ *p*-HPA ในปัสสาวะอย่างง่ายและราคาถูก ซึ่งอาจถูกผสมผสานเข้ากับขั้วไฟฟ้าแบบสกรีนปริ้นท์ในอุปกรณ์ดูแลสุขภาพ เช่น ที่ใช้ตรวจวัดระดับกลูโคส สำหรับพกพาและตรวจสอบได้ด้วยตัวเอง

สาขาวิชาเคมี
ปีการศึกษา 2561

ลายมือชื่อนักศึกษา สมใจ เตียพลกรัง
ลายมือชื่ออาจารย์ที่ปรึกษา
ลายมือชื่ออาจารย์ที่ปรึกษาร่วม Albert Schulte

SOMJAI TEANPHONKRANG : UTILIZATION OF ALLOSTRIC ENZYME ACTIVATION FOR ADVANCED AMPEROMETRIC BIOSENSING. THESIS ADVISOR : ASST. PROF. PANIDA KHUNKAEWLA, Ph.D. 160 PP.

BIOSENSING, ADVANCED AMPEROMETRY, ALLOSTERIC ENZYME, *P*-HYDROXYPHYNYLACETATE, HPAH-REDUCTASE COMPONENT, DISEASE BIOMARKERS

Activating allosteric enzyme modulation can trigger a concentration-dependent a rise in biocatalytic substrate conversion rates. Clearly, allosteric activation is attractive for biotechnology, since related larger product yields will give better process productivity. For amperometric enzyme biosensing, an increased protein biocatalysis facilitates signal amplification and thus improved detection of substrate and/or effector. Realization of advanced amperometric substrate and enzyme effector biosensing for an activating molecule that was, at the same time, appealing as a potential disease biomarker, was actually the main objective of this thesis work.

The enzyme system explored in this project was a well-studied bacterial reductase, namely *Acinetobacter baumannii* C1 that had been shown to convert NADH into NAD^+ and to react faster in the presence of effector *p*-hydroxy-phenylacetate (*p*-HPA). From the medical point of view, it was important that *p*-HPA has relevance as a disease biomarker, in that its urinary elevation is, for instance, reported as a sign of a critical bacterial imbalance in the digestion system on various brain pathologies, too.

As reductase, C1 needs efficient redox recycling for cyclic NADH biocatalysis, which usually is reached via reaction with dissolved oxygen. A side product of continuous C1 action is then detectable, hydrogen peroxide, H_2O_2. In immobilized biosensor configurations artificial redox partners may be offered to C1 for redox recycling and sensing. Within this frame work, the practical thesis work successfully accomplished:

- C1-based amperometric NADH and *p*-HPA biosensing, with the enzyme reacting in solution with substrate, O_2 and effector and cathodic Prussian blue-modified screen-printed electrodes in charge of quantification of liberated H_2O_2.
- C1-based amperometric NADH and *p*-HPA biosensing, with the enzyme fixed in an Osmium (III)-based redox polymer and biocatalysis quantified with and without allosteric activation via Os (II)/(III) redox transfer at the electrode.
- Application of Os (III) redox polymer/C1 biosensors for the quantification of traces of the disease biomarker *p*-HPA in model and artificial urine samples.

The above achievements are seen as the foundation of a simple and cheap urinary *p*-HPA analysis that may be integrated on screen-printed electrode platforms into glucose meter-type portable healthcare devices, and as such serve for personal home inspections.

School of Chemistry

Academic Year 2018

Student's Signature Somjai Teanphonkrang

Advisor's Signature

Co-advisor's Signature

ACKNOWLEDGEMENTS

I would like to express my deepest appreciation to my Ph.D. advisors, Prof. Dr. Albert Schulte, School of Biomolecular Science and Engineering, Vidyasirimedhi Insititute of Science and Technology (VISTEC) and Assist. Prof. Dr. Panida Khunkaewla, School of Chemistry, Suranaree University of Technology (SUT), for providing me the great opportunity to work on this project and enable me to pursue successfully a Ph.D. degree in Chemistry. Their continuous guidance, support and ideas made the efforts interesting to me, gave me a lot of inspiration, helped me to learn new things and finally made this thesis successful.

This research project would of course not have been possible without the kind financial support through the Royal Golden Jubilee Ph.D. Program of the Thailand Research Fund and without the provision of good research facilities by the Biochemistry-Electrochemistry Research Unit at Suranaree University of Technology and the Elektroanalytik and Sensorik Laboratory at the Ruhr University of Bochum. My sincere gratitude goes hence to these three institutions and involved people.

I am also deeply grateful to Prof. Dr. Pimchai Chaiyen, School of Biomolecular Science and Engineering, VISTEC and Assist. Prof. Dr. Jeerus Sucharitakul, Department of Biochemistry, Chulalongkorn University for support, not only through provision of the allosteric enzyme of my Ph.D. research project but also for productive discussions and suggestions about general aspects of enzyme allostery and details of the C1 reductase. And I would like to thank Prof. Dr. Wipa Suginta, School of

Chemistry, SUT for her valuable guidance in reductase C1 binding studies via Isothermal Calorimetry and her help with general enzyme kinetic issues.

My appreciation furthermore goes to Prof. Dr. Wolfgang Schuhmann and Dr. Adrian Ruff from the Analytische Chemie Elektroanalytik und Sensorik (ELAN), Analytical Chemistry - Center for Electrochemical Sciences (CES), Ruhr-University, Bochum, Germany. Their friendly, dedicated and skilled supervision during my one year as a Guest Graduate Research Student in the Bochum ELAN laboratory made my stay scientifically a success and personally an enjoyable experience.

Bettina Stetzka is thanked for her kind help in administrative issues and the organization of my research visit to Bochum. All other "ELAN" group members are acknowledged for offering a nice and friendly working environment throughout my stay, as well as for a lot of time enjoyable together at and off work.

I would also like to thank all lecturers in School of Chemistry who through their education in the Graduate Program have strengthen my foundation in Chemistry, which help understanding and interpreting own experimental data.

I wish to thank also all my colleagues in the Biochemistry-Electrochemistry Research Unit, Suranaree University of Technology for giving me all the emotional support that was needed to get through all the difficult times in this Ph.D. journey.

Finally, my deepest gratitude goes to my parents, younger sister, and everyone whom contributed to my success for their unflagging love and unconditional support throughout my life and my studies. They made me who I am today and have given me a happy life which is beyond words. I am very lucky to have them in my life.

Somjai Teanphonkrang

CONTENTS

Page

CONTENTS (Continued)

Page

CONTENTS (Continued)

Page

CONTENTS (Continued)

Page

CONTENTS (Continued)

Page

LIST OF TABLES

LIST OF FIGURES

LIST OF FIGURES (Continued)

LIST OF FIGURES (Continued)

LIST OF FIGURES (Continued)

LIST OF FIGURES (Continued)

LIST OF FIGURES (Continued)

LIST OF FIGURES (Continued)

Figure **Page**

LIST OF ABBREVIATIONS

$\Delta°G$	Gibbs free energy change
ΔC_p	Heat capacity change
ΔH	Enthalpy change
ΔS	Entropy change
°C	Degrees Celsius
µA	Microampere
µL	Microliter
µM	Micromolar
µmol	Micromol
^{13}C-NMR	Carbon nuclear magnetic resonance
^{1}H-NMR	Proton nuclear magnetic resonance
ACR	Albumin to creatinine
Ag	Silver element
Ag/AgCl	Silver-Silver chloride
AMP	Adenosine monophosphate
AP	Alkaline phosphate
AU	Artificial urine
BG	Berlin green
C	Concentration
Ca^{2+}	Calcium ion

LIST OF ABBREVIATIONS (Continued)

CaM	Calmodulin protein
CE	Capillary electrophoresis
Cu	Copper element
CV	Cyclic voltammetry
CYP 46A1	Cytochrome P450 family 46 subfamily A member 1
DET	Direct electro transfer
DHPA	3, 4-dihydroxyphenylacetate
DIPEA	*N*, *N*-diisopropylethylamine
DMSO	Dimethyl sulfoxide
EDEA	2, 2'-(Ethylenedioxy)bis(diethylamine)
FAD	Flavin adenine dinucleotide
FMN	Flavin mononucleotide
FSCV	Fast scan cyclic voltammetry
GPb	Glycogen phosphorylase b
GC	Gas-chromatography
GOx	Glucose oxidase
H_2O_2	Hydrogen peroxide
HPAH	*p*-Hydroxyphenylacetate 3-Hydroxylase
HPAH-C1	*p*-Hydroxyphenylacetate 3-Hydroxylase reductase component
HPAH-C2	*p*-Hydroxyphenylacetate 3-Hydroxylase oxygenase

LIST OF ABBREVIATIONS (Continued)

	component
HPLC	High performance liquid chromatography
I	Current
ITC	Isothermal titration calorimetry
k	Reaction rate constant
K^+	Potassium ion
K_a	Association constant
K_D	Dissociation constant
kJ	Kilojoule
LC	Liquid-chromatography
mg	Milligram
m-HPA	3-Hydroxyphenylacetate
RE	Reference electrode
PBS	Phosphate buffer solution
C	Concentration
I	Current
MHz	Megahertz
mL	Millilitre
mM	Millimolar
mmol	Millimole
MS	Mass-spectrometry

LIST OF ABBREVIATIONS (Continued)

n	Stoichiometry number
nA	Nanoampere
NADH	Nicotinamide adenine dinucleotide
NaOH	Sodium hydroxide
o-HPA	2-Hydroxyphenylacetate
Os	Osmium element
P(SS-GMA-BA)-Os	Poly (4-vinylbenzenesulfonate-glycidyl methacrylate-butyl acrylate)-osmium
PB	Prussian blue
PBS	Phosphate buffer solution
PEGDGE	Poly (ethylene glycol) diglycidyl ether
p-HPA	4-Hydroxyphenylacetate
ppm	Part per million
PQQ-GDH	Pyrroloquinoline quinone glucose dehydrogenase
Pt	Platinum element
PVP-C6	Poly (vinyl pyridine)-hexanoic acid
PVP-Os	poly (vinyl pyridine)-osmium
PW	Prussian white
PY	Prussian yellow
R^2	Regression coefficient
rpm	Round per minute

LIST OF ABBREVIATIONS (Continued)

s	Second
SPE	Screen printed electrode
T	Temperature
t	Time
TLC	Thin layer chromatography
TSTU	*N, N, N′, N′*-Tetramethyl-O-(N-succinimidyl) uronium tetrafluoroborate

CHAPTER I

INTRODUCTION

Within the past century tremendous technological progress has been made in the area of electronic hard- and software, and accordingly all electrical devices that integrate them for the governance of sophisticated functions underwent an enormous improvement, too. The excellent opportunities that came with the electronics advancements are easiest noticeable for everybody in the television, mobile phone communication and computer sections. TV sets, for instance, grew from the first black and white knob-controlled very bulky versions with two channels at best into high-tech systems with mini-processor controlled color viewing of hundreds of channels on super flat (Figure 1.1A), large and light high-resolution screens. Hand-size smart and ultra-light mobile telephones with fast computer-like functions that connect wirelessly to the signaling networks with high-speed data transfer replaced, on the other hand, the first-generation massive and heavy cell phones of the 1960ies and 70ies with call option (Figure 1.1B), only. And personal computers matured from large apparatuses with very limited storage capacity into portable kits with Terabyte hard-drives and ultrafast software execution (Figure 1.1C). Profiting from the modern technology behind these milestone accomplishments was of course also the standard of electrochemical equipment. High-tech single or multi working electrode potentiostats with down to femtoampere current and nanosecond time resolution capabilities, for instance, became easily available for reasonable prices and their application led, further supported by

integration of advanced computer-controlled detection schemes, to great progress in the overall quality of electrochemical analysis, namely of voltammetry, amperometry and potentiometry.

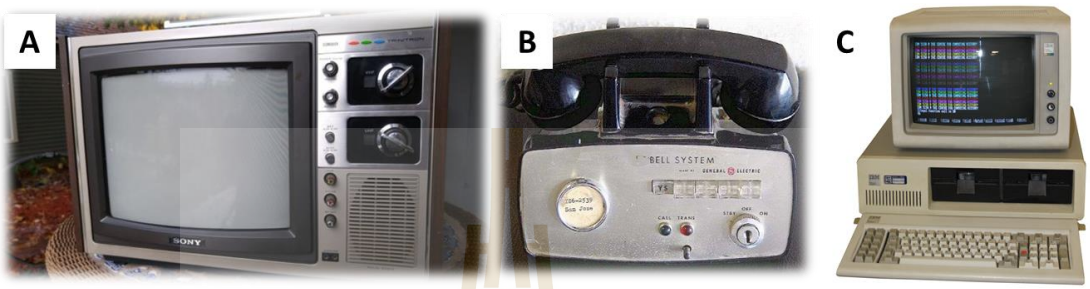

Figure 1.1 (A) TV sets, grew from the first black and white knob-controlled very bulky versions. (B) The first-generation massive and heavy cell phones of the 1960ies and 70ies with call option. (C) Personal computers matured from large apparatuses.

In the area of medical diagnosis, the above trend to advanced instrumentation facilitated the appearance of advanced electrochemical enzyme, antibody/antigen and DNA biosensing devices for healthcare applications. The most prominent success cases are by far the handheld enzymatic blood glucose meters that are used by masses of diabetes sufferers around the world for their daily blood screens, at home or anywhere else. The central subject of this PhD thesis laboratory work is actually a similar electrochemical enzyme biosensing, however, not with ordinary enzymes as, for instance, the glucose oxidase of the commercial glucose meters, but with special protein versions that are susceptible to allosteric activation. With such allosteric biocatalysts, the binding of an allosteric activator molecule (the ‘effector’) actually induces acute local changes in the protein structure arrangements, which tune the embedded catalytic site to a higher speed of substrate turnover into product. The goal of this particular thesis

efforts was to demonstrate, for the first time, that incorporation of an allosteric enzyme into simple amperometric biosensor architectures can be utilized for enhanced substrate quantification, on the one hand, and for trace detection of the allosteric activator itself, on the other hand. The prototype enzyme system was a well-studied bacterial reductase that had been shown to convert NADH as substrate into NAD^+ and was known to do that job faster in presence of *p*-hydroxy-phenylacetate (*p*-HPA) as allosteric effector that accelerates the NADH-to-NAD^+ reaction.

To set above frame of the thesis in more detail, the following thesis chapter will introduce the basics of enzymes, enzyme allostery and enzyme biosensing. Chapter three will then handle the existing literature on the enzyme choice here, which is a *p*-HPA reductase, and review briefly the so far forwarded examples of enzyme biosensing with allosteric enzymes, for both inhibiting and activating stimuli. Finally, the applied experimental methodologies will be explained, results be presented and discussed and, last but not least, a conclusion and future outlook will be provided at the thesis closure.

CHAPTER II

BASIC FACTS ON THESIS-RELATED SUBJECTS

As mentioned in the preliminaries before his Ph.D. thesis focuses on the development of an advanced electrochemical enzyme biosensor assay that ultimately is meant to be for the detection and quantification of a urinary disease biomarker. To lay the foundation for an understanding of the thesis objectives the first subsection of this chapter will provide the basic principles behind the roles and function features of the key component of the target biosensors, actually enzymes. The second subchapter will then inform how enzymes are immobilized as signalling entities onto electrochemical sensor surfaces and brought there to function for the selective and sensitive quantification of their substrates. And in the third and last chapter subsection the special case of allosteric enzymes will be described, a distinction be made between allosteric enzyme inhibition and activation, and enzyme inhibition and activation biosensor assays be outlined in their fundamental methodology.

2.1 (Redox) Enzymes

Enzymes are proteins biocatalysts that enable a myriad of physiological metabolic reactions in the human/mammalian body and as such they are dispensable for the maintenance and activity of general life. Actually, almost the entire set of chemical reaction occurring inside the individual cells of a living organism are dependent on the catalytic drive by enzymes. The effect of enzymes on a biochemical

reaction is best explained by the energy changes that must occur during the conversion of substrate (*S*) to product (*P*) refer to the inset of Figure 2.1, (Flynn and Wall, 1966).

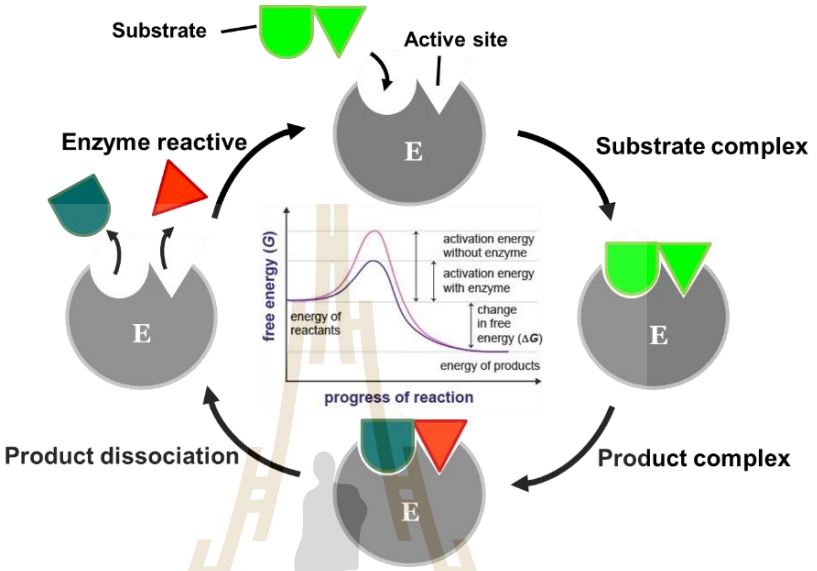

Figure 2.1 The diagram depicts, as example, an exergonic reaction, in which energy is lost for substrate to product formation. The activation energy needed for the reaction to proceeded is shown as lower with the enzyme catalyst than the enzyme without catalyst. The figure shows the catalytic cycle of an enzyme. (i) The substrate bind with the active site. The enzyme then goes through conformational changes in order to better accommodate the substrate. (ii) Substrate held in active site by weak interaction. (iii) Active site can lower Ea and speed up the reaction. (iv) Substrates are convert to products. (v) Products are released or dissociated. (vi) Active site is available for new substrate molecules.

As clear from the presentation of above Figure 2.1, work by lowering the activation energy (E_a), thereby increasing the rate of chemical reactions. On the basis of their chemical nature, enzymes can be classified into two types: (i) simple enzymes,

which consist of only a protein and (ii) holoenzymes or conjugated enzymes, which consist of an apoenzyme (inactive) and a functional co-factor. A cofactor is a non-protein chemical compound that is required for an enzyme activity. The cofactors can be subclassified as either inorganic ions or complex organic molecules called coenzymes (Hashim and Adnan, 1994). A coenzyme that is tightly or even covalently bound is termed a prosthetic group and serves as carrier of electrons or active chemical groups (Cox and Nelson, 2008). Some enzymes or enzyme complexes require several cofactors for running their function successfully.

Embedded into the protein structure of a functional enzyme is the catalytic (or active site). The catalytic site is a three-dimensional region of an enzyme where substrate molecules bind (substrate specificity) and undergo a chemical reaction. Figure 2.1 illustrates that the catalytic activity of enzymes involves affinity binding of their substrates to the specific regions of the active site structure to form an enzyme-substrate complex (ES). While bound to the active site, the substrate is converted into the product of the reaction, which is then released from the enzyme.

In biochemistry, various enzyme kinetic theorys and equations are used to describe the rate of enzymatic reactions by relating the reaction rate v_o (rate of formation of product or rate of consumption of substrate) to [S], the concentration of substrate. The simplest and best-known model is the Michaelis-Menten enzyme kinetics:

$$v = \frac{d[P]}{dt} = \frac{V_{max}[S]}{K_m + [S]} \qquad \text{(eq.1)}$$

where V_{max} is the maximal reaction velocity at enzyme-saturating substrate concentration and K_m is the Michaelis-Menten constant at which the reaction rate is half of V_{max}. A graphical display of the Michael-Menten equation is shown below in Figure 2.2.

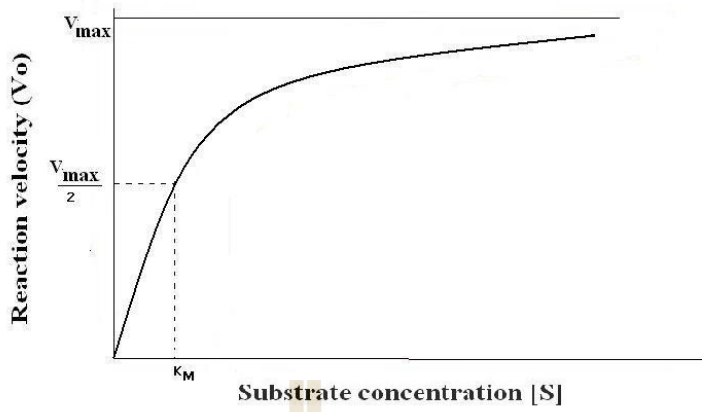

Figure 2.2 Plot of the reaction rate for an enzymatic substrate to product conversion that obeys the Michaelis–Menten kinetics. The v_o vs. [S] curve follows the mathematical expression given by Michaelis-Menten equation (eq.1) and moves towards a plateau at high, saturating substrate exposure levels (Boyle, 2005).

Redox enzymes are a special class of biocatalysts that support substrate oxidations or reductions through effective electron-withdrawing or electron-donating abilities. A very prominent example of a redox enzyme is glucose oxidase, which is major driver of physiological glucose combustion and the selective biological recognition element of most commercial blood glucose meters. Since redox enzyme are changing their oxidation state in course of substrate interaction through loss or gain of electrons, they need to be recycled after individual substrate conversion into product for repetitive action. Reach of redox recycling is gained through contact with so-called redox mediators. Native redox mediator for oxidases, including glucose oxidase, is, for instance, molecular oxygen, O_2, that is dissolved in blood and the cytoplasm of living cells. On the other hand, a number of other dissolved redox active components of the body fluids and even artificial redox compound can serve as recycling partners of

oxidases and the many other redox enzymes.

2.2 Allosteric enzymes

Allosteric enzymes represent a subset of enzymes that are unique compared to the conventional enzymes in their ability to react to variations in environmental conditions spontaneously with an adaptation of their function and performance. These enzymes are thus heavily involved in the control and regulation of central biological processes such as cell signalling and metabolism.

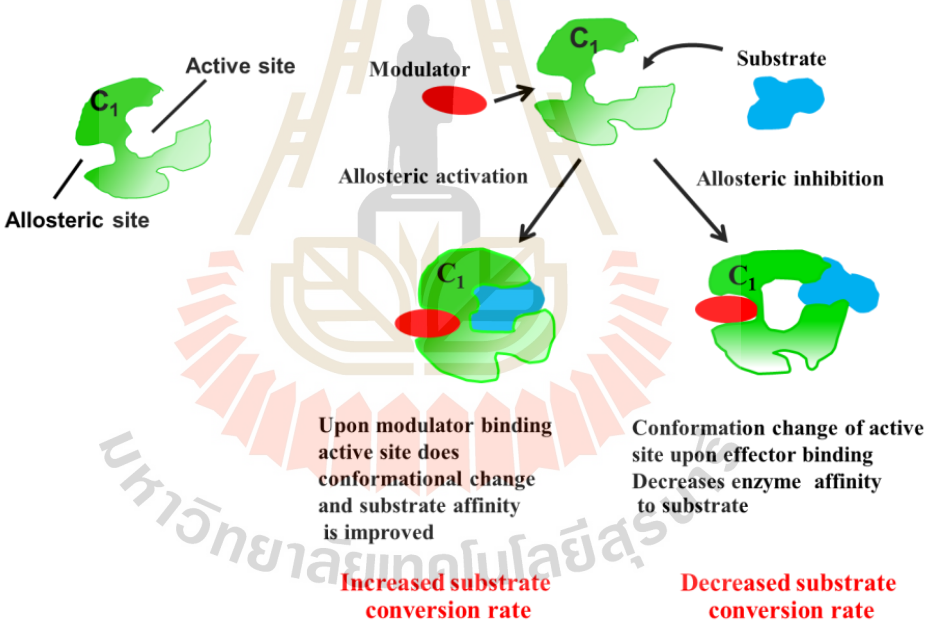

Figure 2.3 Exposure of an allosteric enzyme with an extra binding site for an allosteric effector to effector. Activator or inhibitor binding noticeably changes the conformational protein appearance, also or just in the catalytically active structure region. The induced structure modulation then up- or down-regulates the effectiveness of substrate affinity binding in the catalytic site and accordingly modulates substrate-product turnover rates to higher or lower values.

Behind the observation of an allosteric substrate turnover rate increase or decrease is an affinity binding of an effector molecule at a specific site on the protein surface. Binding leads to noticeable rearrangements in the 3-D protein structure which then take an impact on the strength of enzyme-substrate complex formation (refer to Figure 2.3). Structure changes that induce better enzyme-substrate interaction (= a better affinity between the two) will increase specific biocatalytic reaction rates (‘allosteric activation) while a slowdown of turnover is observed for a worsening of enzyme/substrate affinity (“allosteric inhibition”). Allosteric effectors may be specific ligands, ions, or proteins (Di Cera, 2009; Swain and Gierasch, 2006; Villaverde, 2003; Zhu and Anslyn, 2006; Zorn and Wells, 2010).

Native role and importance of allosteric enzyme activation and inhibition is to allow individual cells in complex and widespread tissue of higher organisms to adjust local enzyme activity to local physiological and pathological needs. Since quite a few enzymes are, on the other hand, explored in biotechnology for the directed synthesis of high-value saleable chemicals the option of yield improvement via allostery exploitation is in the business section certainly an appealing issue. And as mentioned before and outlined in more detail below, enzyme biosensing can benefit from an allostery of the key sensor component in terms of the reach of advancements of sensitivities and detection limits and the move to otherwise unapproachable analytes.

2.3 Electrochemical biosensing with allosteric enzymes

Biosensors are analytical tools that are based on an electrical coupling of an immobilized biological recognition element (BREs) to a signal transducer and an electronic amplifier. Based on the type of transducer used, biosensors have been divided

into optical, calorimetric, piezoelectric and electrochemical biosensors (Chaubey and Malhotra, 2002). BREs may be enzymes, antibodies/antigens, aptamers, single-stranded DNA, cell receptor molecules or even whole cells (Bhalla *et al.*, 2016). Relevant for this PhD thesis is, however, the utilization of enzymes for electrochemical, specifically amperometric, analytical biosensing. Figure 2.4 shows the schematic of the cascade of redox events that lead for a conventional electrochemical oxidase enzyme biosensor, as example, to electrical signal generation in terms of measurable current flow. The system involves three main functional components: (i) the biological recognition element (BREs) which is here an oxidizing enzyme that provides selectivity

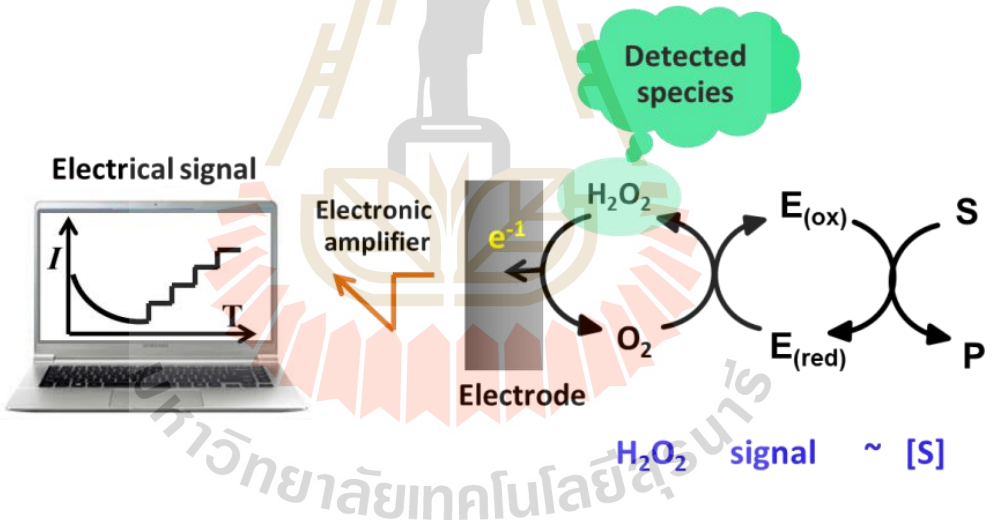

Figure 2.4 Schematic diagram showing the pathway of signal generation for an electrochemical amperometric enzyme biosensor that is exposed to substrate as the analyte. Here, the enzyme is an oxidizing protein biocatalyst and dissolved O_2 is as redox mediator in charge of the enzyme‘s redox state recycling. Measured species at the electrode is H_2O_2; possible is cathodic or anodic detection at appropriate negative or positive working potentials.

for the target substrate molecules; after reaction with substrate then reduced enzyme is re-oxidized by the mediator oxygen to be primed for the next cycle of biocatalysis, (ii) an electrode transducer that converts H_2O_2 from enzyme redox recycling into electrical current through interfacial anodic oxidation and (iii) a signal processing system that measures the current and transfers it into storable form (Niraj *et al.*, 2012).

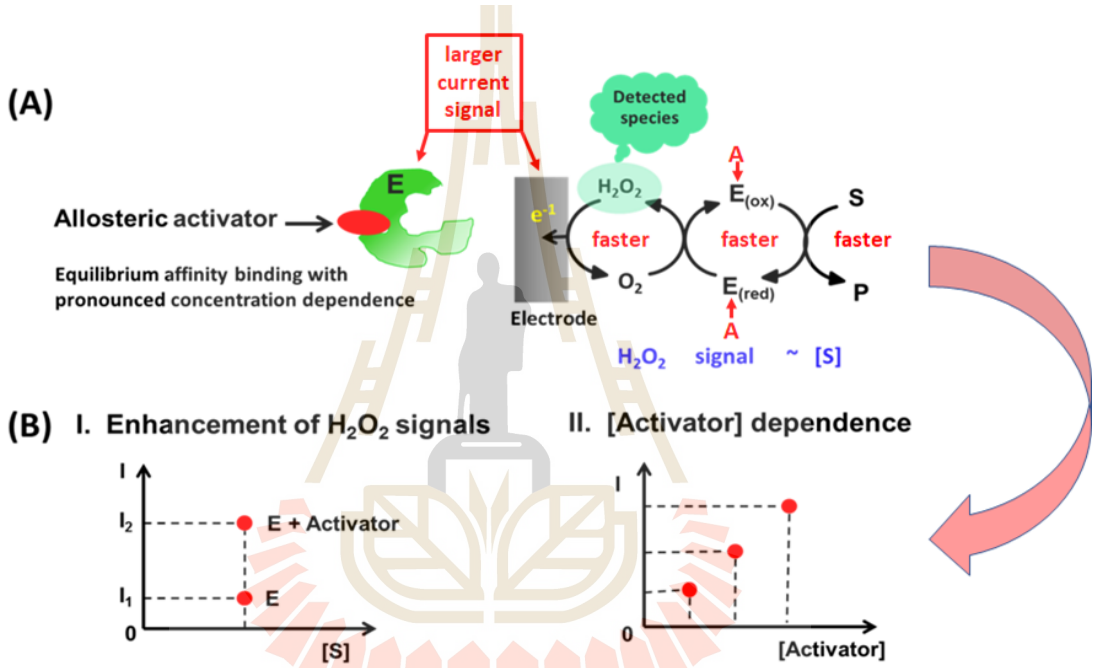

Figure 2.5 (A) Schematic illustration of the principles of amperometric biosensing with an immobilized allosteric "oxidase"-type enzyme of oxygen mediation. (B) Joint presence of enzyme and activator molecules in measuring buffer will lead to an occupation of allosteric bonding sites and then to the stimulating modulation of substrate conversion. For a given substrate concentration larger H_2O_2 currents as compared to absence of effector will be observed (BI). The concentration dependence of enzyme/activator affinity binding should, in principle, allow quantification of the activator through plots of sensor current versus [A] (BII). If the allosteric activator is a disease biomarker the scheme could be exploited for medical diagnosis.

So far considered has been the case of amperometric biosensing with normal, non-allosteric enzymes in action on top of electrode transducers such as noble metal or glassy carbon disks. Options for the quality of signalling are changing when the protein biocatalyst shows pronounced liability to allosteric activation. Figure 2.5 illustrates that distinct situation. On the electrode immobilized is an allosteric enzyme that responds to the bonding of an activator molecule with speedier chemical conversion of substrate. As a result, enzyme recycling is also accelarated, more detectable H_2O_2 is available for signal creation for a given substrate concentration and the current for the particular condition enhanced (refer to Figure 2.5BI). The association of the allosteric effector with its enzyme partner is an affinity binding process. A well-expressed concentration dependence of allosteric turnover rate modulation is thus expected (2.5BII) and seen as chance to use current recordings at fixed substrate levels as methodology for the quantification of the allosteric effector. Though this type of detection is technically rather simple, it has surprisingly not really worked with until now, at least not in the most basic configuration possible. Existing exploitations will be discussed not here but in the later subsection ,State of the Art, Literature Review.

CHAPTER III

RESEARCH OBJECTIVES

Introduced was in the starting thesis chapters its general framework, which is actually advanced medical disease biomarker electroanalysis with an allosteric enzyme biosensing assay in amperometry mode. Choice of allosteric protein was for the prototype work a bacterial reductase, namely the C1 unit of 2-component *p*-hydroxyphenyl-acetate hydroxylase (HPAH) from *Acinetobacter baumannii*. C1 is allosteric to *p*-hydroxyphenyl-acetate (*p*-HPA), which also is urinary biomarker of a bad condition in the gastrointestinal tract, mainly of small intestinal bacterial and fungal overgrowth and of various brain pathologies, too. In a point-to-point list, the conducted research project aimed at:

- The development of C1-based amperometric NADH and *p*-HPA biosensing, with the enzyme reacting in solution with substrate, O_2 and effector and cathodic Prussian blue-modified screen-printed electrodes in charge of quantification of liberated H_2O_2. Target output is the novel analytical scheme and one publication in a quality peer-reviewed journal.
- The development of C1-based amperometric NADH and *p*-HPA biosensing, with the enzyme functionally immobilized into an adapted Osmium (III)-based redox polymer and biocatalysis quantified with and without allosteric activation via Os (II)/(III) redox electron transfer at the electrode. Target output is the novel analytical scheme and one publication in a quality peer-reviewed journal.

- Application of the developed schemes, favourably the Os (III) redox polymer/C1 biosensing, for the quantification of traces of the disease biomarker *p*-HPA in model and artificial urine samples. Target output is a novel suggestion for urinary disease biomarker analysis with the potential to be incorporated into a handheld ‘glucose meter’-type device for personal screening at home and one publication in a quality peer-reviewed journal.

CHAPTER IV

STATE OF THE ART, LITERATURE REVIEW

4.1 *p*-Hydroxyphenylacetate hydroxylase-reductase (C1): kinetic properties and allostery

Target of the PhD thesis was an electrochemical urinary *p*-HPA biosensor assay that exploited for signal generation an activation allostery of a specific reductase enzyme unit of the soil-based microorganism *Acinetobacter baumannii*. In *A. baumannii* the reductase is functional as the "C1" subunit of the two-component enzyme system *p*-hydroxyphenylacetate hydroxylase (HPAH), which is responsible for biocatalytic chemical conversion of *p*-HPA into di-hydroxyphenylacetate (DHP). The second enzymatic HPAH subunit (referred to hereafter as "C2") is a monooxygenase that governs the desired *p*-HPA hydroxylation into 3,4 dihydroxy-phenylacetate (DHPA) as final product (Chaiyen *et al.*, 2001; Thotsaporn *et al.*, 2004). The enzymology of HPAH was intensively studied, in particular by Chaiyen, Sucharitakul and coworkers, and the basic biochemical, structural and kinetic properties of C1, C2 and the C1/C2 agglomerate have been disclosed in a comprehensive series of their scientific reports. C1 and C2 are actually separate protein who operate independently in terms of biocatalytic functions. However, for *p*-HPA to DHPA conversion their distinct activities are coordinated through the activation of NADH oxidation ($FMNH^-$ generation) on the C1 component (Phongsak *et al.*, 2012; Sucharitakul *et al.*, 2005; Sucharitakul *et al.*, 2007). The process starts with a C1-driven oxidation of substrate β-

NADH to β-NAD^+, leaving the C1 cofactor FMN in reduced form ($FMNH^-$) in the catalytic protein pocket. As the binding of $FMNH^-$ to C1 is weaker compared to the binding of oxidized FMN, $FMNH^-$ dissociates from C1, freely diffuses and can be delivered to C2 via an intermolecular give-and-take action (Sucharitakul *et al.*, 2014). In the presence of molecular oxygen, the C2-$FMNH^-$ complex reacts with oxygen to form a reactive intermediate, C4a-hydroperoxy-FMN which can catalyze the hydroxylation of *p*-HPA to result in final products i.e. DHPA and oxidized FMN (Ruangchan *et al.*, 2011; Sucharitakul *et al.*, 2006; Tongsook *et al.*, 2011). As the binding affinity of oxidized FMN and C2 is low, the oxidized FMN is released from C2 and back-trafficked to C1, prompting the reductase to be ready for next catalytic cycles. Important in the context of this study was that although C1 does not use HPA as a substrate, HPA can bind to C1 and act as an effector to increase the NADH oxidation activity. Transient kinetics results show that the effective allosteric *p*-HPA stimulus on C1 is achieved through an increase of the binding affinity of substrate β-NADH and the related acceleration of the reaction rate (k) of NADH oxidation (Sucharitakul *et al.*, 2005). Therefore, the C1 reductase was able to serve as an ideal novel redox enzyme model for inclusion into redox polymer biosensor preparations. Offered in the equations 2-5 below for a summary of enzymatic and chemical events that finally lead to DHPA production from a *p*-HPA input:

$$C1\text{-}(FMN)_{ox} + NADH \rightarrow C1\text{-}(FMN)_{red} + NAD^+ \quad \text{(eq.2)}$$

$$C1\text{-}(FMN)_{red} + C2 \rightarrow C1 + C2\text{-}(FMN)_{red} \quad \text{(eq.3)}$$

$$C2\text{-}(FMN)_{red} + p\text{-HPA} \rightarrow C2 + DHPA + (FMN)_{ox} \quad \text{(eq.4)}$$

$$C1\text{-}(FMN)_{ox}{:}p\text{-HPA} + \beta\text{-NADH} \rightarrow C1\text{-}(FMN)_{red}{:}p\text{-HPA} + NAD^+ \quad \text{(eq.5)}$$

- **Equation 1** refers to the biocatalytic substrate conversion of allosteric reductase component (C1) of HPAH ($NADH \rightarrow NAD^+$; $(FMN)_{Ox} \rightarrow (FMN)_{red}$)
- **Equation 2** refers to a transfer of reduced FMN from C1 to the oxygenase component (C2) of HPAH.
- **Equation 3** refers to the biocatalytic hydroxylation of *p*-HPA to DHPA by primed C2.
- **Equation 4** refers to the biocatalytic activity substrate conversion of allosteric reductase component (C1) of HPAH in presence of allosteric activator *p*-HPA.
- Due to positive allosteric stimulation reaction rate *k*(4) is significantly larger than reaction rate *k*(1).

The $NADH \rightarrow NAD^+$ conversion activity of reductase C1 is allosterically amplified by the phenolic compound *p*-HPA; however, in above cited studies it was shown that not only *p*-HPA but also some other aromatic compounds with similar chemical structure can act as effectors to, though with lesser power. The identified C1 activities in presence of various activators, scaled to the one valid for *p*-HPA taken as 100%, analogues are listed in Table 4.1 for 10 selected substrates.

Obviously, *p*-HPA with the hydroxyl group in *para*-position was best activating C_1 partner but the two compounds *m*-HPA and phenylacetate could at quite close rates also up tune the enzymatic conversion cycle. Summarized in Figure 4.1 are the findings of the Chaiyen and Sucharitakul studies e.g. (Sucharitakul *et al.*, 2007; Sucharitakul *et al.*, 2014) on the properties of the C_1 reductase subunit of HPAH. Most relevant to the

Table 4.1 Substrate specificity of HPAH from *A. baumannii* (Chaiyen *et al.*, 2001).

Substrate analogue	Relative NADH oxidase activity (%)
No substrate	1.7
p-Hydroxyphenylacetate	100
m- Hydroxyphenylacetate	97.7
o-Hydroxyphenylacetate	4.8
p-Chlorophenylacetete	10.3
p-Fluorophenylacetate	37.6
p-Nitrophenylaceteate	2.0
4-Hydroxy-3-methoxyphenylacetate	45.4
Phenylacetate	96.5
3-(4-Hydroxyphenyl)propionate	35.9
p-Hydroxybenzoate	2.6
p-Nitrophenol	2.6

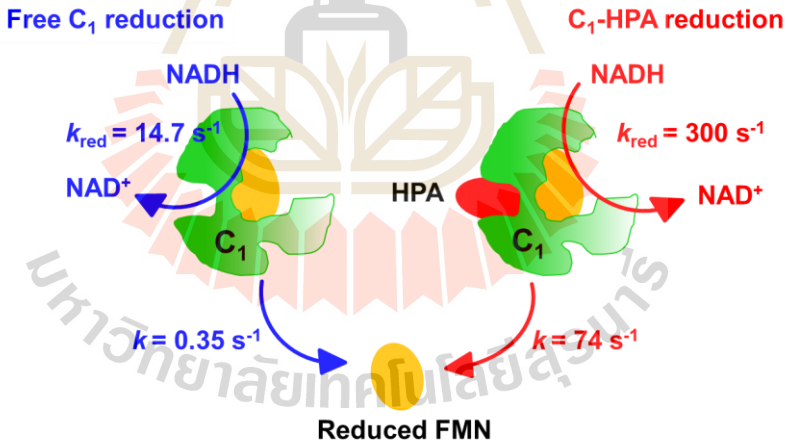

Figure 4.1 Allosteric C_1-*p*-HPA binding increases the reduction rate of FMN and reduced FMN dissociation from the C_1 complex. The blue-colored left section of the graphic represents the situation in absence of *p*-HPA; reaction of FMN with NADH is rather slow at $14.7s^{-1}$. The red-colored right section of the graphic represents the situation in presence of fully stimulating *p*-HPA level at which the FMN site reduction is fastest, at $300s^{-1}$.

work of this doctoral thesis is the enhancement of the conversion of NADH into NAD^+ due to the presence of *p*-HPA: in fact, the allosteric affinity binding of *p*-HPA to the designated area on the C_1 protein surface significantly multiplies the turnover rate by a factor of about 20 times. Accordingly, more H_2O_2 would, for example, be generated in a biosensing exploitation of C1 at a particular NADH level, an effect that can serve as basis for the establishment of advanced H_2O_2 current-based NADH and *p*-HPA detection schemes.

4.2 C1 enzyme biosensor signalling via amperometric detection of hydrogen peroxide

Above mentioned biochemical studies had shown that isolated C_1 on its own is a potent converter of NADH into NAD^+, with dissolved molecular oxygen (O_2) used as partner for required enzyme redox recycling. H_2O_2 is, on the other hand, a well assessable by-product of cyclic C_1/NADH/O_2 interactions and, as shown in Figure 4.2, H_2O_2 production is up scaled by allosteric stimulation through *p*-HPA. Biosensor activity in terms of substrate conversion is usually tested in an electrochemical workstation as shown in Figure 4.3, by the detection of a species that is proportional to conversion rate.

Common for the electrochemical characterization of a biosensor with an enzyme that is recycled through redox with dissolved oxygen (as, for instance the glucose oxidase or the C1 of this study) is the anodic detection of by-product of enzyme recycling H_2O_2 . To enhance anodic H_2O_2 measurements advanced materials with electro-catalytic impact on faradaic H_2O_2 sensing have been used as supplements of the immobilization layer of enzymes on the electrode surface, often in form of

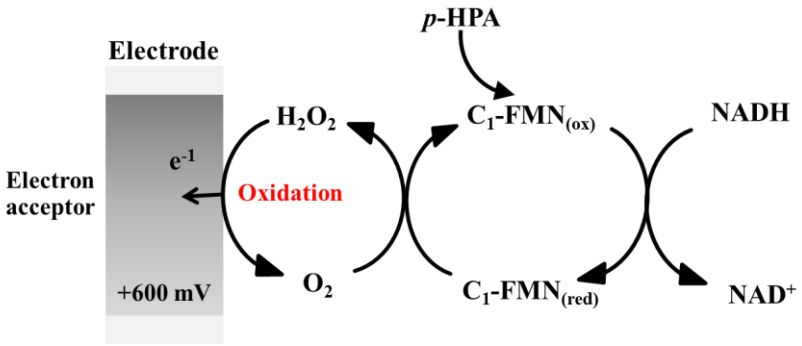

Figure 4.2 Schematic of the dissolved or immobilized C_1 reaction with substrate NADH and the conversion of substrate-NADH into NAD^+; dissolved O_2 is here utilized as redox mediator for enzyme redox recycling. H_2O_2 product is generated via the C_1/NADH/O_2 interaction and usually detected through an oxidation of H_2O_2 at working electrode surface that are polarized at high enough positive potential (e.g. +600 mV). H_2O_2 generation is enhanced when enzyme C1 is activated to higher turnover rates through *p*-HPA binding.

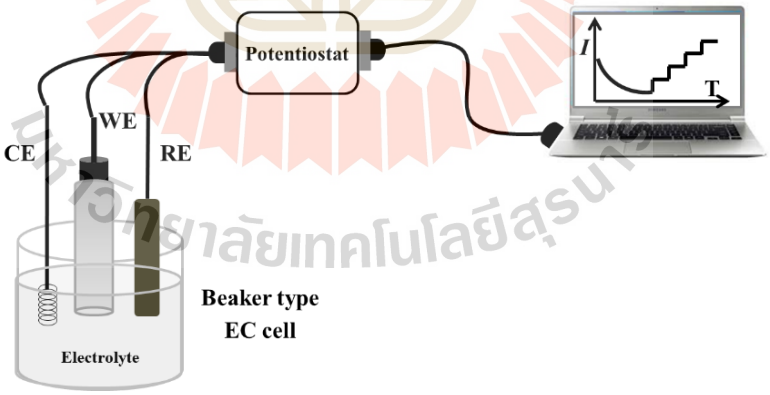

Figure 4.3 Schematic of a typical electrochemical workstation with a three electrode configuration as used for biosensor measurements. Implemented are a working (WE), counter (CE) and reference electrode (RE), respectively. A computer with suitable software helps executing the electroanalytical schemes, e.g. amperometry or cyclic voltammetry, and data storage and post-measurement analysis.

nanomaterials or nanoparticles (Siangproh *et al.*, 2011), conducting polymers (Gerard *et al.*, 2002), quantum dots (Dong *et al.*, 2013; Muthurasu and Ganesh, 2014) and mesoporous materials (Bai *et al.*, 2007; Lee *et al.*, 2009). In general, amperometric enzyme biosensor-type of measurements have received significant attention due to the merger of advantages such as high selectivity and sensitivity (J. Wang, 2008).

However, the common anodic H_2O_2 amperometry is for biosensors with the C_1 reductase as allosteric recognition element problematic for reasons that are stressed in Figure 4.4. NADH and the allosteric activator molecule *p*-HAP are both oxidizable species (Figure 4.4A, B) and they would get oxidized on an electrode surface that is polarized to anodic potentials for H_2O_2 detection. Aiming on C1/NADH/*p*-HPA biosensing substrate and allosteric effector would thus act as interference of the H_2O_2 signaling of enzyme activity as they have to be in solution as reaction partners of C1 and their contributions to anodic current cannot be distinguished from the electrical H_2O_2 signal. Fortunately, H_2O_2 is a special molecule that can be oxidized and reduced (Figure 4.4 C) while the same is not true for NADH and *p*-HPA. A move from anodic to cathodic H_2O_2 detection at favorable negative instead of critical positive detection potential offers thus a way-out of the interference problem and should, in principle at least, allow the functional operation of a C1 biosensor including allosteric activation via phenolic effector *p*-HPA.

To be considered is the fact that cathodic H_2O_2 reduction relates to an electron transfer process that kinetically is not that well favored and slow at normal electrode surfaces such as gold, platinum or carbon/graphite sensors disks or cylinders. Recommended and successfully applied has thus been a chemical modification

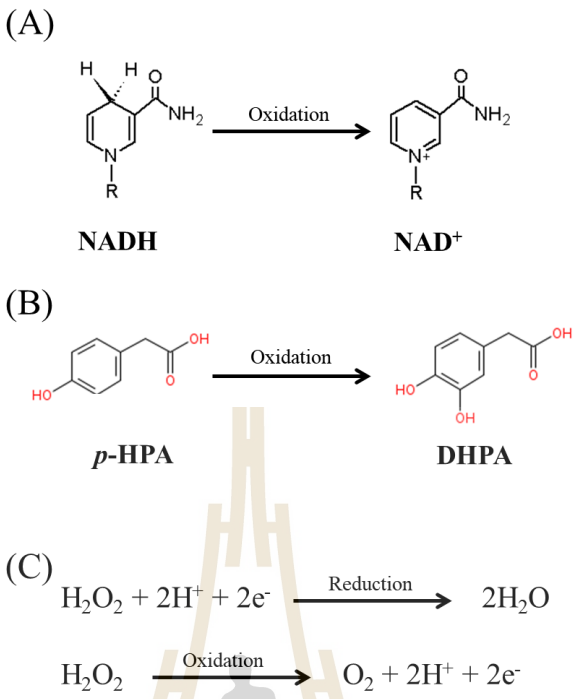

Figure 4.4 Representation showing the change that occur when (A) NADH is oxidized to NAD^+, (B) *p*-HPA is oxidized to DHPA and (C) H_2O_2 is reduced to water or oxidized to oxygen.

electrode surfaces with thin layers of a species that can be a catalyst for H_2O_2 electro-reduction. Electrodes coated with a conducting polymer (Rahman *et al.*, 2004), an iodide-modified Au electrode (Miah and Ohsaka, 2006), micro tubular Te adsorbed on Pt electrode (Guascito *et al.*, 2011), coenzyme adsorption on a carbon felt (Y. Wang and Hasebe, 2011), a cyclopentadienyl ruthenium thiolate schiff base-on-Au electrode (Ticha *et al.*, 2014) and graphene/CNT nanocomposite encapsulated Au nanoparticles (Abdelwahab, 2016) have been reported as suitable for the support of cathodic H_2O_2 detection. Jaikaew *et al*. reported recently that electrical cable-based copper disk electrode served well as cathodic H_2O_2 detection platform of oxidase biosensors (Jaikaew *et al.*, 2016). And a well investigated catalytic electrode coating for efficient

cathodic H_2O_2 electro-reduction are thin films of Prussian blue (PB) on the surface of the electrode (Karyakin, 2001). PB electrode modifications have found a widespread use in the biosensor field because of the elimination of common anodic interferences such as ascorbic acid, uric acid, paracetamol etc. (Francesco Ricci *et al.*, 2007; F. Ricci and Palleschi, 2005). PB films on sensor surface may be created via pure chemical depositions or via electrochemical coating procedures. Some chemical, physical and electrochemical properties of PB are described below:

- The characteristic cyclic voltammogram of a PB thin-film electrode coating is shown in Figure 4.5A PB (Karyakin, 2001). In between the observed two sets of redox peaks the oxidation state corresponds to PB. At elevated cathodic potentials PB reduction is induced and Prussian White (PW) formation is accompanied with loss of the blue color. PB to PW conversion is reversible.
- At high positive (anodic) potentials PB converts to its fully oxidized form denoted as Berlin Green (BG) or Prussian Yellow (PY). PB to BG (PY) conversion is reversible.
- PB has a basic cubic structure consisting of alternating iron(II) and iron(III) located on a face center cubic lattice (Figure 4.5B) in such a way, that the iron(III) ions are surround octahedrically by nitrogen atoms, and iron (II) ions are surround by carbon atoms. (Herren *et al.*, 1980). Distinguished is between two a soluble and the other insoluble forms of PB, (Figure 4.5C-D) (Itaya *et al.*, 1982). It has been demonstrated that the PB electrochemical activity is supported in the presence of K^+ ions (Garcıa-Jareno *et al.*, 1998).

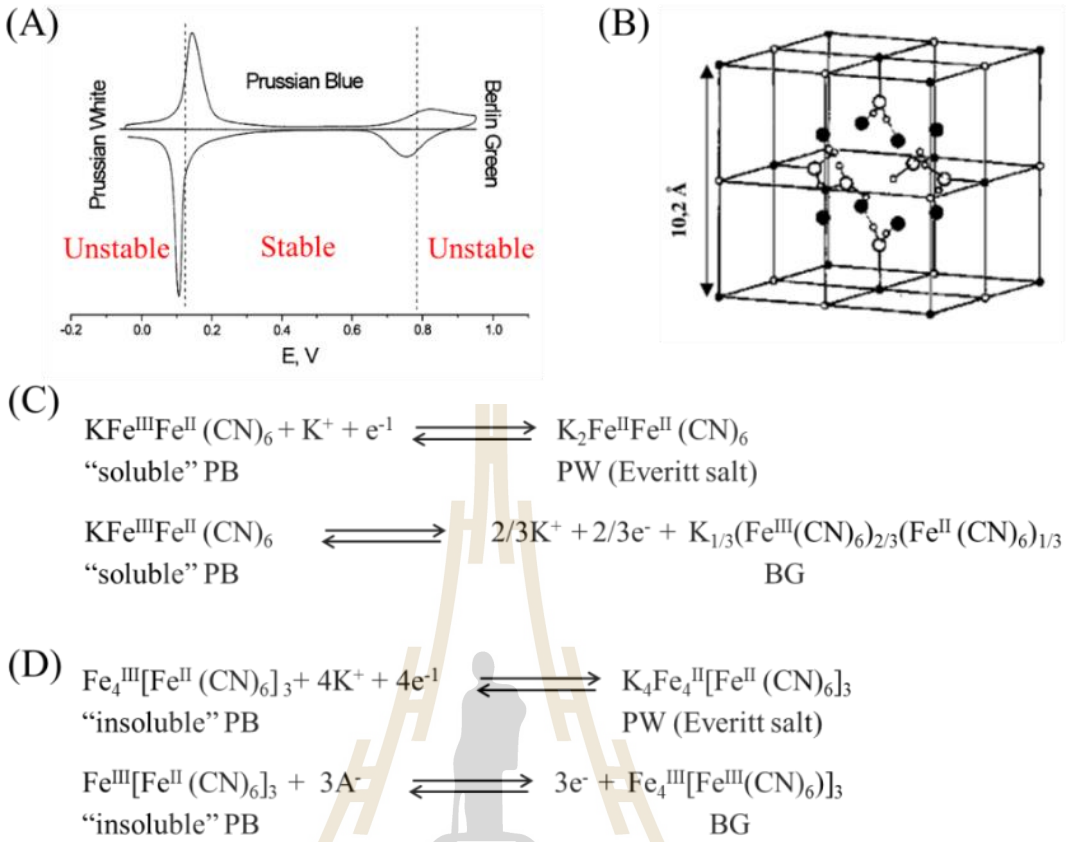

Figure 4.5 (A) Cyclic voltammogram of a Prussian blue (PB) modified electrode showing the reduction and oxidation peaks of PB (Karyakin, 2001). (B) Unit cell of PB; (•) Fe^{3+}, (◦) Fe^{2+} (Herren *et al.*, 1980). (C) Redox processes of "soluble" PB (Ellis *et al.*, 1981). (D) Redox process of "insoluble" PB (Itaya *et al.*, 1982)

Screen-printed electrodes (SPE) as shown in Figure 4.6 (Albareda-Sirvent *et al.*, 2000) were successful for the detection of many analytes (Ivanildo Luiz de Mattos *et al.*, 2003) and they were favored for a lot of applications because they are fast in response, cost-effectiveness, high selectivity and sensitivity. Another advantage of SPEs is that they can easily be produced in large quantities via automated inkjet printing on prepared polymer plates.

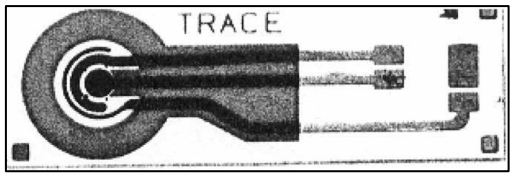

Figure 4.6 Representative photograph of the design of screen printed electrodes (SPEs); the size of the carrying plate is 51x16 mm; the electrodes were placed via screen-printing technology (Trace GmbH Braunschweig, Germany). Working electrodes may be made of metal (e.g. Au, Pt, Ag) or carbon ink; the other two electrodes in the screen-printed electrode set can serve as reference and counter electrodes (Ivanildo Luiz de Mattos *et al.*, 2003).

In context of the work of this study important is that SPEs were successfully modified with thin PB layers for cathodic H_2O_2 measurements at potentials against oxidation of ascorbic acid, uric acid, drugs such as paracetamol and enzyme substrates such as NADH. An example of a characteristic redox couple for PB on a PB-modified SPE is shown in Figure 4.7A, in the presence and absence of H_2O_2 (Cinti *et al.*, 2014). The cathodic peak, indicating formation of PW, was shifted slightly to more negative potential, and was increased in the magnitude. The anodic peak was also shifted to more negative potentials and was reduced in peak current. These effects are explainable considering the mediation of the reductive electro-catalytic reactions according to the scheme in Figure 4.7B.

The well-pronounced cathodic response of the PB-SPEs towards H_2O_2 can be made use of for quantitative amperometric H_2O_2 detection at, e.g. 0.0 V vs. Ag/AgCl reference electrodes (Cinti *et al.*, 2014). Screen-printed electrodes chemically modified with functional PB films showed good sensor characteristics for the detection of H_2O_2

at low potential. This type of H_2O_2 sensing is anodic interference free at moderately cathodic working potentials (e.g. 0 to -200 mV) (I. L. de Mattos *et al.*, 2000).

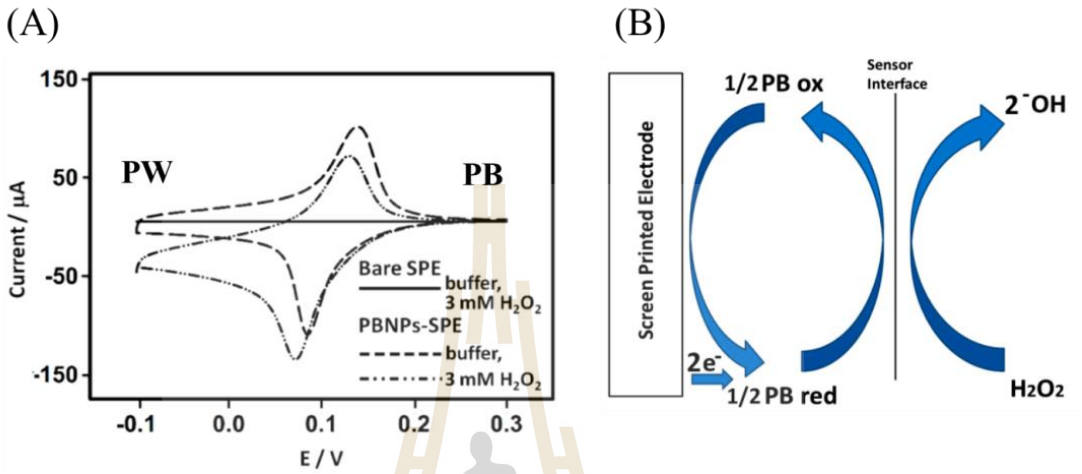

Figure 4.7 (A) Cyclic voltammograms of bare SPE in 3 mM H_2O_2 (solid line), SPE modified with 20 cycles for PB deposition in buffer (dashed line) and 3 mM H_2O_2 (dashed-dotted line) (A). (B) Mechanism of the catalytic H_2O_2 reduction mediated by PB (Cinti *et al.*, 2014).

Note that in the first part of this thesis a PB-assisted low-potential cathodic H_2O_2 electroanalysis will be explored for the first time as a novel non-biochemical assay for thorough inspection of enzyme allostery, via the example of the C1 reductase, and as a readout for a C1-based NADH and *p*-HPA biosensing. Choice of low-potential measurement of H_2O_2 was, as will be demonstrated in the Results & Discussion section, suitable to avoid the *p*-HPA/NADH interference on H_2O_2 signaling of bare or allosterically up-tuned C1 conversion of NADH.

Allosterically up-tuned C1 conversion of NADH relies on pronounced affinity binding of the allosteric effector molecule *p*-HPA to a distinct ligand site on the C1

protein surface Isothermal Titration Calorimetry (ITC) was also used to look at the C1/*p*-HPA binding characteristics. ITC is a high-accuracy biochemical method especially primed for the evaluation of binding affinities of proteins with various coupling partners and with broad impact on protein studies and protein biotechnology (Doyle, 1997). Determined is the heat change that occurs in course of the interaction of, e.g. and enzyme and its substrate molecules (Freyer and Lewis, 2008; Martinez *et al.*, 2013). Heat may be either absorbed or released due to the formation and redistribution of non-covalent bonds when interacting molecules move from the free to the bound state. Identified heat changes are monitored by the ITC machine (refer to Figure. 4.8) by determining the differential power, applied to the cell heaters, needed for maintaining zero temperature difference between the sample and reference cells while mixing the binding partners. The reference cell normally contains water, while the sample cell contains one of the binding partners and a stirring syringe holding the other binding partner (ligand). Titration ligand into protein partner, each ligand injection results in a heat pulse integrated in terms of time (μcal/sec vs. time) and normalized for concentration to generate a titration curve of kcal/mol vs. molar ratio (ligand/protein) (Falconer, 2016; Leavitt and Freire, 2001; Song *et al.*, 2015). A set of isotherm is obtained and fitted to a binding model to find about the number of binding site (*n*), the equilibrium constant (*K*), Gibbs free energy of binding process (Δ*G*) and enthalpy change of binding (Δ*H*). Finally, the obtained data reveals the entropy change of binding (Δ*S*) (Saboury, 2006).

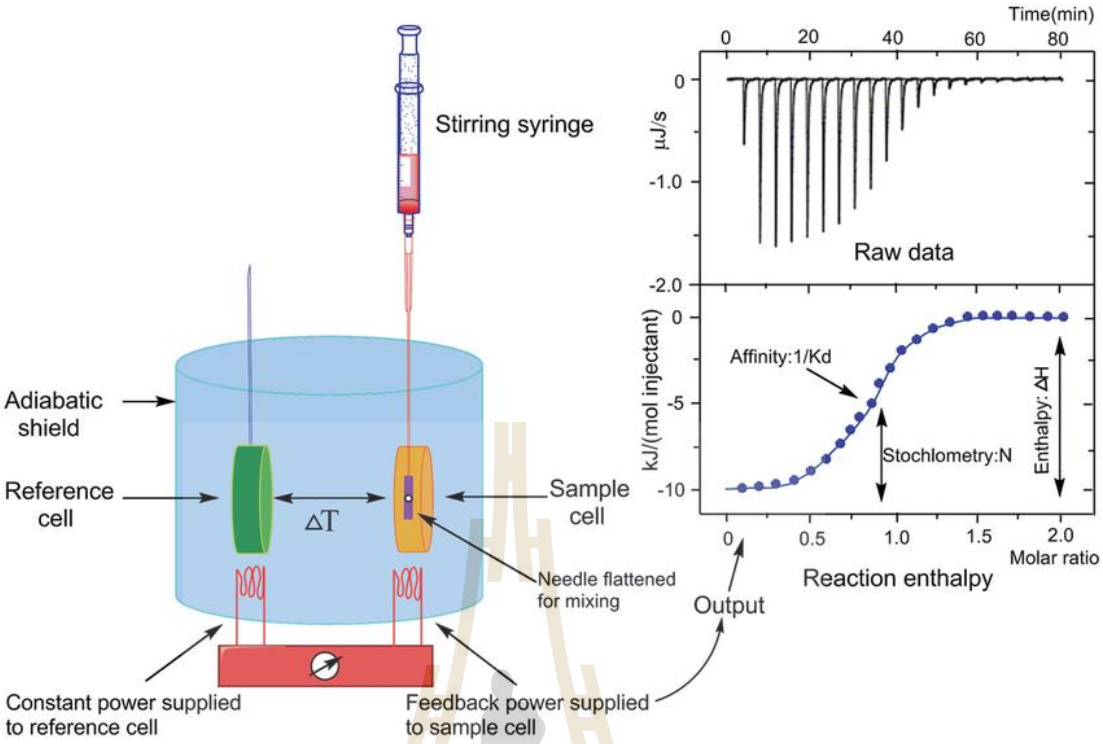

Figure 4.8 Schematic representation of an isothermal titration calorimeter (left) and a characteristic titration experiment (upper right) with its evaluation (lower right). In (upper right) picture, the titration thermogram is represented as heat per unit of time released after each injection of the ligand into the protein (black), as well as the dilution of ligand into buffer (blue). In the lower right picture, the dependence of released heat for each injection vs. the ratio between total ligand concentration and total protein concentration is represented. Circles represent experimental data and the line corresponds to the best fitting to a model considering *n* identical and independent sites. The syringe is inserted in the sample cell and a series of injections are made (Song *et al.*, 2015).

ITC has been widely used biological technique for studying the formation of dissociation of molecular complexes. For example, Ollila *et al*. (2001) used the ITC

methodology for the characterization of bile salt/cyclodextrin interactions. Rajarthnam and Rösgen (2014) described how ITC can be effectively used to gain a valuation of the thermodynamics signatures for drug discovery studies. And ITC-experiment allowed under anaerobic conditions the thermodynamic characterization of two substrates binding to the metal site in homophotocatechuate 2, 3-dioxygenase (HPCD) (Henderson *et al.*, 2016).

4.3 Enzyme biosensor signalling via redox polymer utilization

In the above section electrochemical enzyme biosensing took advantage of an enzyme recycling via dissolved oxygen redox mediation and consequently formed H_2O_2 detection for signal generation. However, more modern reagent-free versions of enzyme biosensors take advantage of the embedment in a redox polymer matrix that has randomly distributed redox sites available for enzyme recycling. The development of redox polymer-based biosensing has its foundation in the early work of Adam Heller on advanced sensors of such a design used for blood glucose meters (Heller, 1990) and was extended then by many others (Schuhmann, 2002).

For the example of a glucose oxidase-based biosensor, possible pathways for enzyme recycling are sketched in Figure 4.9. Dissolved oxygen (as handled in the previous section) or dissolved artificial redox species may be exploited as enzymatic redox partners. Many enzymes have buried active sites in order to prevent the indiscriminate exchange of electrons with other redox proteins and to assure selectivity (Aoyama *et al.*, 1988). In order to transfer electrons between the redox active site and the electrodes, mediators such as osmium complexes (Gregg and Heller, 1991), ferricyanide (Mor and Guarnaccia, 1977), quinones (Williams *et al.*, 1970) and

ferricinium complexes (Crumbliss *et al.*, 1986) are used. And direct electron transfer contact with the electrode surface is a chance to reset the enzyme to original oxidation state after it reacted and exchanged electrons with substrate but difficult to achieve. In redox polymer biosensor, on the other hand, the dissolved artificial redox entity is actually covalently anchored into a specially adapted polymer that at the same time functions as an immobilization sensor layer for enzyme entrapment (Refer to Figure 4.10). Redox sites (e.g. a metal atom such as an Os (III) or a proper organic molecule) that are in touching distance to an immobilized enzyme molecule accept an electron from the protein, which turns the biomolecule back to oxidized state ready for next substrate conversion while itself it becomes reduced.

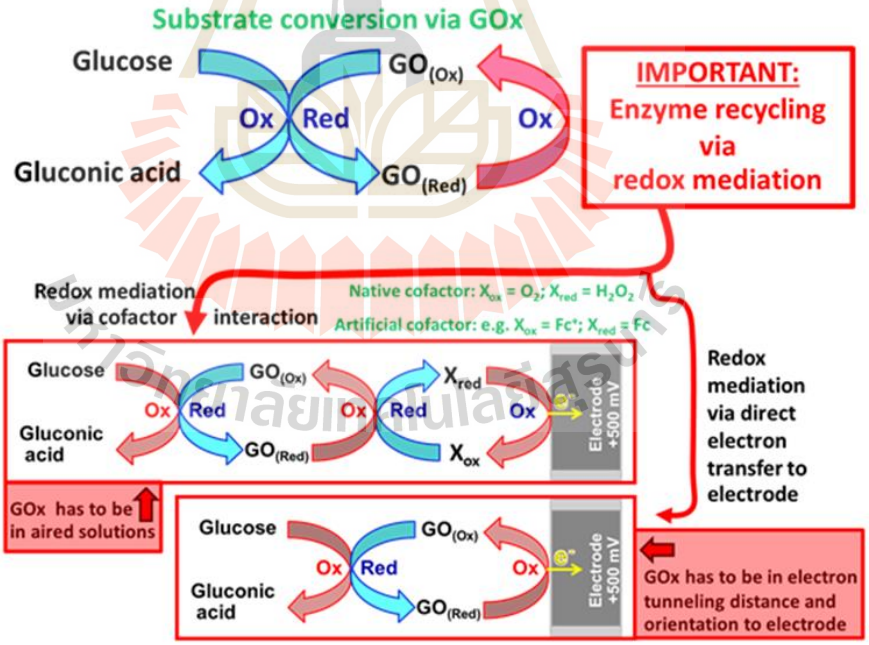

Figure 4.9 Possibilities for enzyme redox recycling in amperometric biosensors.

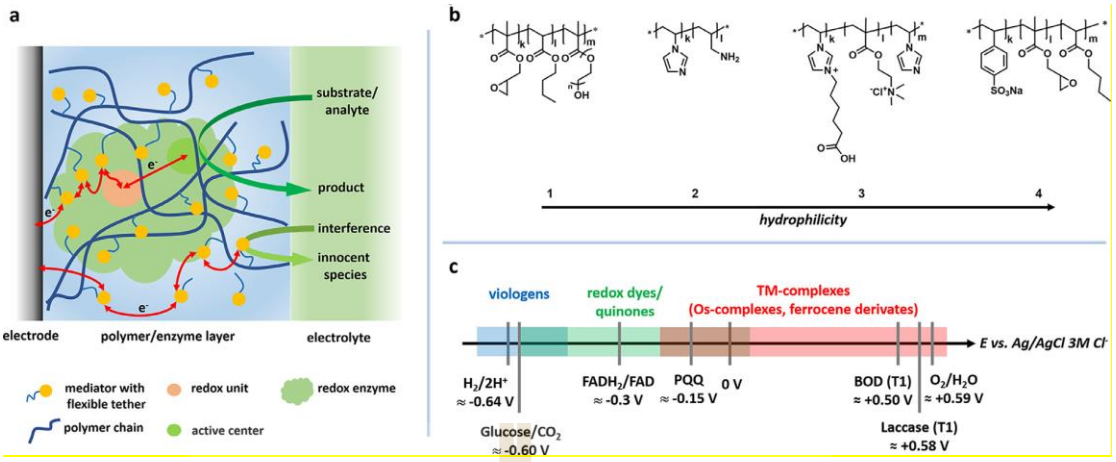

Figure 4.10 (a) Schematic of a redox polymer-based enzyme biosensor, (b) molecular structures of various functional polymer backbones ordered according to their hydrophobicity, and (c) potential scale showing the redox potential windows that can be covered by common mediator species and the redox potentials of some important biocatalysts and substrates (Ruff, 2017).

Chained redox interaction with neighbouring other synthetic redox sites delivers sequential via electron hopping received electrons to the electrode surface and generates current in proportion to substrate conversion rate. Choice of the employed mediator molecule and of the fixing polymer matrix allow an adaptation of the redox potential of the system as well as a tailoring of the hydrophobicity, ionic charge, porosity and biocompatibility of the immobilizing and recycling environment to the best needs for the survival and activity guarantee of the protein biocatalyst.

A useful type of covalently fused mediator species in redox polymers are osmium (III) complexes bearing imidazole or pyridine base ligands, since formal potentials are adjustable over a wide range through the introduction of electro-donating or electron-withdrawing groups in the ligand periphery of the metal cation (Heller, 2006;

Ruff, 2017). Another advance of Os-complexes as signaling components of redox polymers is that the ligand sphere of individual redox centers is covalent bonded to the poly backbone which prevents mediator leaching, and thus signaling reliability and long term stability (Heller and Feldman, 2008). Examples of electrodes with Os-complex modified redox polymer/enzyme modifications range from amperometric biosensors for the quantification of glucose (de Lumley-Woodyear *et al.*, 1995; Mano *et al.*, 2003; Ohara, 1995; Pinyou *et al.*, 2016; Prévoteau and Mano, 2012; Taylor *et al.*, 1995).

Since enzyme biosensors with a redox polymer design can be operated reagent-less and in the absence of sufficient supply of dissolved oxygen (even in de-aerated conditions) and the associated sensor surface modification can be automated and used with mass-produced screen printed electrode structures redox polymer biosensing became prime solution for the fabrication of tools for medical point-of-care diagnostics. Also for the target of this PhD thesis the use of a redox polymer was favoured over other alternatives for the reach of an easy to make and use biosensor tool for the detection and quantification of disease biomarker *p*-HPA.

4.4 Enzyme biosensing with allosteric enzymes

Allosteric enzyme biosensing is usually applied to molecular species that modulate the rate of substrate conversion, which in turn monitored by suitable physiochemical transducers. In 2006 year, allosteric properties have been successfully engineered in to proteins for drug design to the development of novel biosensor for therapeutics (Swain and Gierasch, 2006). In addition fundamental capacity is intrinsic to proteins, the properties confers on a proteins the ability to be allosterically modulated in order to shift substrate binding affinity (Zhu and Anslyn, 2006). In this configuration,

the onset of magnitude of the change in the signal amplitude indicate the presence or absence of analyte and its concentration, respectively. In an exploration of this principle Wollenberger and Scheller, for instance, designed an electrochemical biosensor for the analysis of glycogen phosphorylase b (GPb), a heart muscle cell constituent and primary ischemia biomarker that is regulated both through allosteric control by adenosine monophosphate (AMP) and through phosphorylation (Wollenberger and Scheller, 1993). This used a three enzyme cascade that involved functional corporation between GPb and an alkaline phosphatase (AP)/glucose oxidase (GOx) supplementation to the biosensor immobilization matrix, translating GPb action on glycogen into a quantifiable anodic hydrogen peroxide sensor current (seen in eq. 6-10). Although GPb was couple to the sensor surface indirectly through secondary (AP) and tertiary (GOx) enzyme, this early study proved that the couple of allosteric enzyme electroanalysis was feasible for both activator and enzyme substrate detection.

$$\text{Glucose}_n + P_i \longrightarrow \text{Glucose}_{n-1} + \alpha\text{-G1P} \qquad \text{(eq.6)}$$

$$\text{GPb} \underset{-\text{AMP}}{\overset{+\text{AMP}}{\rightleftharpoons}} \text{GPa} \qquad \text{(eq.7)}$$

$$\alpha\text{-G1P} \xrightarrow{\text{AP}} \alpha\text{-Glucose} + P_i \qquad \text{(eq.8)}$$

$$\alpha\text{-Glucose} \xrightleftharpoons{\text{MR}} \beta\text{-Glucose} \qquad \text{(eq.9)}$$

$$\beta\text{-Glucose} + O_2 \xrightarrow{\text{GOx}} \text{Gluconolactone} + H_2O_2 \qquad \text{(eq.10)}$$

In the case of biosensors employing allosteric redox enzyme, direct electrical connection of the protein to the signal-generating transducer interface is preferable to cascade detection schemes with multiple enzymes. Activatory and inhibitory allosteric modulation of redox enzymes have been reported for a number of systems, for example brain cytochrome P450 46A1 activation by neuroactive compounds (Mast *et al.*, 2017). 3-hydroxy-3-methyl-glutaryl coenzyme A reductase inhibition by corrole, a natural

tetrapyrole-base antioxidant (Haber *et al.*, 2013) and control of Cu-containing bacterial nitrate reductase by exogenous organo-chemical ligands (Wijma *et al.*, 2006).

However, utilization of redox enzyme allosteric behaviour for quantitative amperometric or voltammetric electroanalysis propose is, to the best of our knowledge, limited of one proof-of-principle study that used sophisticated protein engineering to convert a PQQ-glucose dehydrogenase in to an allosteric electrochemical Ca^{2+} sensor (Figure 4.11) with simple amperometric glucometer readout (Guo *et al.*, 2015).

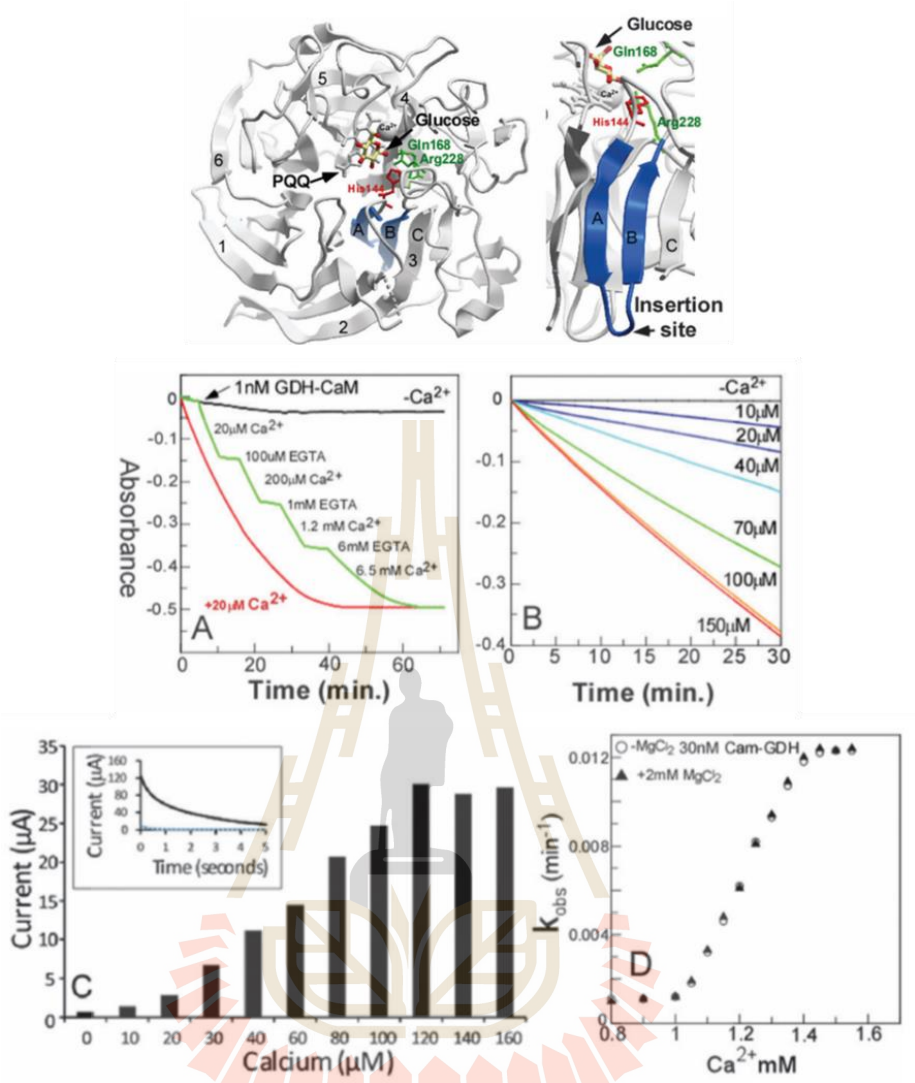

Figure 4.11 The redox enzyme PQQ-glucose dehydrogenase (on top view) as used in a Ca^{2+} selective biosensor. (A) Spectrometric analysis of PQQ-GDH activity with different concentrations of Ca^{2+}, measured at 600 nm in presence of 20 mM GOx and 1.0 nM GDH-CaM. (B) As in A, but with 3 mM GDH-CaM exposed to rising levels of Ca^{2+}. (C) Response of GDH-CaM chronoamperometric electrode to rising Ca^{2+} level, at applied potential of +0.4 V vs. imbedded Ag reference strip, inset plot, *I/t* curve of the applied potential +0.4 V at two representation Ca^{2+} concentrations (0 and 100 μM). (D) A plot the observed initial reaction rates of 3 nM GDH-CaM in the presence of 20 mM glucose and 1.1 mM of the specific Ca^{2+} chelator BAPTA (Guo *et al.*, 2015).

4.5 *p*-Hydroxyphenylacetate (*p*-HPA) as disease biomarker

The small molecule**,** *p*-HPA is a naturally occurring electroactive phenolic compound. It is slightly soluble in water and formed in humans by the metabolism (intermediates in the microbial degradation) of aromatic amino acids (Blakley, 1977; Gracin and Rasmuson, 2002; Kishore *et al.*, 1976; Pometto and Crawford, 1985). It is ingredient of numerous food intake (such as olives, cocoa beans, oats, mushrooms beer and etc.) (Nardini and Ghiselli, 2004; Papadopoulos and Boskou, 1991) and all human tissues and biofluids (Shanaiah *et al.*, 2007). As metabolic product *p*-HPA is finally excreted through the kidney pathway into urine and in there among the many indicators of healthy bodily function and a predictors of certain disease risk (Zamora-Ros *et al.*, 2014). Actual *p*-HPA metabolism is known to be influenced by factors such as gender, age, body mass index (BMI), renal function, gut microbiota activity, recent use of antibiotics and genetic trials (Williamson and Clifford, 2010; Zamora-Ros *et al.*, 2011). The detection of abnormally elevated levels of this molecule is a useful diagnostic tool for patients with gastrointestinal or toxicological symptoms (R. Chalmers *et al.*, 1979; Lord and Bralley, 2008), intestinal bacterial cell overgrowth (“Dysbiosis”) (R. Chalmers *et al.*, 1979), Neurodegenerative diseases (e.g. Major depressive disorder and Parkinson’s) (An and Gao, 2015; Fava and Kendler, 2000; Luan *et al.*, 2015), Diabetic nephropathy (Stec *et al.*, 2015) and Gastric cancer (Jung *et al.*, 2014).

Considering its role as disease marker, the quantification of *p*-HPA is of relevance for medical analysis, and straightforward detection schemes for simple on-site monitoring and point-of-care diagnostics of urinary samples are highly desirable. The routine protocols for urinary *p*-HPA detection include currently the use of gas chromatography (R. A. Chalmers *et al.*, 1976; Tanaka *et al.*, 1980) and, more recently,

applications of combined techniques such as chromatographic separation coupled to mass spectrometry (GC-MS) or electrochemical detection, ^{1}H and ^{13}C nuclear magnetic resonance (NMR) experiments and capillary electrophoresis. In particular, GC-MS was successfully employed as a screening method for varying urinary *p*-HPA in small-bowel disease and bacterial overgrowth syndrome (R. Chalmers *et al.*, 1979; Stec *et al.*, 2015) and even for the analysis of neonatal urine samples (Hoehn *et al.*, 2008). Furthermore, high resolution ^{1}H-NMR analysis was used for quantification of *p*-HPA changes in urinary metabolite profiles (Adamko *et al.*, 2007) and chemical *p*-HPA derivatization allowed the detection of the biomarker by ^{13}C-NMR spectroscopy (Shanaiah *et al.*, 2007). Finally, high performance liquid chromatography with voltammetric detection in the column eluate was used to assay *p*-HPA in cerebrospinal fluid (Kobayashi *et al.*, 1982). All these analytical approaches work well for the quantification of *p*-HPA but the requirement for time-consuming pre-treatment of samples (e.g. derivatisation of *p*-HPA (Hoffmann *et al.*, 1989; Hušek *et al.*, 2016; Kobayashi *et al.*, 1982)) and the need for rather complex analytical setups (often combinations of two different techniques) are drawbacks to the implementation of easily- established and -applied point-of-care diagnostics.

Purely electrochemical approaches to the detection of *p*-HPA or its derivatives were also considered since these compounds are electroactive and can be oxidized at suitable anodic potentials. Fast scanning cyclic voltammetry with scan rates of up to 600 V s-1 was, for instance, employed to detect *p*-HPA with a carbon fiber microelectrode in tissue samples after stimulation with dopamine (Shin *et al.*, 2015). However, the oxidation potential of *p*-HPA is rather high (≈ +1.0 V vs. a pseudo-reference Ag/AgCl wire (Shin *et al.*, 2015) which might cause interference through

electrochemical reactions of other urinary components (e.g. oxidation of ascorbic acid, paracetamol or uric acid). Moreover, fast-scan cyclic voltammetry requires special potentiostat, low-noise electrochemical setups and microelectrodes and a high level of operator expertise, rendering such applications unpractical for point-of-care diagnostics. A recent whole-cell biochemical assay with electrochemical readout involved the voltammetric detection of redox-active pyocyanine, the cellular production rate of which is controlled by *p*-HPA, enabling indirect determination of the target biomarker but with rather low sensitivity and selectivity (Dierckx *et al.*, 2015).

Table 4.2 provides a list of normal and abnormal concentrations of *p*-HPA in human urine that have been observed during the analysis of samples from a variety of people with the existing strategies for analyte determination. Normal and abnormal urinary levels of *p*-HPA ranged from 1.7 to 917.0 μmol/mmol creatinine ranges (influenced by e.g. age and gender, shows in Table 4.2). Chromatography with spectroscopic end column detection as major screening method was capable to provide quantitative results of *p*-HPA and offered high enough sensitivity and selectivity but a disadvantage was the need of expensive and bulky instrumentation. Instrument operation as well as data interpretation of this high-end instrumentations also required the expertise of a competent well-trained personnel (Woods *et al.*, 2013). Besides, the lengthy sample preparation for GC/MS/MS, and the many experimental factors that affect chromatography/spectroscopy performance (e.g. sample concentration, matrix, analyte type, buffer and purity, purity of organic solvents, purity of curtain gas and collision cell gas, run time and number of sample run) are against widespread use in local hospitals or general physician places (Ojanperä *et al.*, 2012). That's why it was considered here worth to explore and develop a detection sensor scheme base on

electrochemical platform which can better sensitivity, accessibility and portability at a much lower start-up and instrument maintenance cost.

Table 4.2 List of normal and abnormal concentrations of *p*-HPA in human urine.

Conditions	Value (µmol/mmol creatinine)	Age	Gender	Reference
Normal	6.0 (2.4 - 9.7)	Adult (>18 years old)	Both	Bouatra *et al*., 2013
Normal	(5.8 – 12.0)	Adult (>18 years old)	Female	Husek *et al*., 2016
Normal	< 185.8	Infant (0 – 1 year old)	Male	Bastug *et al*., 2014
Normal	44.6 +/- 29.0	Infant (0 – 1 year old)	Both	Pampini *et al*., 1974
Normal	9.68	Adult (>18 years old)	Male	Shaykhutdinov *et al*., 2009
Normal	917.0 +/- 341.8	New-born (0 – 30 days old)	Both	Hoehn *et al*., 2007
Normal	11.0 (3.5 – 22.0)	Adult (>18 years old)	Both	Hoffmann *et al*., 1989
Normal	7.0 (2.8 – 11.0)	Children (1 – 3 years old)	Both	Mckibbin *et al*., 1969
Normal	24.2	New-born (0 – 30 days old)	Both	Boulat *et al*., 2003
Normal	20.3	Children (1 – 13 years old)		
Normal	31.4	Adolescent (13 – 18 years old)		
Normal	24.2 (8.6 – 73.2)	New-born (0 – 30 days old)	Both	Guneral & Bachmann, 1994
Normal	36.7 (8.4 – 142.0)	Infant (0 – 1 year old)		
Normal	31.4 (9.7 – 184.4)	Children (1 – 3 years old)		
Normal	7.4 +/-4.4	Adult (>18 years old)	Both	Jones *et al*., 2005
Normal	1.68 – 101.7	Children (1 – 3 years old)	Both	Achaintre *et al*., 2016
Normal	12.0+/-1.4	Adult (>18 years old)	Male	Loke *et al*., 2009

Table 4.2 List of normal and abnormal concentrations of *p*-HPA in human urine (Continued).

Condition	Value (µmol/mmol creatinine)	Age	Gender	Reference
Normal	24.2	New-born (0 – 30 days old)	Both	Boulat *et al*., 2003
Normal	36.7	Infant (0 – 1 year old)		
Normal	24.2	New-born (0 – 30 days old)	Both	Boulat *et al*., 2003
Normal	16.3 (3.2 – 180.2)	Adolescent (13 – 18 years old)		
Normal	10.5	Adult (>18 years old)	Both	Zamora-Ros *et al* ., 2016
Fumarase deficiency	24.5	Infant (0 – 1 year old)	Male	Bas tug *et al*., 2014
Phenylketomuria	44.6 +/-66.1	Children (1 – 13 years old)	Both	Rampini *et al* ., 1974
Preterm infant	428.0 +/- 164.0	Infant (0 – 1 year old)	Both	Hoehn *et al*., 2007
Meningomyelo coele	25.0 (7.0 – 50.5)	Adult (> 18 years old)	Both	Mikibbin, 1969
Lung cancer	16.0 +/- 15.0	Not specified	Both	Wishart *et al*., 2008

CHAPTER V

RESEARCH METHODOLOGY

5.1 Chemicals and Materials

Table 5.1 List of chemicals.

Chemical	**Supplier**
p-Hydroxyphenylactetate 3-Hydroxylase, (HPAH) reductase component (C_1), (34 kDa)	Research enzyme from two collaborators from Chulalongkorn and Mahidol University Bangkok, Thailand.
Sodium phosphate monobasic, (NaH_2PO_4)	Carlo ErbaReagentiSpA, Rodano, Italy.
di-Sodium hydrogen phosphate anhydrous, (Na_2HPO_4)	Carlo ErbaReagentiSpA, Rodano, Italy.
Hydrochloric acid, (HCl), 37%	Sigma Aldrich, Kansas, USA.
Sodium hydroxide, (NaOH)	Sigma Aldrich, St.Louis-Missouri, USA.
Dimethyl sulfoxide-d_6, (DMSO-d_6), 100%	Sigma Aldrich, St.Louis-Missouri, USA.
Sodium 4-vinylbenzenesulfonate, ($C_8H_7NaO_3S$)	Sigma Aldrich, St.Louis-Missouri, USA.
Poly-(4-vinylpyridine), (PVP), 160 kDa	Sigma Aldrich, St.Louis-Missouri, USA.

Table 5.1 List of chemicals (Continued).

Chemical	Supplier
2, 2'-Azobis (2-methylpropionitrile), $(CH_3)_2C(CN)N=NC(CH_3)_2CN$, 98%	Sigma Aldrich, St.Louis-Missouri, USA.
N,N,N',N'-Tetramethyl-O-(N-succinimidyl)uronium tetrafluoroborate (TSTU)	Sigma Aldrich, St.Louis-Missouri, USA.
N,N-diisopropylethylamine (DIPEA)	Sigma Aldrich, St.Louis-Missouri, USA.
Toluene, (C_7H_8)	Acros-Organics, Geel, Belgium.
Osmium (IV) potassium chloride, (K_2OsCl_6)	Sigma Aldrich, St.Louis-Missouri, USA.
Poly (ethylene glycol) diglycidyl ether, (PEGDGA)	Sigma Aldrich, St.Louis-Missouri, USA.
2,2'-(Ethylenedioxy) bis (ethylamine), (EDEA), 98%	Fluka Chemika, Buchs, Switzerland.
Hydrogen peroxide solution, (H_2O_2), 30%	Carlo ErbaReagentiSpA, Rodano, Italy.
β-Nicotinamide adenine dinucleotide, reduced disodium salt hydrate, (β-$C_{21}H_{27}N_7O_{14}P_2$)	Acros Organics, Geel, Belgium.
Potassium chloride, (KCl)	Carlo ErbaReagentiSpA, Rodano, Italy.
2-Hydroxyphenylacetate, (*o*-$C_8H_7O_3$)	Acros Organics, Geel, Belgium.
3-Hydroxyphenylacetate, (*m*-$C_8H_7O_3$)	Acros Organics, Geel, Belgium.

Table 5.1 List of chemicals (Continued).

Chemical	Supplier
4-Hydroxyphenylacetate, (*p*-$C_8H_7O_3$)	Acros Organics, Geel, Belgium.
3-(4-Hydroxyphenyl) propionate, ($C_9H_{10}O_3$)	Acros Organics, Geel, Belgium.
4-Hydroxy-3-methoxyphenylacetate, ($C_9H_{10}O_4$)	Acros Organics, Geel, Belgium.
Ward's® Artificial Urine	Ward's science, Ontario, Canada.
Urea, ($CH4N_2O$)	Carlo ErbaReagentiSpA, Rodano, Italy.
Creatinine hydrochloride, ($C_4H_7N_3O$ HCl)	Sigma Aldrich, St.Louis-Missouri, USA.
Sodium chloride, (NaCl)	Carlo ErbaReagentiSpA, Rodano, Italy.
Potassium dihydrogenphosphate, (PH_2PO_4)	Carlo ErbaReagentiSpA, Rodano, Italy.
Sodium sulphite, (Na_2SO_3)	Carlo ErbaReagentiSpA, Rodano, Italy.
Ammonium chloride (NH_4Cl)	Carlo ErbaReagentiSpA, Rodano, Italy.

5.2 Instrumentations

- An electrochemical workstation 910 PSTAT mini (Metrohm Instruments, Herisau, Switzerland) was used the amperometric biosensor experiments with dissolved C1 enzyme in interaction with dissolved substrate NADH and effector *p*-HPA and also for screen printed electrode characterization via cyclic voltammetry.

- An electrochemical workstation CHI 1030 multichannel potentiostat (CH instruments, Inc., Austin, USA) was used for characterization of all redox polymer biosensor experiments in Bochum, at the Ruhr-University in Professor Schuhmann's laboratory and all related electrode characterization there via simple amperometry and cyclic voltammetry.
- A thermomixer type Comfort (Eppendorf Co., Ltd., Bangkok, Thailand) was used to incubate and mix buffer solutions, substrate solution and enzyme solution.
- A double beam UV-vis spectrophotometer (PG Instrument Ltd., Leicester, TX, UK) was used for a photometric enzyme assay at 458 nm, the wavelength, of FMN-absorption spectrum.
- A MicroCal PEAQ-ITC-isothermal titration calorimeter (Malvern instrument Ltd., Malvern, UK) was used for a label-free Isothermal Calorimetry (ITC) inspection of HPA/C_1 binding affinity.
- An NMR DPX200 spectrometer (Bruker, Billerica, USA) with a ^{1}H and ^{13}C resonance frequency of 200.13 MHz and 50.32 MHz was used for characterizations of redox polymer.
- A Cary 60 UV-vis spectrophotometer (Agilent, Santa Clara, USA) was used for recording the absorption spectra of redox polymers.
- An electron ionization (ET) mass spectrometric VG AutoSpec spectrometer (Jeol, Akishima, Japan) was used for inspections of redox polymers.

5.3 Electrodes

- Prussian blue modified screen printed carbon electrode (PB-SPEs) from RUSENS Ltd., Moscow, Russia.
- Commercial glassy carbon disk electrodes with 3 mm diameter (BAS® Analytical Instrument, Inc., West Lafayette, IN, USA).
- Graphite rod electrodes of 3 mm diameter from Alfa-Aesar Sigma Aldrich Spruce, USA.
- Gassy carbon electrode disks of 3 mm diameter from Alfa-Aesar Sigma Aldrich Spruce, USA.
- A counter electrode made of a platinum wire that is drilled to a spiral at the bottom.
- A reference electrode made of silver wire (Ag/AgCl/3 M KCl).

5.4 Cathodic HPAH-C1 biosensing with enzyme in solution

5.4.1 Characterization and use of PB-modified SPEs for C1/*p*-HPA electrode.

The layer of PB on the electrode surface of commercial PB-modified SPEs is very thin. Catalytic effectiveness of the PB/SPEs for H_2O_2 reduction was inspected via cyclic voltammetry in presence and absence of different concentration of H_2O_2 in supporting electrolyte containing 50 mM PBS (pH 7). The employed electrochemical configuration is shown in Figure 5.1.

Amperometric experiments for the inspection of C1/NADH interaction with and without allosteric *p*-HPA activation were performed at room temperature using

10 mL of a 50 mM PBS (pH 7) as supporting electrolyte. The amperometric current H_2O_2 current was continuously monitored at an applied potential of -100 mV (to avoid anodic interferences). A given volume of C1 and *p*-HPA stock solution were added to the stirred solution. NADH (50 μM) was later added to the stirred electrode, while recording the corresponding constant potential current vs. time.

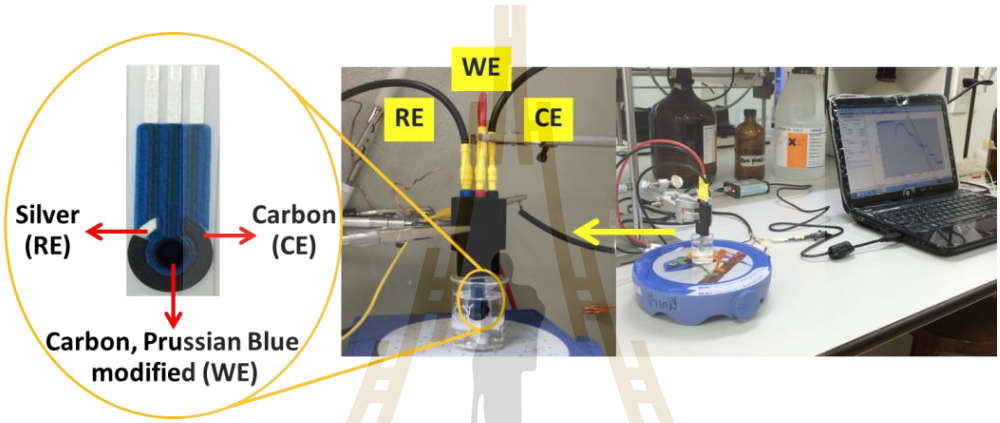

Figure 5.1 Electrochemical cell set-up with PB-SPEs connected to 910 mini potentiostat and with a laptop computer for system control and data acquisition and storage. This system was used for all electrochemical C1/*p*-HPA experiment with adjusted C1 functioning in solution.

5.4.2 ITC characterization and inspection of C1/*p*-HPA binding affinity

The instrument constantly monitors the temperature of the cells to maintain thermal equilibrium (Figure 5.2). Titrations were performed by injection of titrant (allosteric activator *p*-HPA) into the C_1 sample solution with an interval of 120 s at a constant stirring rate of 750 rpm, 25 °C (number of injections is 13). The reaction energy for C1- *p*-HPA affinity binding results in a temperature difference between sample and reference cells. A feedback system is maintaining a null temperature

different; the required energy for heat change is measured and stored. The amount of heat absorbed or heat release (as the feed-back signal) will be detected via ITC in less than 10 s. Then plotting integrated rated of the heat change against the molar ratio of C_1 /*p*-HPA, the binding stoichiometry number (*n*), the association constant (K_a), dissociation constant (K_D) and the enthalpy change (ΔH) are directly determined by fitting the data using the one site independent binding model provided by the instrument (MciroCal PEAG Analysis Software). The entropy change (ΔS) is obtain by calculation using the equation of $\Delta G = -RT\ln K_a$ and $\Delta G = \Delta H - T\Delta S$, where ΔG is free energy change, *R* is the Faraday constant and T is absolute temperature.

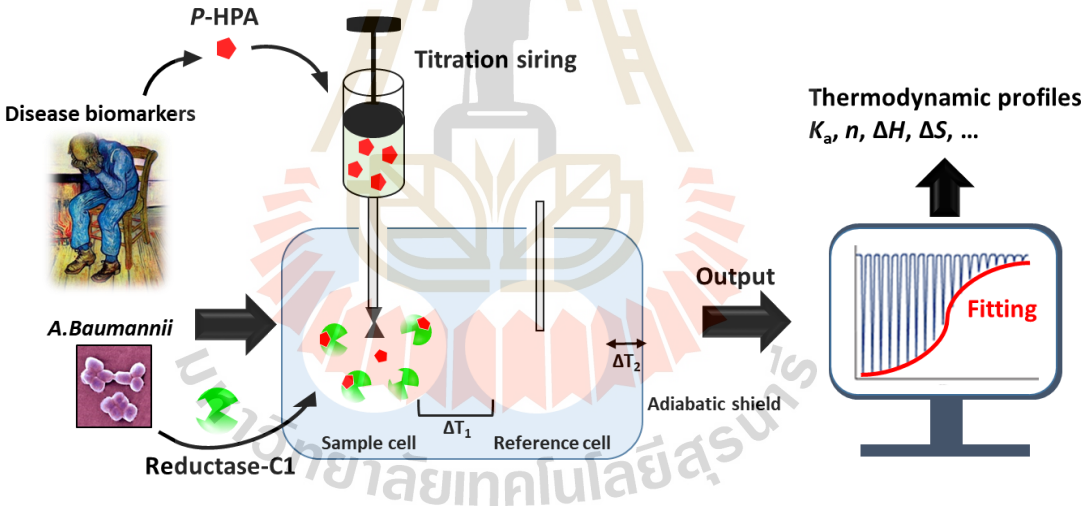

Figure 5.2 Representative diagrams of typical power compensation ITC. Major features of this type of instrument such as the reference and sample cells, syringe for adding titrant (allosteric activators), and adiabatic shield are noted in the figure. This figure shows an over simplification of how the power applied by the instrument to maintain constant temperature between the reference and sample cells is measured resulting in the instrument signal.

5.5 Amperometric HPAH-C1 biosensing with the enzyme immobilized on the electrode surface in a redox polymer assay

5.5.1 Preparation and application of PVP-Os/C1 modified graphite electrodes for the quantification of NADH

At the beginning, a commercial 3 mm-diameter PEEK-insulated glassy carbon disk working electrode was polished on a soft polishing pad soaked with alumina suspensions of 0.05 µm particle diameter, water rinsed and dried. The electrode was used for measurements of the voltammetric response of the free Os-complex; a 1 M KCl/water solution was used as supporting electrolyte. Disk-shaped working electrodes for the preparation of amperometric PVP-Os/C1 modified biosensors were home-made from 3 mm-thick graphite rods. Their cylindrical surfaces were made a smooth surface via P400 and P2500 sandpaper-polishing, respectively and the structures were then water/ethanol rinsed and dried, and tightly sealed with Teflon tape (PTFE) coating to form a 3 mm-diameter disk face exposed as active area (refer to Figure 5.3). Electrolyte for all biosensor tests was 50 mM PBS at pH 7.

All polymer and enzyme/polymer modified electrodes were prepared by a simple drop-casting process as shown in Figure 5.3, too. The preparation of the PVP-Os/C1 modified electrodes was conducted as follows: 4 µL of C1 in 50 mM PBS, pH 7 (36.4 mg mL^{-1}), 4 µL of PEGDGE in water (11.40 mg mL^{-1}), 5 µL of PVP-Os in water (46.5 mg mL^{-1}) and 7 µL of PBS (50 mM, pH 7), giving a mass ratio of 3:1:5 of C1/PEGDGE/PVP-Os, were thoroughly mixed and 5 µL of this solution (with overall concentrations of 12 mg mL^{-1} polymer, 12.28 mg mL^{-1} crosslinker and 7.3 mg mL^{-1} enzyme) were drop-casted onto graphite disk electrode and allowed to dry. For

electrode prepared without crosslinker PEGDGE, 5 μL of PVP-Os (46.5 mg mL^{-1} in water), 4 μL of C1 (36.4 mg mL^{-1} in PBS) and 11 μL of PBS (50 mM, pH 7) were mixed and 5 μL of this solution (with 12 mg mL^{-1} polymer and 7.3 mg mL^{-1} enzyme) was drop-casted onto the graphite electrode. For the preparation of the P(SS-GMA-BA)-Os/C1 electrodes, 7.5 μL of P(SS-GMA-BA)-Os in water (16 mf mL^{-1}), 4 μL of C1 in PBS (36.4 mg mL^{-1}) and 8.5 μL of BPS (50 mM, pH 7) were mixed and 5 μL of this solution (with overall concentrations of 6 mg mL^{-1} polymer and 7.3 mg mL^{-1} enzyme) was drop-casted onto graphite electrode. The modified electrodes were dried 2 h under ambient conditions and then stored at 4°C until use.

Cyclic voltammetric experiments for graphite electrode modified with polymer and enzyme/polymer, characterizations were performed at room temperature using 4 mL of 50 mM PBS (pH 7) containing 2.5 mM and 5.0 mM of NADH; scan range for the potential was -0.4 to 0.2 V at scan rate 2 mV s^{-1} in the presence and absence of allosteric activator *p*-HPA.

Amperometric experiments for C1/NADH interactions with allosteric activation via *p*-HPA exposure and a redox polymer readout of substrate conversion were performed at room temperature using a 4 mL of 50 mM PBS (pH 7) by monitoring the “Os (II/III)” current continuously at an applied potential of -100 mV vs. Ag/AgCl/3 M KCl reference electrode. Initially, high concentration (500 μM) of *p*-HPA was added to the stirred electrolyte solution. Then NADH was later added to the stirred electrodes, while recording constant potential current vs. time curves. All measuring solutions were thoroughly deoxygenated by bubbling Ar through the solution for at least 30 min.

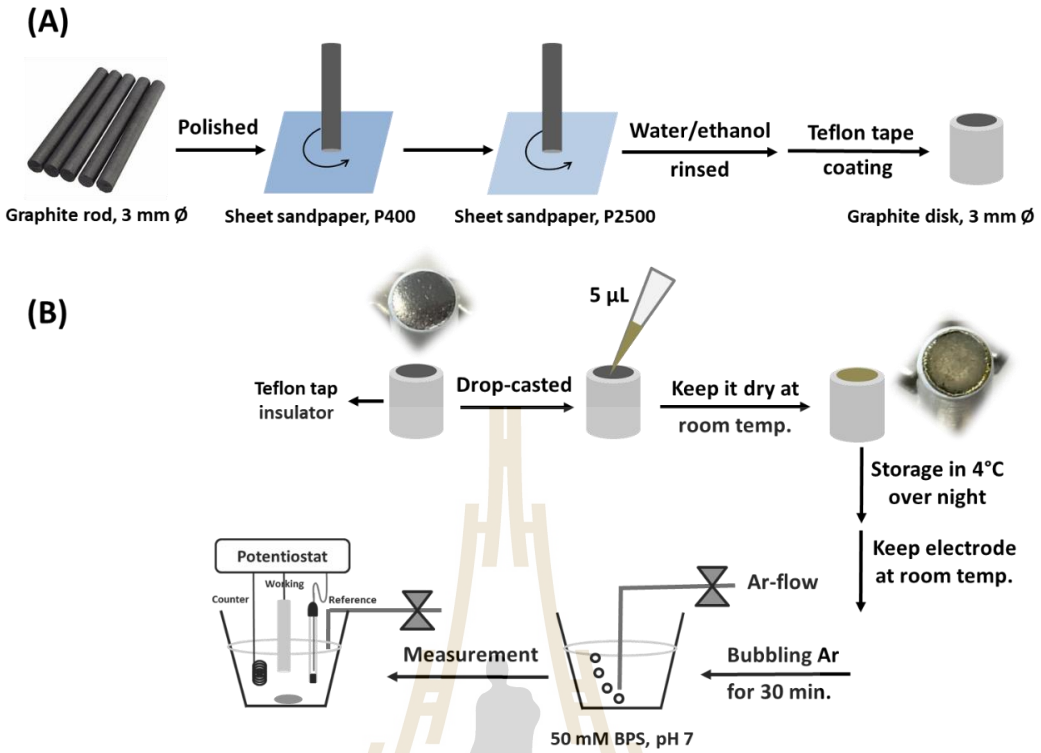

Figure 5.3 Schematic diagrams of (A) the home-made from 3 mm-thick graphite rods that had their cylindrical stem were polished with different grid size of sandpaper and tightly sealed into a Teflon tape coating then water/ethanol rinsed and dried 3 mm-diameter disk face exposed as active area. (B) The PEGDGE/PVP-Os/C1 modified graphite electrode for the NADH biosensor assay.

5.5.2 Preparation and application of P(SS-GMA-BA)-Os/C1 modified glassy carbon electrode and application for urinary *p*-HPA biomarker detection

Before electrode modification, a commercial glassy carbon electrode (3mm, Ø) was polished on a soft polishing pad soaked with alumina suspension of 0.05 µm particle diameter then water rinsed and dry, respectively. The polymer/enzyme modified electrodes was prepared by the standard drop-casting process as seen in Figure 5.4. The preparation of the P(SS-GMA-BA)-Os/C1 modified electrode was conducted

as the following: 6 µL of C1 in 50 mM PBS, pH 7 (36.4 mg mL^{-1}), 5 µL of EDEA in water (10.12 mg mL^{-1}) and 9 µL of P(SS-GMA-BA)-Os (16 mg mL^{-1}), give a mass ratio of 4:1:3 of C1/EDEA/P(SS-GMA-BA)-Os, were thoroughly mixed and 5 µL of this solution (with overall concentration of 10.95 mg mL^{-1} C1, 2.5 mg mL^{-1} EDEA and 7.2 mg mL^{-1} P(SS-GMA-BA)-Os) was drop-casted onto glassy carbon electrode. The modified electrodes were dried 2 h under ambient conditions and then stored at 4 °C until use.

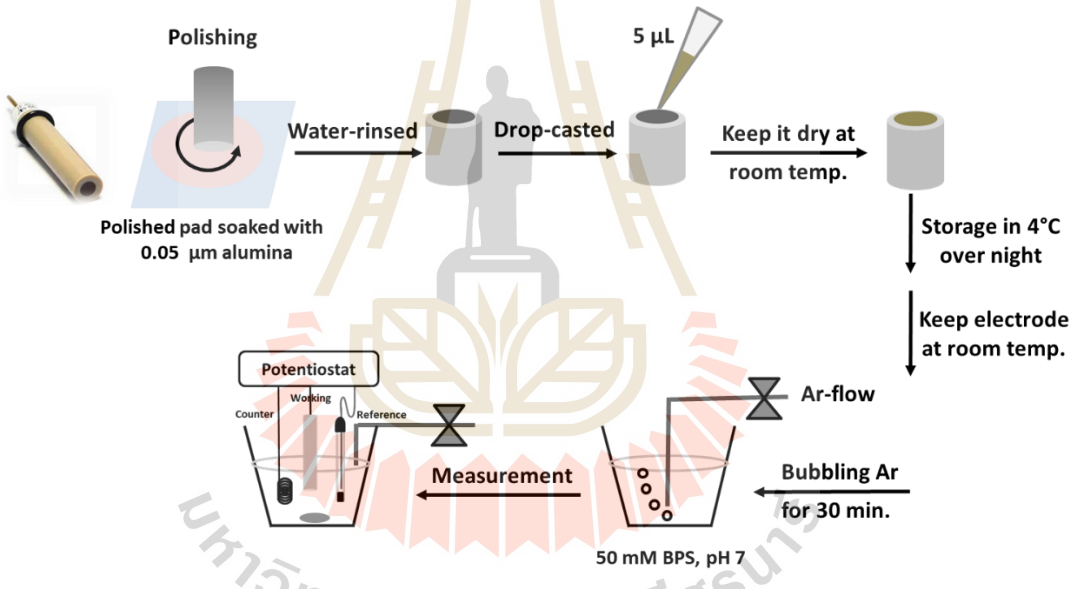

Figure 5.4 Schematic diagrams of the glassy carbon disk electrode (3 mm of diameter) that was polished with suspended 0.05 µm alumina then water rinsed and the EDEA/P(SS-GMA-BA)-Os/C1 modified glassy carbon electrode for the *p*-HPA biosensor assay.

Amperometric experiments for concentration dependence of *p*-HPA-induced allosteric amplification of C1/NADH activity, visualization and quantification

were performed at room temperature using a 5 mL of 50 mM PBS (pH 7) by monitoring the current continuously at an applied potential of -100 mV vs. Ag/AgCl/3 M KCl reference electrode. Initially, 500 µM of NADH was added to the stirred electrolyte solution. Then different concentrations of *p*-HPA was later added step by step to the stirred electrodes, while recording at constant detection potential the current vs. time curves. All measuring solutions were thoroughly deoxygenated by bubbling Ar through the solution for at least 30 min.

CHAPTER VI

RESULTES AND DISCUSSION

6.1 Electrochemical visualization and valuation of enzyme allostery with pre-dissolved HPAH-C1

6.1.1 Amperometric characterization and use of PB-SPEs for C1/*p*-HPA electrode

Aimed at was a sensitive H_2O_2 amperometry as non-biochemical assay for the electrochemical visualization and valuation of enzyme allostery, with allosteric reductase-C1 component from HPAH used as a model biocatalyst. The principle of the desired C1 activity assay is schematically exposed in Figure 6.1. Enzymatically produced H_2O_2 is in the C1/NADH/*p*-HAP system not the only electrochemical oxidizable substance as the substrate of C1, NADH, and the allosteric C1 activator, *p*-HPA, also can undergo oxidations at anodic working electrode potentials for sufficient H_2O_2 detection. The correct choice of the applied potential at the electrode is thus fundamental to avoid anodic NADH and *p*-HPA disturbances to the analytically relevant H_2O_2 current. Best is actually a cathodic instead of anodic H_2O_2 detection as NADH and *p*-HPA are only liable to electro-oxidation but not reduction, while H_2O_2 can either be reduced or oxidized at working electrodes, depending on the applied polarization. So that, the H_2O_2 current measurements are free of a signal contribution from interfering species.

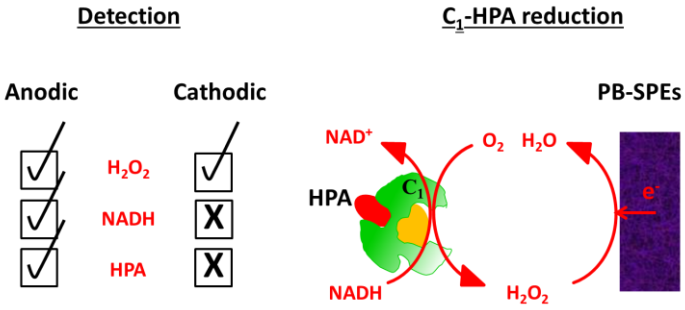

Figure 6.1 Schematic illustration of the electrochemical assay for reductase-C1 activity at applied potential of -100 mV vs. Ag/AgCl reference electrode.

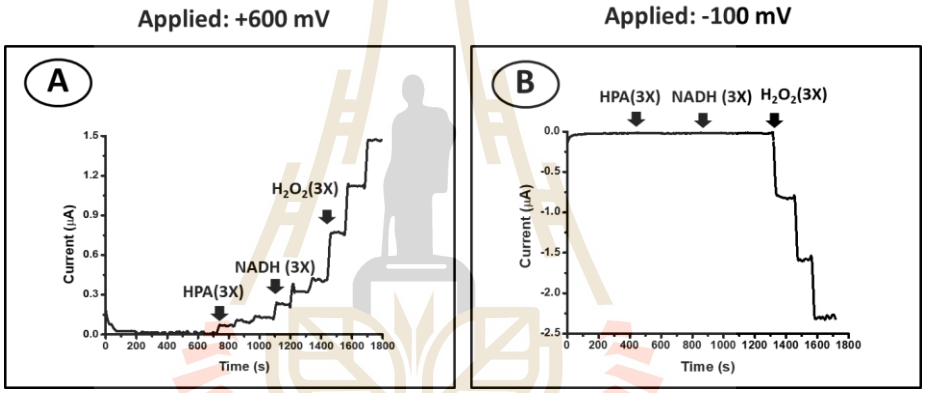

Figure 6.2 Chronoamperograms at a Prussian blue-modified screen printed electrode in response to additions of (1) allosteric C1 activator *p*-HPA, (2) C1 substrate NADH and (3) H_2O_2 at (A) a working electrode potential of +600 mV vs. reference electrode and (B) a working electrode potential of -100 mV vs. reference electrode.

The current traces in Figure 6.2 provide nice evidence for the phenomena of interference influence at anodic H_2O_2 detection potential, +600 mV (Figure 6.2A) and reach of interference-free H_2O_2 measurement at cathodic (-100 mV) operation of PB-SPEs (Figure 6.2B). Optimal since interference-free working potential was thus -100 mV since here current contributions from C1 substrate-NADH and

allosteric activator *p*-HPA are effectively compressed.

6.1.2 Valuation of cathodic H_2O_2 amperometry at PB-SPEs

The characteristic redox properties of PB on PB-SPEs were expected to facilitate a good cathodic detection of H_2O_2, at, for instance, a moderately negative potential of -100 mV vs Ag/AgCl reference electrode. To demonstrate this capability, amperometry trials were carried out in PBS (50 mM, pH 7) in a stirred conventional beaker-type three-electrode electrochemical cell.

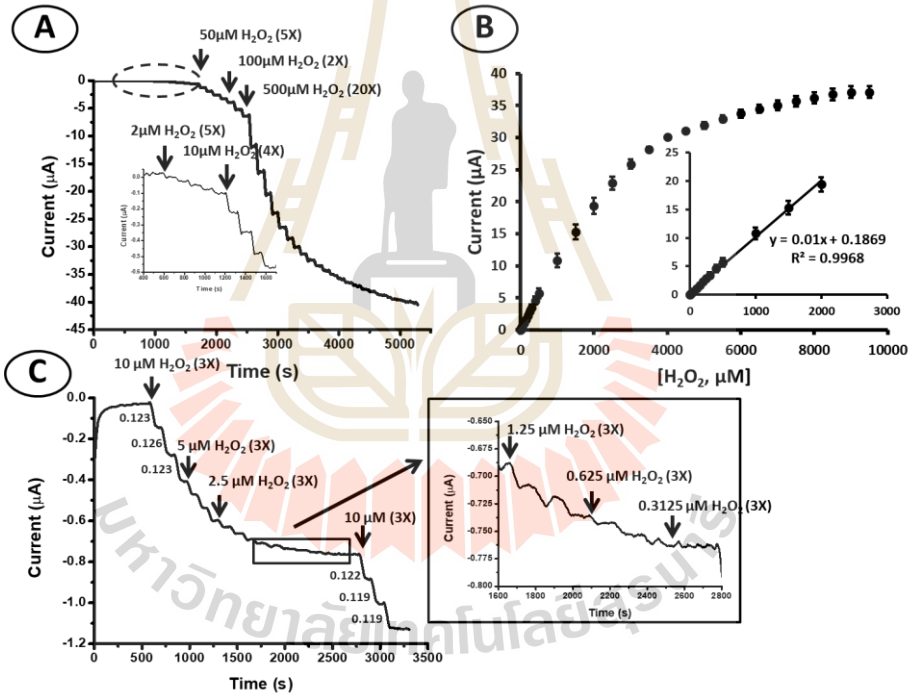

Figure 6.3 Representative cathodic H_2O_2 amperometric measurement at constant potential of -100 mV vs. RE. (A) Chronoamperogram for gradually increasing H_2O_2; the inset is a zoom into the region of the lowest concentration of H_2O_2. (B) Background subtracted H_2O_2 reduction currents vs. H_2O_2 concentrations, valid or the data in (A). (C) Demonstration of the detection limit of 0.625 μM.

Figure 6.3A shows a typical amperometric response of a PB-SPE to sequential addition of a small aliquots of H_2O_2 stock solution to continuously stirred supporting electrolyte. The chronoamperogram, actually an *I* vs. *t* curve, visualizes in step-like pattern the increase in cathodic H_2O_2 current as the analyte level is raised; the inset of Figure 4.3A is the response for incremental H_2O_2 elevations as small as 2 and 10 µM, respectively. The calibration curve for the H_2O_2 amperometry of Figure 6.3A is shown in Figure 6.3B. Obtained was a well-pronounced concentration dependence with, as the inset of the graph forwards, a linearity from 1.0 up to 2,000 µM. The practical detection limit was about 0.625 µM (Figure 6.3C).

6.1.3 Amperometric H_2O_2 quantification on cathodic PB-SPEs

The performance of PB-SPEs for amperometric assessments of sample H_2O_2 levels in the common standard addition mode was investigated with the aim to reveal the sample recovery of H_2O_2 quantification of known analyte concentration in spiked supporting electrolyte.

Figure 6.4A exposes for a typical amperometric quantification of H_2O_2 in a model sample by the standard addition method the acquired amperometric current trace with the plateaus that refer to buffer alone, then to the known sample supplementation with 100 µL rise in solution, and finally for the three standard additions of H_2O_2. Figure 6.4B is the constructed standard addition curve for the data in Figure 6.4A. The H_2O_2 levels in the samples were determined graphically via linear regression line extrapolation to zero current or via calculation based on the regression line equation. Triplicate repetitions of an assessment of a 100 µM adjusted H_2O_2 level revealed a % recovery of 109.00 ± 1.68 (refer also to Table 6.1). With this reasonable performance the methodology was further applied for the quantitative analysis of the

H_2O_2 generation by action of C1 and NADH, in absence and presence of allosteric effector *p*-HPA.

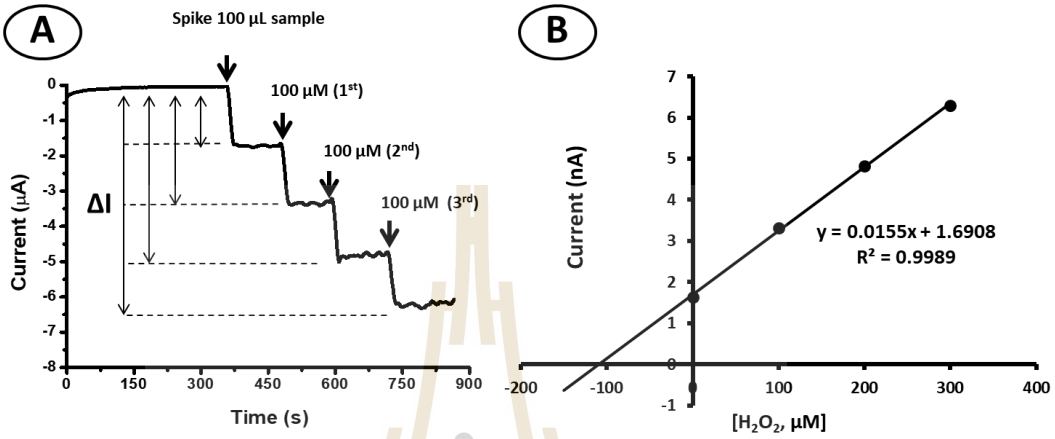

Figure 6.4 Amperometric quantification of H_2O_2 in a model sample by the standard addition method. (A) Typical amperometric *I-t* curve, initially recorded in buffer alone, then after addition of known volume of a sample with 100 µL of H_2O_2 and solutions with additional H_2O_2 supplementations. (B) The construction of the standard addition curve and the linear regression plot for the data in (A).

6.1.4 NADH amperometry at PB-SPEs with allosteric-C1 activation

Knowing about their quality for H_2O_2 analysis PB-SPEs were applied for the determination of the enzymic reaction between C1 and NADH in absence and presence of a high level of allosteric activator *p*-HPA, which in either case delivers H_2O_2 as product into the solution where the biocatalysis takes place, to lesser or larger extent. C1 was dissolved in measuring buffer, a 50 µM NADH was added and amperograms at immersed PB-SPEs were recorded from just before substrate addition till the rise in anodic peroxide current came to end and a current plateau was reached.

A set of typical cathodic current recordings of such a trial aimed at electrochemical allostery visualization is displayed in Figure 6.5A. Reproducibly, the observed rise in H_2O_2 levels was much faster in the presence of allosteric activator *p*-HPA, which is an identification of the accelerating *p*-HPA impact on the biocatalytic reaction of C1/NADH and the associated higher rate of H_2O_2 production through biocatalytic NADH to NAD^+ conversion. The speed of the generation of H_2O_2 got actually 11.5-fold larger by full allosteric activation, at 100 μM of *p*-HPA.

For different NADH supplementations revealed was a marked increase in the final plateau level but times for the reach of the plateau currents were obviously longer for larger substrate supplementations (data not shown). The corresponding calibration curve is shown in Figure 6.5B and confirmed a linearity (inset) from 5 to 600 μM. Figure 6.5C is representative H_2O_2 chronoamperogram from a standard addition trial that aimed at NADH determination through electrochemical inspection with a C1 reductase that was heavily stimulated by 100 μM of *p*-HPA. Initially, 50 μM of NADH was adjusted in the PBS (50 mM, pH 7) and the solution was then further supplemented with three consecutive aliquots of standard solution of NADH. Figure 4.5D is the constructed standard addition curve for the data in Figure 6.5C. The adjusted NADH 'sample' levels were again determined graphically via linear regression line extrapolation to zero current or via calculation based on the regression line equation. Triplicate repetitions of an assessment of the 50 and a 5 μM adjusted NADH level revealed a passable % recovery of 109.16 ± 2.57 and 95.53 ± 6.00, respectively (refer also to Table 6.1).

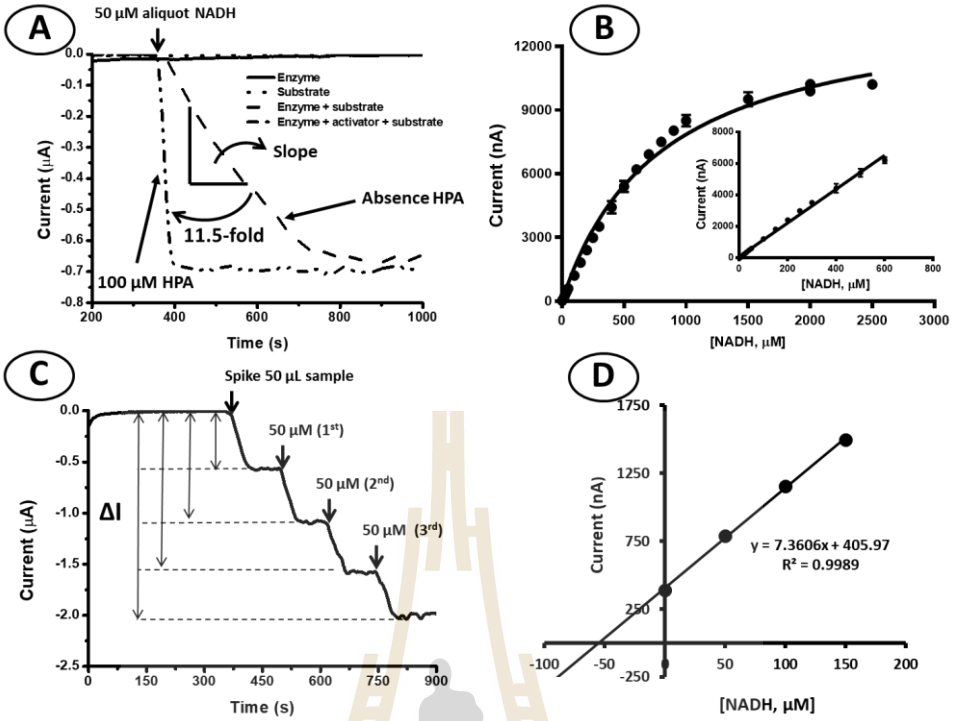

Figure 6.5 Amperometric *I-t* curve that monitors the reaction of C1/NADH via cathodic H_2O_2 detection at -100 mV vs. reference for a Prussian blue-modified screen printed electrode. (A) The current trace in the absence and presence of high, 100 µM, *p*-HPA as allosteric activator. (B) Calibration plot derived from the mean values of a triplicate replication of NADH measurements as shown (A) but for increasing adjustments of NADH solution levels. (C) NADH determination in the standard addition mode; amperometric plateaus were determined for buffer alone, buffer spiked with 50 µM (sample), and buffer plus sample and additional NADH supplementations (standard additions). (D) The construction of the standard addition curve and the linear regression plot for the data in (C). Data points are the means and error bars the standard deviation for three sample measurements.

Table 6.1 Application of C1-based enzyme biosensing at Prussian blue-modified screen printed electrodes for the quantification of H_2O_2 and NADH in model sample solutions of known levels: Demonstration of the % recovery performance.

Analyte	**Adjusted**	**Found**	**% Recovery**
*H_2O_2, µM (n=3)	100.00	109.00 ± 1.68	109.00 ± 1.68
**NADH, µM (n = 3)	50.00	54.58 ± 0.86	109.16 ± 2.57
	5.00	4.78 ± 0.30	95.53 ± 6.00

It was known from the published biochemical C1 studies that not only *p*-HPA but also other structurally similar chemical compounds could bind to the its allosteric site and trigger allosteric activation of the enzyme's NADH conversion rates, though not to same extent. To check whether biosensing with dissolved C1 could expose the compound specificity of allosteric activation electrochemical inspection of C1/NADH interaction was carried under the rule of the aromatic compounds that are shown together with *p*-HPA in Figure 6.6. The actual C1 turnover rates were examined at room temperature by amperometric H_2O_2 electroanalysis at PB-modified SPEs, while Isothermal Calorimetry (ITC) measurements with the set of phenol derivatives was done to get information about the quality of their binding affinity to C1.

Figure 6.7 present the amperometric *I-t* curves that visualize the time course of H_2O_2 due to the reaction of C1 with NADH, however, without any and for the reaction in the presence of the different allosteric activator analogues of Figure 6.6, including *p*-HPA. All tested compounds apparently could bind to the allosteric site of C1 and amplified C1/NADH turnover rates, but, as expected, with different power. The *o*-HPA, for example, with the hydroxyl group in the *ortho*-position to the acidic

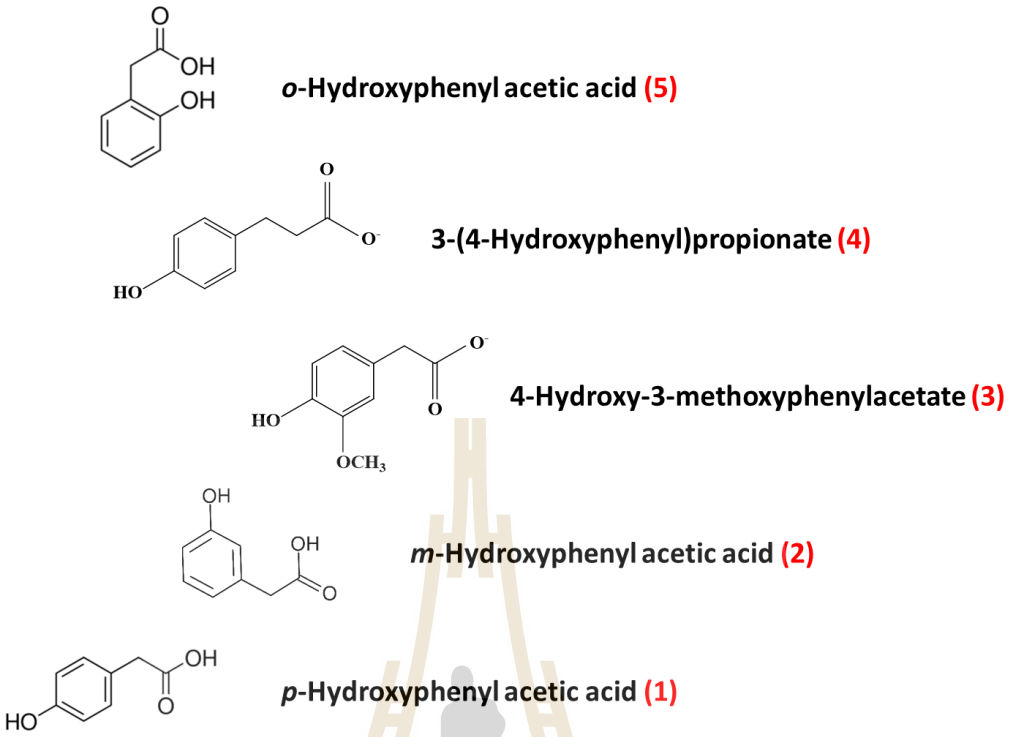

Figure 6.6 Four phenolic compounds with similar chemical structure as *p*-HPA that – to more or less extent – have the power to act as allosteric activators of C1 and amplifiers of C1/NADH turnover rates.

aliphatic side chain, showed lowest C1/NADH activity (curve slope as term proportional to the rate of H_2O_2 production and thus enzyme activity was 1.23 nA s^{-1} while *p*-HPA created the best allosteric activation (curve slope as term proportional to the rate of H_2O_2 production and thus enzyme activity was 13.5 nA s^{-1}). The ranking of the allosteric power of the tested allosteric phenol compounds, as visualized by the electrochemical trial outcome in Figure 6.7 was (differentiated by their curve slopes, sorted best to worse):

p-HPA→m-HPA→4-Hydroxy-3-methoxyphenylaceate→3-(4-Hydroxyphenyl) propionate→*o*-HPA

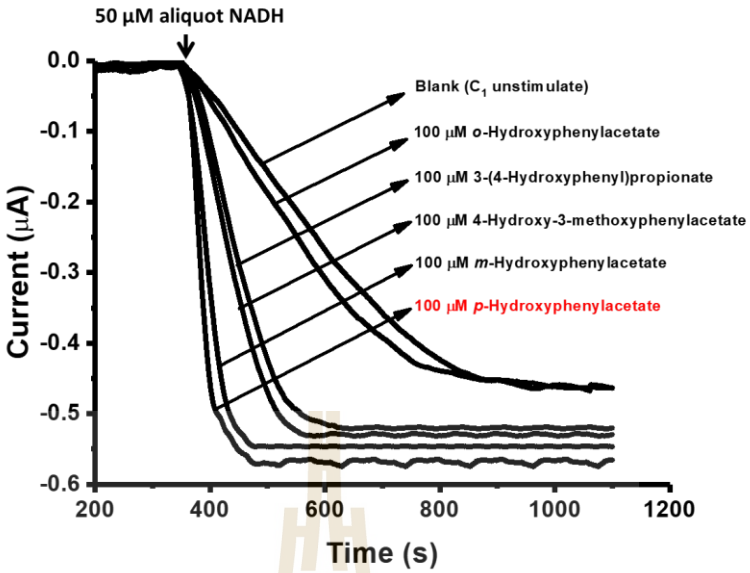

Figure 6.7 Amperometric *I-t* curves for the interactions of the C1 (1.0 µM)/NADH (50 µM) with four different allosteric activators analogues. Traces have been monitored at cathodic H_2O_2 detection potential (-100 mV vs. RE) with PB-modified SPEs.

This order was exactly in line with the prediction that could be made based on the early biochemical C1 studies by Chaiyen, Sucharitakul and coworkers and own affinity binding studies with C1 and the effector set via ITC experiment (see below). Figure 6.8 is a very simple representation of the binding process between C1 and an allosteric activator molecule. A linear arrangement of the phenolic OH^- and the second side chain in the *ortho* isomer seems to be in favor of effective molecular interaction and strong allosteric activation power while the placement of the side group in *meta* and *ortho* positions of the aromatic ring obviously causes sterical hindrance and lesser acceleration of enzymatic consumption of substrate.

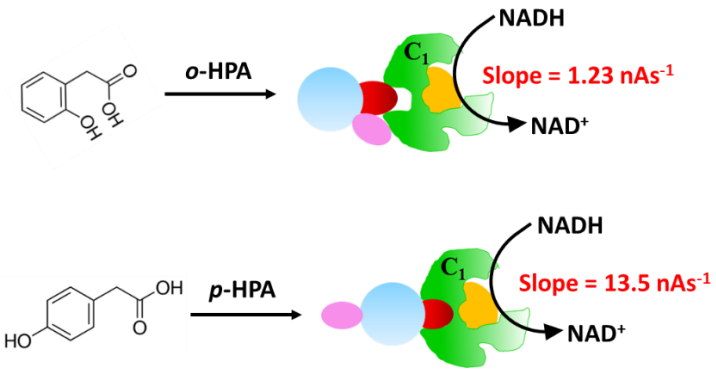

Figure 6.8 Simplified schematic comparing H_2O_2 production rates of C1 in presence of stimulating phenols with their additional aliphatic COOH group in *ortho* or *para* position. *Para* arrangement favors allosteric impact while the *ortho* placement is less successful.

6.1.5 ITC characterization and inspection of C1/*p*-HPA binding affinity

As mentioned in Section V., ITC is used for measuring the heat that is associated with molecular interactions and extract from determined heat values important thermodynamic parameters for the binding of e.g. small molecules to ligand sites on larger (bio-) macromolecules. The heat release or uptake due to exothermic or endothermic molecule contacting may involve temperature changes of only fractions of a degree but the variations are highly specific, universal and detected by the very sensitive ITC calorimeter. Obtained ITC data provides insights in the strength of the binding affinity and the mechanism of binding. Looked at here by ITC was the allosteric interaction between the C1 reductase binding and the five phenolic compounds of the electrochemical tests in the previous section.

Routinely, all ITC experiments were carried out at 25 °C, the sample

cell was filled C1 solution (100 μM) in PBS (50 mM, pH 7). The ligand (e.g. *p*-HPA) was prepared to a concentration of 1.5 mM in the same PBS (50 mM. pH 7). The titration was then performed at constant stirring rate of 750 rpm by injecting small aliquots of ligand solution (here: 3.2 μL each) into the sample cell with 150 s (1^{st} injection) and 120 s (2^{nd} to 13^{th} injections) delay between individual injections.

Shown in Figure 6.9A is a representative ITC recording with the typical signal pattern in the measured differential heat change vs. time plots ligand that refer to the thermodynamic nature of the prime effector *p*-HPA to C1 molecular bonding process. Each injection of ligand into the sample cell gave rise to a heat of reaction, caused by the formation of the complexes between effector and the allosteric enzyme. The magnitude of the heat changes decreased from one injection of effector to the next, because less and less *p*-HPA molecules were able to perform complex formation due to gradual consumption of binding partners in course of the titration. The binding experiments and the acquired calorimetric traces served to measure association constant for the *p*-HPA/C1 complex formation, as well as reveal the stoichiometry for their reaction with each other and the value of the binding enthalpy (ΔH). The equilibrium association constant (K_a), equal to the reciprocal of the equilibrium dissociation constant K_D, the binding stoichiometry number (n), the entropy change (ΔS) and Gibbs free energy ($\Delta°G$) terms became available as thermodynamic parameters when plotting the measured ΔH vs. molar ratio of binding partners and let the customized analysis software of the ITC instrument appropriately fit the resulting binding isotherms (refer to Figure 6.9B). All observed thermodynamic values for the five phenol compounds of interest are summarized in Table 6.2.

Visualization on the thermodynamic parameters in form of a binding signature plot (inset of Figure 4.9B) makes it easy to identify how the enthalpic component dominates the sign of Δ°*G* and thus the thermodynamic probability of the binding process. For the couple shown, that is *p*-HPA/C1, the complex formation is strongly driven by enthalpy change (ΔH = - 89.2 ± 1.89 kJ mol^{-1}). Enthalpic support of affinity reactions is typically originating from hydrogen bonding and Van der Waals interactions between structural elements of the binding partners. The distinct Δ*H*/*T*Δ*S*/Δ*G* fingerprint of the *p*-HPA/C1 couple may thus indicated that enthalpic polar/hydrophilic forces are governing binding and the bonding pressure in the allosteric affinity site of C1.

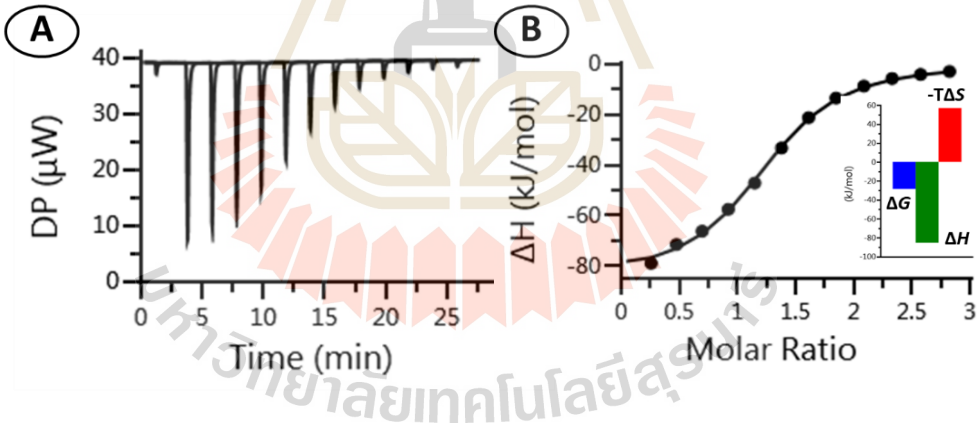

Figure 6.9 (A) Calorimetric traces (heat flow) as observed upon injecting at 25 °C 3.2 µL ligand solution (1.5 mM of *p*-HPA, $V_{tot.}$ = 38.80 µL, into the sample cell that filled with C1 solution (100 µM, V = 280 µL). The heat of reaction, Δ*H*, is obtained as the integration of the calorimetric traces. (B) The Wiseman plot resembles the theoretical fit of the binding isotherm with acquired fit parameters were K_D, Δ*H*, Δ°*G*, -TΔ*S* and 1:1 stoichiometry. The binding signature plot (inset) of the *p*-HPA and C1.

In analogy to the ITC trial with *p*-HPA the thermodynamics of the other four allosteric activators of C1 (as displayed before in Figure 6.6) with different chemical structures compared to *p*-HPA have been inspected via calorimetric measurements. Shown in the left panels of Figure 6.10A-E are all acquired ITC recordings with the measured differential heat changes plotted vs. time. As expected, the injections of the different phenolic compounds into the sample cell containing C1 gave rise to exothermic heat of reactions, cause by the formation of inclusion complexes between activators and C1 and again they decreased injection by injection of activators, as observed in the initial *p*-HPA trial. Curve data was transferred into thermodynamic parameters by fitting the binding isotherm (right panels, Figure 4.10). The summary of all of thermodynamic values is provided in Table 6.1.

Figure 6.11 shows the set of heat integrated isotherms for five tested systems while Table 6.2 summarized all important thermodynamic parameters of the set. All compounds apparently could bind to the allosteric active site-C1, however, with different power. The affinity strength from ITC testing compared well to the one obtained in the earlier amperometric analysis with PB-SPEs. *o*-HPA, with it hydroxyl group in *ortho*-position, showed in the ITC trial the weakest affinity to C1 (K_D = 98.8 ± 36.6 μM) while *p*-HPA related to strongest binding (K_D = 10.2 ± 1.2 μM). The other compounds ranked with respect to C1 binding strength in between the the ortho and para derivatives, in the same sequence as revealed electrochemically. The outcome from ITC characterization can indicated that the C1 enzyme interacts with its phenolic effectors in favorable way with a negative reaction enthalpy (= integrated heat release) but hampered by a positive reaction entropy. However, the Gibbs-free energy of reaction is negative throughout, which means the binding between allosteric activators

and C1 happens spontaneously. The stoichiometry between allosteric site-C1 and allosteric activator was revealed as 1:1, one C1 unit binds one phenolic molecule for activity boosting.

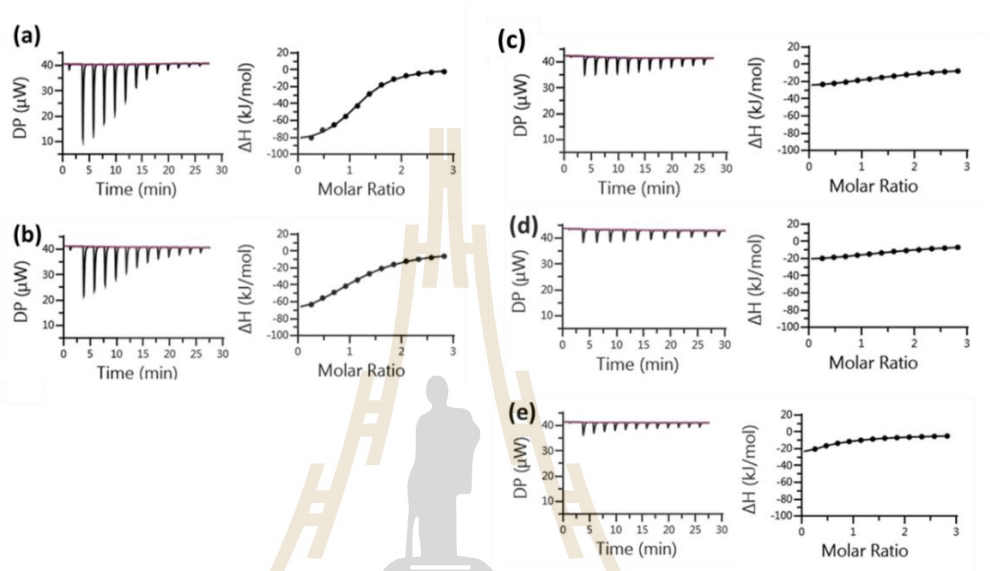

Figure 6.10 Calorimetric traces (heat flow) observed upon injecting 3.2 µL of 1.5 mM ligand solutions for (a) *p*-HPA; (b) *m*-HPA; (c) 3-(4-Hydroxyphenyl) propionate; (d) 4-Hydroxy-3-methoxyphenylacetate and (e) *o*-HPA into the sample cell (V = 38.8 µL) containing C1 solution (100 µM). Experiments were performed at 25 °C, heat of reactions were obtained from the integration of the calorimetric traces. The Wiseman plot resembles the theoretical fit of the binding isotherm. The acquired fit parameters were K_D, ΔH, ΔG, $-T\Delta S$ and 1:1 stoichiometry (n), respectively.

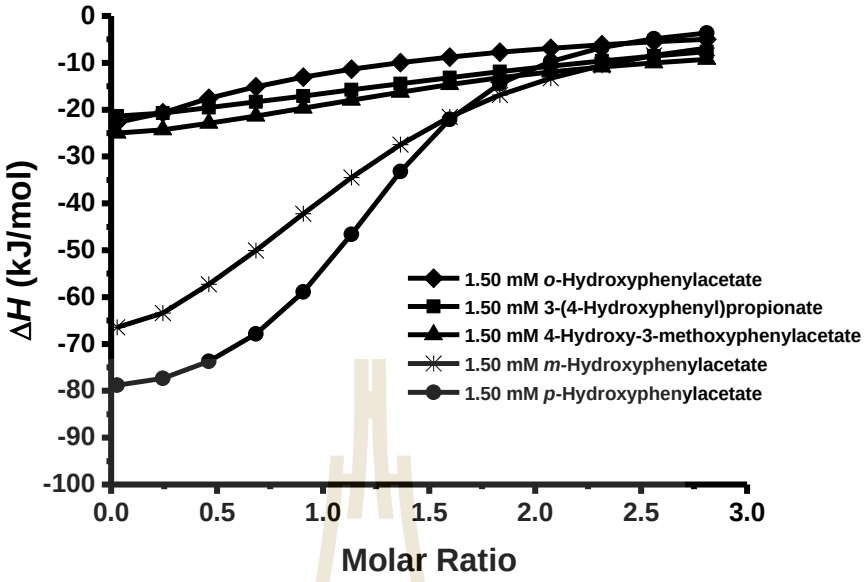

Figure 6.11 Display of the heat integrated isotherm of five tested allosteric activators of the C1 reductase. The corresponding affinity reactions took place in PBS (50 mM, pH 7) at 25 °C; obtained raw data was analyzed with the software of the ITC setup to extract the relevant thermodynamic values (K_D, ΔH, ΔG, -TΔS and stoichiometry (n)).

Table 6.2 Observed thermodynamic parameters for the interactions of five phenolic effectors of C1 reductase. Presented values are the means and standard deviations of triplicate repetitions of measurements (n = 3).

Activator analogues	Conc. (mM)	K_D (µM)	ΔH (kJ/mol)	ΔG (kJ/mol)	$-T\Delta S$ (kJ/mol)	N (sites)
1. *o*-Hydroxyphenylacetate	1.50	98.80 ± 36.60	-54.90 ± 22.00	-22.90	32.10	-
2. 3-(4-Hydroxyphenyl) propionate	1.50	84.90 ± 23.60	-32.50 ± 4.73	-23.30	9.24	-
3. 4-Hydroxy-3-methoxy phenylacetate	1.50	50.70 ± 3.51	-26.10 ± 0.72	-24.50	1.58	0.86 ± 0.60
4. *m*-Hydroxyphenylacetate	1.50	31.40 ± 0.83	-83.30 ± 0.75	-25.70	56.50	1.12 ± 0.20
5. *p*-Hydroxyphenylacetate	1.50	10.22 ± 1.21	-82.20 ± 1.89	-28.40	60.80	1.22 ± 0.12

On top of the enthalpy, entropy and Gibbs free energy, the heat capacity (ΔCp) is another major thermodynamic quantity describing the thermodynamics of reaction in general and of biochemical processes of proteins in particular (Prabhu and Sharp, 2005). Here, we have to use the ITC experiments with the C1/*p*-HPA couple at increasing temperatures within the range of 10 to 30 °C for assessments of ΔCp values for the *p*-HPA /C1 affinity reaction. The top panels in Figure 6.12 represent the raw data for selected temperatures while the bottom panel shows the associated heat integrated isotherms, after correction via subtraction of appropriate blank experiments and then fitting with non-linear regression and computed values ΔH, $-T\Delta S$, ΔG and K_D for each temperature are listed in Table 6.3. With increase in temperatures, K_D values increases (refer to Figure 6.13), indicating that the allosteric activator *p*-HPA was more tightly bound to C1 at low temperatures. Also visible in Figure 6.13 us that the released heat, ΔH, decreases, entropy change becomes smaller and the Gibbs Free energy stayed reasonably constant.

Based on basic thermodynamic principles, the heat capacity, ΔC_p, and reaction enthalpy, ΔH relate to each other through the following equation:

$$\Delta C_p = \Delta H/\Delta T \qquad \text{(eq.11)}$$

The heat capacity is thus he slope of ΔH vs. ΔT plots. For the *p*-HPA /C1 affinity reaction ΔC_p was determined as 1.21 kJ $mol^{-1}K^{-1}$, with the slope of the relevant curve in Figure 6.13. The positive ΔC_p change is like to come from extensive additional hydration upon binding of *p*-HPA and charge-related interactions (electrostatic interactions) within the allosteric binding site-C1. As a consequence of the positive value of ΔC_p, the nature of the thermodynamic driving force changes with the increasing temperatures from an enthalpy-driven to entropy-driven characteristic.

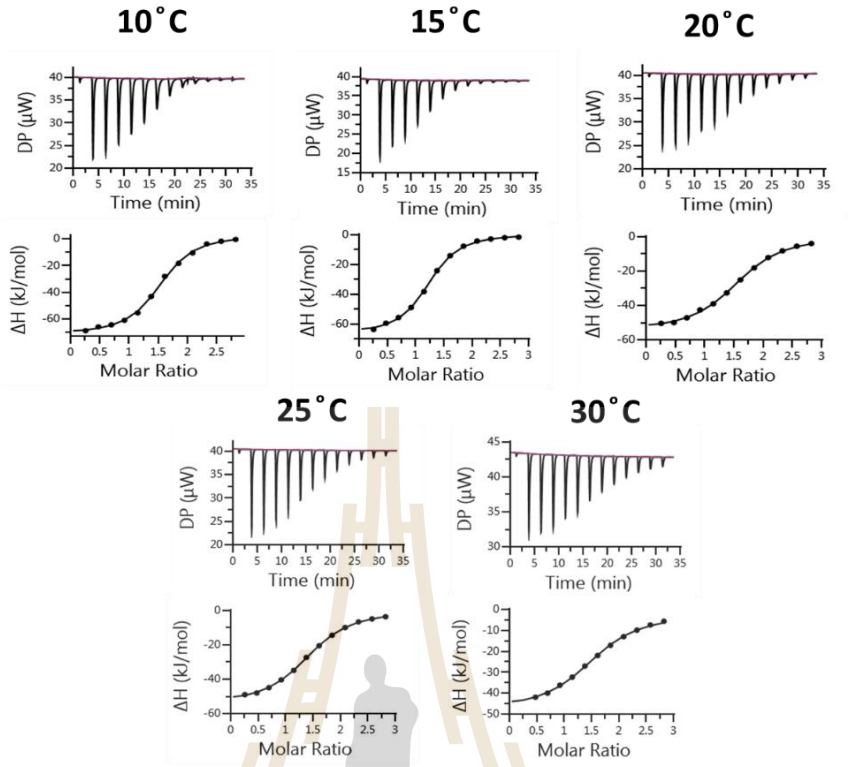

Figure 6.12 Calorimetric traces (heat flow) as observed by injecting 3.2 µL of ligand solutions (1.5 mM *p*-HPA, V = 38.8 µL) into the sample cell that is filled with C1 solution (100 µM, v = 280 µL); the experiment was performed for five temperatures between 10 to 30 °C. The top panel presents the original calorimetric traces. The bottom panels show the heat of reactions (corrected by subtraction of appropriate blank experiments) and fitted with a non-linear regression. Identification of best fit parameters for K_D, ΔH, ΔG, $-T\Delta S$ and 1:1 stoichiometry (n) was task of the ITC data analysis software.

Table 6.3 Thermodynamic quantities for the interactions between allosteric activator *p*-HPA and C1 at temperature of 10, 15, 20, 25 and 30 °C.

Temp. (°C)	K_D (μM)	ΔH (kJ/mol)	ΔG (kJ/mol)	$-T\Delta S$ (kJ/mol)
10	4.60 ± 1.00	-72.70 ± 1.50	-29.00	43.70
15	6.00 ± 0.60	-66.30 ± 1.50	-28.80	35.70
20	9.80 ± 1.00	-60.90 ± 4.40	-28.20	32.20
25	10.20 ± 0.30	-57.00 ± 2.70	-28.50	28.70
30	15.30 ± 1.50	-47.00 ± 2.00	-28.00	19.00

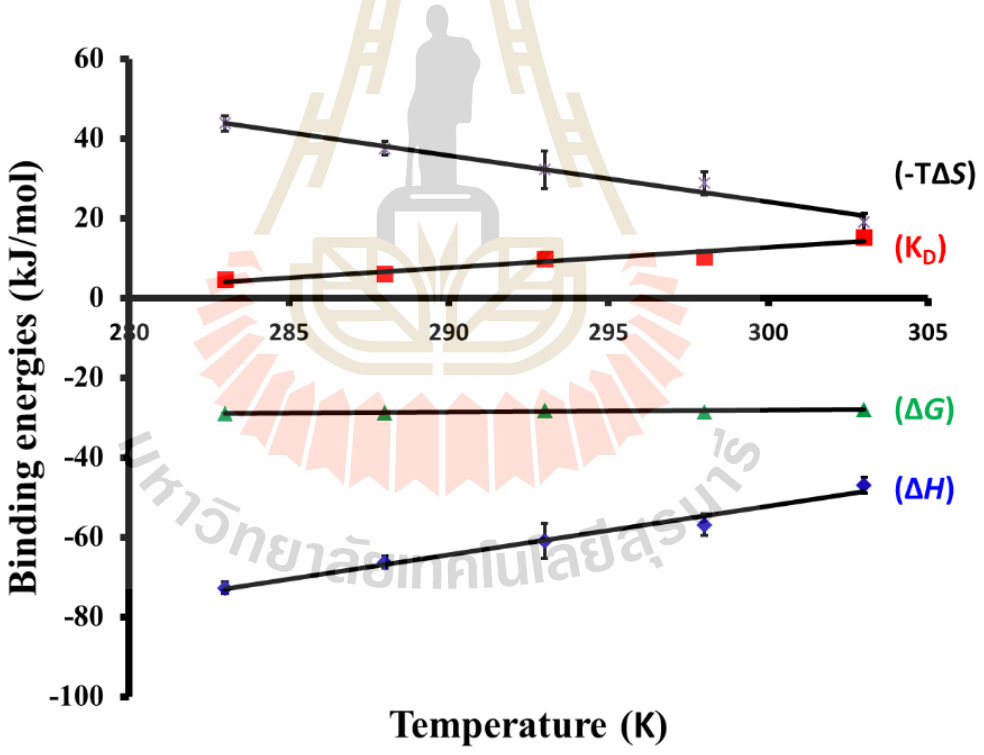

Figure 6.13 Display of the temperature dependence of the K_D, ΔH, ΔG, $-T\Delta S$ valued for allosteric C1/*p*-HPA interaction, tested at 10, 15, 20, 25 and 30 °C. ΔC_p for the binding of *p*-HPA to C1 is equal to the slope of linear of the ΔH vs. T plot.

6.1.6 Amperometric quantification of disease biomarker *p*-HPA with PB-SPEs

The exploitation of H_2O_2 as side product of C1/NADH/O_2 turnover was excellently possible through detection at low potential on PB-SPEs. For a given NADH C1 exposure, the H_2O_2 current generation got actually attenuated by full allosteric activation *p*-HPA (the best allosteric activator, as confirmed via electrochemical tests in 6.1.4 and the standard ITC experiment in 6.1.5). For innovative amperometric *p*-HPA analysis, PBS solutions with pre-dissolved C1 were challenged with NADH addition of defined and constant level while the concentration of *p*-HPA was varied and the H_2O_2 current monitored. As expected the rate of NADH to NAD+ conversion by enzymic C1 action was dependent on the concentration of activator molecule *p*-HPA and this effect is well illustrated in Figure 6.14A. Displayed there are the amperometric response for addition of 50 µM NADH in to stirred PBS (50 mM, pH 7) containing different *p*-HPA concentrations, recorded at H_2O_2 detection potential of -100 mV. Apparently, each amperogram, valid for a particular *p*-HPA concentrations, saw a rise in H_2O_2 current after NADH addition and the slope of the trace increased with increasing *p*-HPA level.

As evidenced in Figure 6.14B, plots of the slope of the H_2O_2 trace vs. actual solution *p*-HPA level approached saturation at higher *p*-HPA values. The inset of calibration curve is a display of the linear range for *p*-HPA detection, which reproducibly stretched up to about 100 µM with an $R^2 = 0.9947$. The lowest practically detectable *p*-HPA concentration was estimated to be about 1.0 µM. Curves as in Figure 6.14B can be interpreted as electrochemically derived binding curves and they are the first of this kind known. Furthermore, the accomplishment of very good analytical

figures of merit for C1 biosensing-based *p*-HPA electroanalysis is seen as a possible starting point for the development of a technically simple testing scheme for diagnostic trace *p*-HPA biomarker quantifications in human body fluids such as blood and, most important, urine.

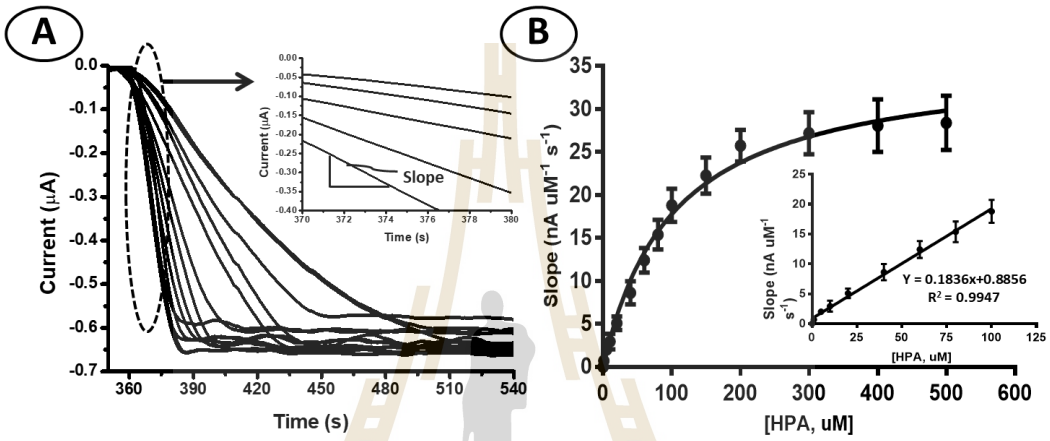

Figure 6.14 Amperometric *I-t* curves for the reaction of C1 (1.0 μM)/substrate-NADH (50 μM) for increasing solution levels of allosteric effector *p*-HPA. H_2O_2 currents are monitored at cathodic detection potential (-100 mV) at PB- modified SPEs. A marked difference in the slopes of the upcoming current signals in the present of varied *p*-HPA was observed; [*p*-HPA] 0, 1, 5, 10, 20, 40, 60, 80, 100, 150, 200, 300, 400 and 500 μM, respectively. (B) Plots of the slopes of the *p*-HPA-induced H_2O_2 signals vs. [*p*-HPA]. They can be interpreted as electrochemically derived binding curves.

6.2 Fabrication of C1/redox polymer-modified electrodes for the detection and quantification of NADH and *p*-HPA

6.2.1 C1 to electrode with Os(III)-complex modified redox polymers

The reductase-C1 component of HPAH uses FMN as redox cofactor for the oxidation of NADH. Hence, for the electrical wiring of this enzyme to an electrode surface two prerequisites have to be fulfilled by the redox matrix: (i) the potential of the redox mediator has to be low enough to avoid significant oxidation of NADH at the mediator and at the electrode (note that the electrode potential has to be adjusted to the redox potential of the mediator for detection); and (ii) the potential has to be considerably more positive than that of the FMN coenzyme, to ensure fast electron transfer between the enzyme and the mediator and thus efficient signal generation.

Since significant oxidation of NADH at graphite electrodes occurs only at potentials well above -100 mV vs. Ag/AgCl/3 M KCl (refer to Figure 6.15) and the potential of the FMN domain is rather negative (≈ -400 mV vs. Ag/AgCl/3 M KCl, depending on the protein environment), the mediator should have a potential within this region. The potential of Os-complexes, on the other hand, can easily be tuned by the coordination of either electron-withdrawing or electron-donating ligands to the metal center. Mao *et al*. (2003), for example, reported the synthesis of a low potential Os-complex (Figure 6.16, top) bearing bi-imidazole-based ligands with a redox potential of around -240 mV vs. Ag/AgC/3 M KCl (Figure 6.17). This potential is the within the above mentioned limits. Consequently, this mediator should be suitable for chronoamperometric experiments, interacting with the C1 unit at applied potential that do not cause simultaneous NADH oxidation at the electrode. For polymer preparation, this mediator was attached to two different backbones to yield the redox polymers PVP-

Os and P(SS-GMA-BA)-Os (Figure 6.16, bottom). The synthesis of the PVP-Os, described by Mao *et al*. (2003), was originally used for the electrical wiring of glucose oxidase. In PVP-Os, the mediator is attached to a hexanoic acid-modified poly(4-vinylpyridine) backbone (PVP-C1-acid) by activation of the acid moieties with *N*,*N*,*N′*,*N′*-tetramethyl-*O*-(*N*-succinimidyl) uranium tetra fluoroborate (TSTU) and the subsequence reaction of the active ester with complex 5 by amide formation (Figure 6.16 and the synthesis was showed in Figure A.1). The novel polymer P(SS-GMA-BA)-Os was synthesized starting by the co-polymer P(SS-GMA-BA), which contains electrophilic epoxide functions with the backbone (see the synthesis part in Figure A.4). The epoxides can be used as anchoring sites for attachment of complex 5, by including a ring opening reaction of the –COC- moiety with the primary amino group in 5 at elevated temperature, using a base catalyst (Figure 6.16 and the synthesis was showed in Figure A.3. Polymer PVP-Os has a positively charged backbone due to the alkylated pyridine moieties. In contrast, P(SS-GMA-BA)-Os has a negatively charged backbone, due to the sulfonate groups in the styrene-base co-monomer (Figure 6.16: note that at pH 7 sulfonate groups are fully ionized). Both polymers are very hydrophilic and thus provided a solvated environment for the reductase-C1. Moreover, the redox potentials of the modified polymers were estimated from cyclic voltammograms, measure with drop-cast films in phosphate buffer saline (BPS, 50 mM) at pH 7, to be -190 mV (PVP-Os) and -220 mV (P(SS-GMA-BA)-Os) vs. Ag/AgCl/3 M KCl (Figure 6.17B and C).

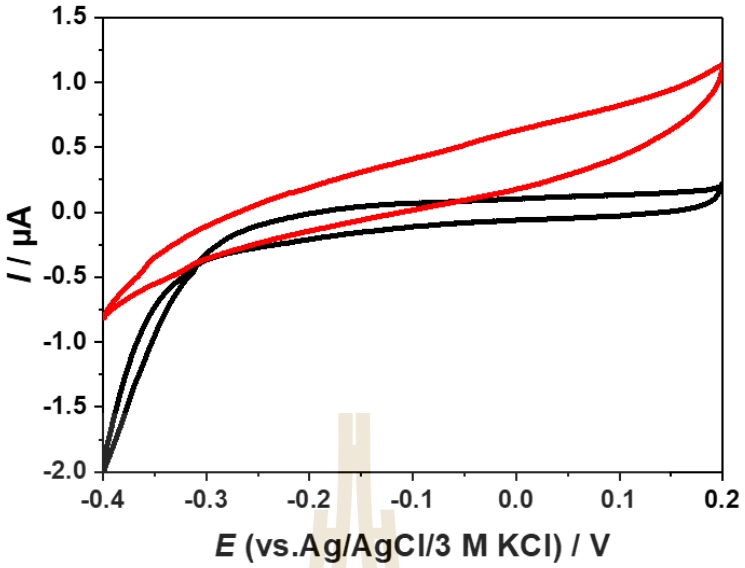

Figure 6.15 Cyclic voltammograms of a bare graphite electrode in the absence (black trace) and presence of 5 mM NADH (red trace). Working electrolyte: deaerated PBS (50 mM, pH 7), scan rate: 2 mV s^{-1}. Considerable anodic currents due to the oxidation of NADH at the electrode surface were observed at potentials above -0.1 V vs. Ag/AgCl/3 M KCl.

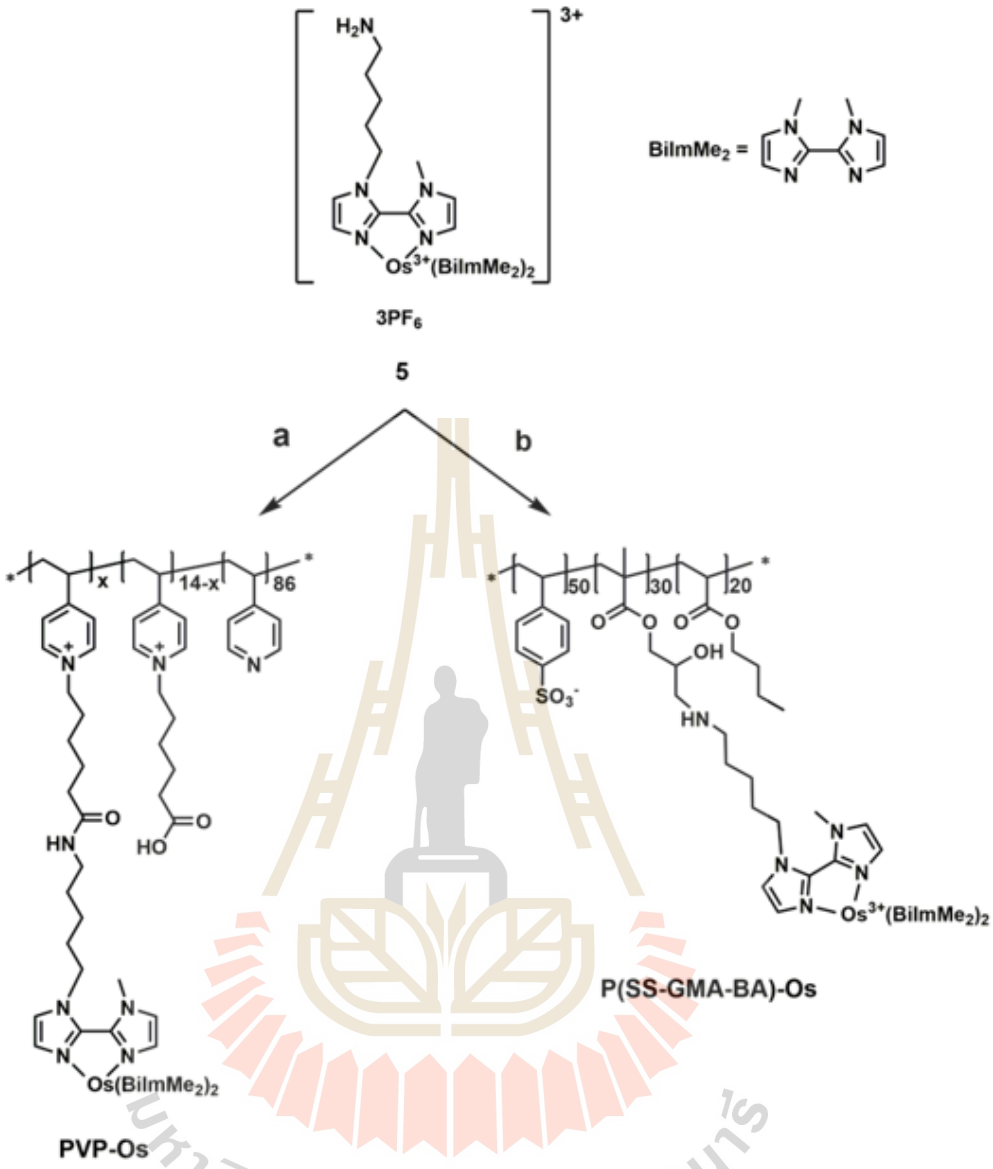

Figure 6.16 Synthesis of the redox polymers PVP-Os and P(SS-GMA-BA)-Os. Complex 5 has a primary amino group within its ligand periphery, which can be used to covalently attach the complex to the activated acid functions in PVP-C6-acid to yield PVP-Os. At evaluated temperatures and with a base catalyst the amino group can also react with electrophilic epoxide functions in P(SS-GMA-BA) to form P(SS-GMA-BA)-Os. Reaction conditions: (a) dry dimethylformamide, PVP-C6-acid, TSTU, DIPEA, room temperature, argon, overnight; (b) water/DMSO, P(SS-GMA-BA), NaOH as base catalyst, 50 °C

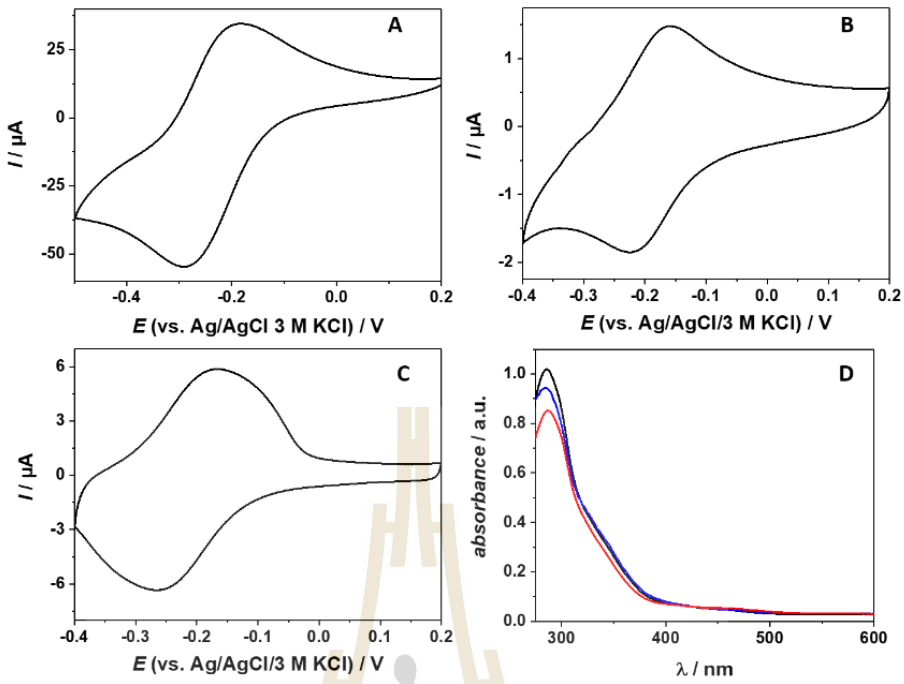

Figure 6.17 Voltammetric (A-C) and UV-vis spectroscopic (D) characterization of dissolved, freely diffusing complex **5** (A and black trace in D) and the polymers PVP-Os (B and blue trace in D) and P(SS-GMA-BA)-Os (C and red trace in D). A – C: Cyclic voltammograms of the free complex **5** (B, 1 M KCl/water, 50 mV s^{-1}) and the redox polymers (B and C, both in PBS, 50 mM, pH 7, 2 mV s^{-1}). The mid-point potentials were estimated to be -0.24 V (**5**), -0.19 V (PVP-Os) and -0.22 V (P(SS-GMA-BA)-Os); potentials refer to Ag/AgCl/3 M KCl reference. Compared to the free Os-complex **5**, a shift of the redox potential for both polymers to more positive values was observed due to the covalent bonding of the mediator to the polymer backbone. The effect is more pronounced for the positively charged polymer PVP-Os. D: UV-vis spectra recorded in DMSO. The spectral appearance of the free complex and the polymers with bound complex are almost identical indicating that the electronic structure of the redox-active complex is not significantly influenced by the attachment to and the nature of the polymer backbone.

6.2.2 The electrochemistry of C1/redox polymer-modified graphite electrodes

Figure 6.18 is a display of a schematic informing about the electrochemical wiring of enzyme C1 to a biosensor electrode surface via redox polymer embedment. From a thermodynamic point of view, the polymer should be able to extract electrons from FMN dependent C1 at a potential suitably below the oxidation potential of NADH at graphite electrodes. Indeed, cyclic voltammograms (Figure 6.19) of graphite electrodes modified with PVP-Os/C1 (Figure 4.19A) and P(SS-GMA-BA)-Os/C1 (Figure 6.19B) films showed a well-defined catalytic response upon the addition of substrate NADH, according to the mechanism depicted in Figure 6.18.

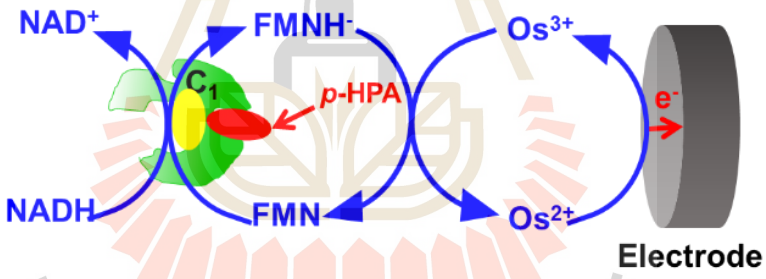

Figure 6.18 Simplified schematic of the electrochemical wiring of C1 under substrate turnover conditions (in presence NADH) via an Os(III)-complex modified redox polymer. For clarity, only the Os-metal centers and their corresponding oxidation states are shown. The allosteric activator *p*-HPA can bind to regulatory site on C1, inducing a conformational change in the enzyme that affects the substrate-binding site. This increases the rate of substrate conversion of NADH to NAD+, which is observable as an increase in Os(II) oxidation current.

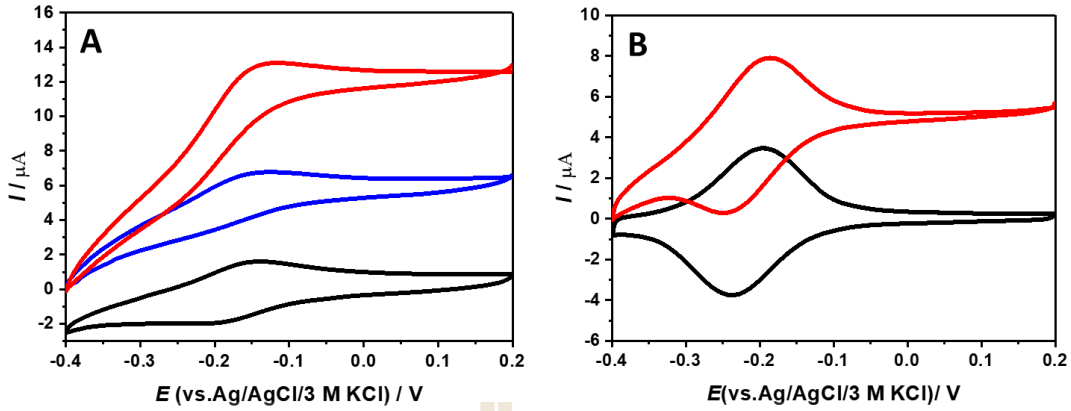

Figure 6.19 Cyclic voltammograms of (A) PVO-Os/C1 and (B) P(SS-GMA-BA)-Os/C1 graphite electrode modifications in the absence (black trace) and presence of NADH (2.5 mM: blue trace, 5 mM: red trace); working electrolyte: deaerated PBS (50 mM, pH 7); all *I-t* curves were recorded at scan rate of 2 mV s^{-1}.

Compared to the anionic polymer backbone in P(SS-GMA-BA)-Os, the positively charge polymer PVP-Os supported much higher catalytic current at, for instant, a NADH concentration of 5 mM (Figure 6.19A and B, red traces). The charge at the polymer base chain apparently influenced the strength of the C1/Os-complex interactions within the matrix and the efficiency of the process was higher in the presence of alkylated cationic pyridine moieties, even with an identical, probably because of the net surface charge of the enzyme molecules, with at pH = 7 is predominantly negative (pI 6.02, calculated with the ExPASy-SIB Bioinformatics Resource portal. GenBank ID: OUM80372.1).

Repulsive forces between entrapped enzyme and the negatively charge backbone P(SS-GMA-BA)-Os thus may hinder the optimal special arrangement of the redox site of the polymer and the biocatalyst, inhibiting electron transfer and thus reducing the observed current, compared to cationic PVP-Os sensor. This emphasized

the importance of the rational design of the redox polymer in achieved effective electrical wiring of the C1 biocatalyst and confirmed similar fundamental finding for other proteins (Ruff, 2017; Heller, 2006 and Milton, 2015). Nevertheless, both polymers tested were able to exchange electrons with C1, though with significantly different efficiencies, which proved that the bacterial reductase could be functionally connected to an electrode surface by means of the redox polymer. Repetitive cyclic voltammograms, acquired with both polymer/enzyme electrodes, shows a stable current response over several cycles (Figure 6.20).

It is known that Os-complex modified polymers can mediate the oxidation of hydro-quinones (Gregg, 1991 and Vering, 1994). Hence, the contributed of Os-complex mediate oxidation of NADH (electronic structure is similar to those of quinones) was evaluated, to ensure that detected current response was solely or mainly electrical communication between the polymer and the biocatalyst. In these tests pure redox polymers was drop-coated into graphite electrode and cyclic voltammograms were recorded in the absence and presence of NADH. PVP-Os modified sensors produced a week anodic current upon addition of NADH (Figure 6.21A), while P(SS-GMA-BA)-Os was virtually unresponsive to this (Figure 6.21B). For both polymer coatings, however, a slight current evaluation at potentials above -50 mV vs. Ag/AgCl/3 M KCl was observed, indicating some oxidation of NADH directly at the graphite electrode surface. Finally, we evaluated the contribution to the response by direct electron transfer (DET) from the enzyme to the electrode, with C1 immobilized by adsorption on the electrode surface by a drop-coating process.

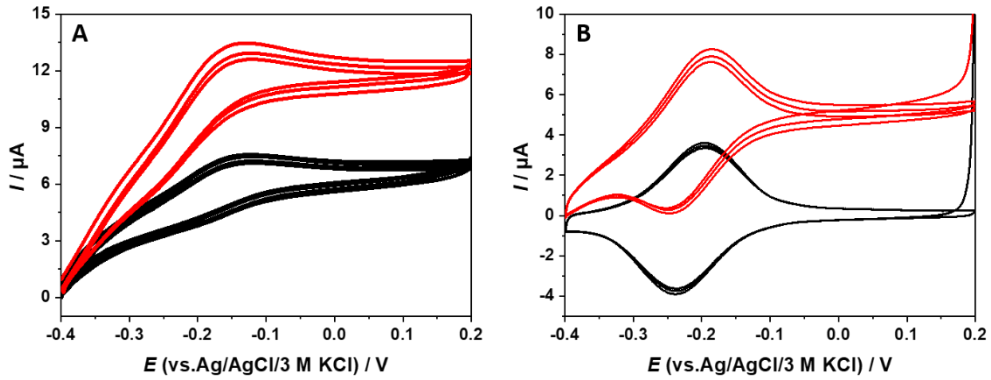

Figure 6.20 Multi-cycle voltammograms of (A) PVP-Os/C1 and (B) P(SS-GMA-BA)-Os/C1 films drop coated on graphite electrodes in deaerated PBS, 50 mM, pH 7. A: 2.5 mM NADH, four consecutive potential cycles (black trace) and 5 mM NADH, three consecutive potential cycles (red trace). B: three consecutive potential cycles in the absence of NADH (black trace) and 5 m NADH, three consecutive potential cycles (red trace); all *I-E* curves were recorded with a scan rate of 2 mV s^{-1}.

Cyclic voltammograms showed only a week anodic current at potentials above -300 mV vs. Ag/AgCl/3 M KCl (Figure 6.22, blue trace), indicating that very little electron transfer occurred between the redox-active protein and the graphite electrode. Not surprisingly, adsorption of C1 alone formed poorly stable enzyme films on the electrode surface. The use of a stabilizing immobilization matrix, i.e. the hydrophilic P(SS-GMA-BA) polymer backbone without bound Os-complexes, increase the signal stability but did not lead to higher catalytic currents (Figure 6.22, red trace). To evaluate the contribution of DET to the detected catalytic currents, a polymer double layer, compose of an underlying C1-free PVP-Os layer and an active PVP-Os/C1 upper layer, was introduced to prevented contract of the protein with the electrode surface.

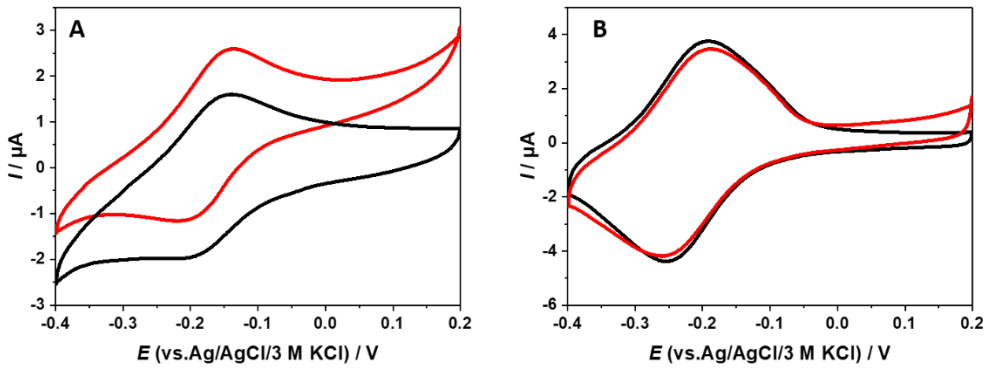

Figure 6.21 Mediated NADH oxidation by means of the redox polymer matrix (A) PVP-Os and (B): P(SS-GMA-BA)-Os. Working electrolyte: deaerated PBS, 50 mM, pH 7; scan rate: 2 mV s^{-1}. A: 5 mM NADH (red trace), B: 2.5 mM NADH (red trace); black traces in A and B refer to measurements in absence of NADH.

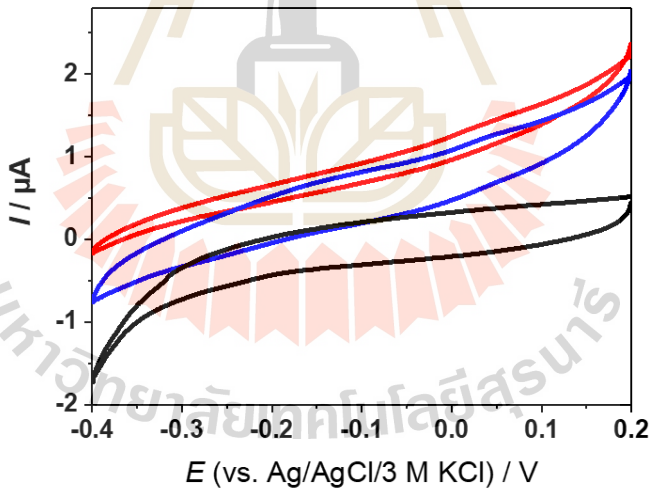

Figure 6.22 Oxidation of NADH with C1 recycling via direct electron transfer (absence of polymer bound Os(III) mediator). Black line: background current recorded with the bare graphite electrode in the absence of NADH; blue line: C1 directly adsorbed onto graphite, 5 mM NADH; red line: C1 embedded in the pristine polymer backbone P(SS-GMA-BA), 5 mM NADH. Working electrolyte: deaerated 50 mM PBS, pH 7, and scan rate 2 mV/s.

For a valid comparison of single layer sensor responses, the absolute amount of immobilized PVP-Os in double layer sensor variants was adjusted to be equal to that in PVP-Os/C1 modified graphite electrodes. Cyclic voltammetry was again used to analyze the behavior of the polymer double layer electrodes. In the presence of NADH a clear catalytic wave was observed for the double layer system (Figure 6.23, red line), however, the catalytic trace in the region of reaction onset was less steep than in the single layer system (Figure 6.23, blue line). At potentials above 0 V vs. Ag/AgCl/ 3 M steady state catalytic currents were reproducibly smaller for the double layer sensor system.

This clear difference between the current traces for PVP-Os//PVP-Os/C1 and PVP-Os/C1-modified visualized the contribution of DET to C1 biosensor signaling. At the same time, the experiment provided further evidence of the effective mediated electron transfer between C1 and the redox matrix. As expected for the double layer sensor architecture, the lowering of the magnitude due to DET suppression was accompanied by a slowed response to substrate addition (Figure 6.23B).

The more mechanistic look at the elementary reaction steps of immobilized C1/redox polymer blends was followed by a detailed evaluation of the analytical performance of such biosensors for the amperometric detection of NADH, obviously with and without allosteric C1 activation. Because of a more favorable signal with regard to current magnitude and response time the chosen sensor layout for all work from now used the single-layered PVP-Os/C1 configuration that has allosteric C1 enzyme entities fixed into an Os-complex loaded and the positively charge redox polymer network.

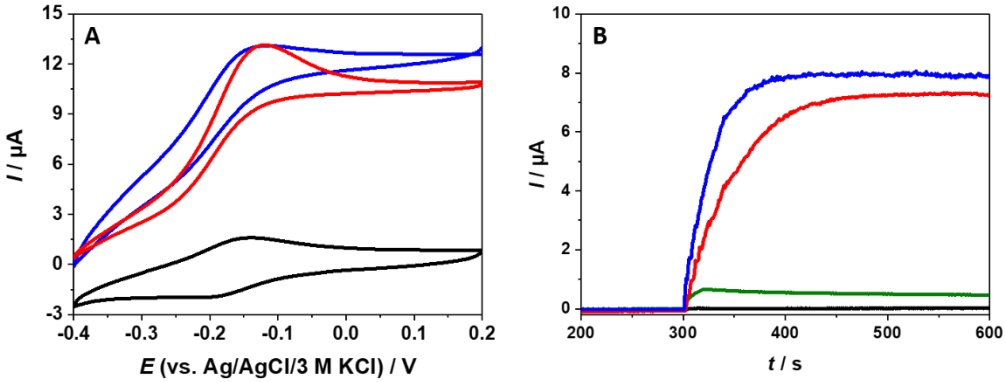

Figure 6.23 Voltammetric and amperometric characterization of the PVP-Os/C1-based double layer (red traces) and single layer (blue traces) biosensor systems. (A) Cyclic voltammetry of the double layer system in the presence of 5 mM NADH (red curve) and the single layer system in the presence (5 mM, blue curve) and absence (black curve) of NADH, scan rate: 2 mV s^{-1}. (B) Chronoamperometry at an applied potential of -100 mV vs Ag/AgCl/3 M KCl (note that at this potential, no significant oxidation of NADH at the electrode is observed, see also Figure 4.15); blue line: 5 mM NADH electrolyte supplementation at 300 s, single layer; red line: 5 mM NADH electrolyte supplementation at 300 s, double layer. Shown for comparison purpose are the background current in the absence of NADH (black curve) and trace for C1 working via direct electron transfer for a 5 mM NADH electrolyte supplementation (green trace). The double layer system had an enzyme-free bottom PVP-Os layer with a PVP-Os/C1 top coat (sensing layer). The single layer system was composed of a single PVP-Os/C1 layer. Working electrolyte was for all measurements deaerated PBS, 50 mM, pH 7.

6.2.3 Demonstration of allosteric *p*-HPA activation for C1/Os(III) redox polymer biosensors; proof of principle tests and sensor characterization trials.

As outlined in the introductory section, molecular activity modulation of allosteric enzyme in redox polymer-based immobilization matrices of biosensor for quantitative analysis has not been explored, certainly not with a simple amperometric biosensor configuration. In initial chronoamperometric measurements (Figure 6.24) PVP-Os/C1 modified graphite electrode responded reproducibly at the potential of -100 mV vs. Ag/AgCl/3 M KCl to the addition of NADH with stepped increases in current, followed by subsequent progression to a new steady state (black trace: 0.5 mM and red trace: 1 mM). Here the anodic sensor current reflects the continuous oxidation by C1 of NADH to NAD^+, which is translated into an electrical signal by redox contact with the transducing electrode surface, along an uninterrupted pathway of tethered Os(III)-sites. Supplementation of the electrolyte with the C1 activator *p*-HPA should induce another current step, though allosteric- stimulation of the catalytic activity of C1. This is shown by the two *I*/*t* traces in Figure 6.24A, in which the addition of *p*-HPA to the buffer with pre-adjusted C1/NADH level produced the expected signal increase.

Calibrations in the common amperometric mode were then carried out with the allosteric C1 biosensor assay for NADH concentration between 50 µM and 500 µM in 100 µM presence (Figure 6.24B, red trace) and absence (Figure 6.24B, black trace) of the allosteric activator *p*-HPA. The current steps produced by incremental elevations of substrates concentration were consistently larger in the presence of *p*-HPA producing a 1.5-fold increase in the sensitivity of amperometric NADH sensing, confirmed by the slopes of the corresponding calibration plots (Figure 6.24C, red and

black traces). It was observed that the initial maximum current slowly declined with time (Figure 4.24B, red trace, valid from the 4th addition of substrate (200 μM) and Figure 6.25 even with a NADH concentration of 50 μM). This first success with a proof-of-principle trial verified the potential of the chosen strategy towards the desired simple *p*-HPA disease biomarker electroanalysis with C1-based biosensing. In the following a few sensor optimizations will be described that led to more stable and sensitive signaling of C1 interaction with NADH and *p*-HPA.

To enhance the response stability of PVP-Os/C1-based NADH biosensors, bi-functional poly(ethylene glycol) diglycidyl ether (PEGDGE) was added as cross-linking against to immobilization layer. PEGDGE contain two electrophilic epoxide functions that readily react at room temperature with amino group on, for instant protein surfaces (Vasylieva *et al.*, 2011). Covalent attachment of C1 to PEGDGE within the immobilization layer was expected to achieve more stable fixation of the enzyme to graphite electrodes. Since the formation of covalent pyridine-epoxide adducts requires elevated temperatures (Dell'Erba and Williams, 2006; Xue *et al.*, 1986) and PEGDGE was used at room temperature, crosslinker binding to residual pyridine moieties in the backbone of the PVP-Os redox polymer was unlikely. However, entangling of PEGDGE and PVP-based polymer chins may contribute to the stabilizing effect (not that a stabilizing effect for PVP based polymers in combination with PEGDGE was reported earlier (Mao *et al.*, 2003) and such chain interweaving may have stabilized the immobilization of C1.

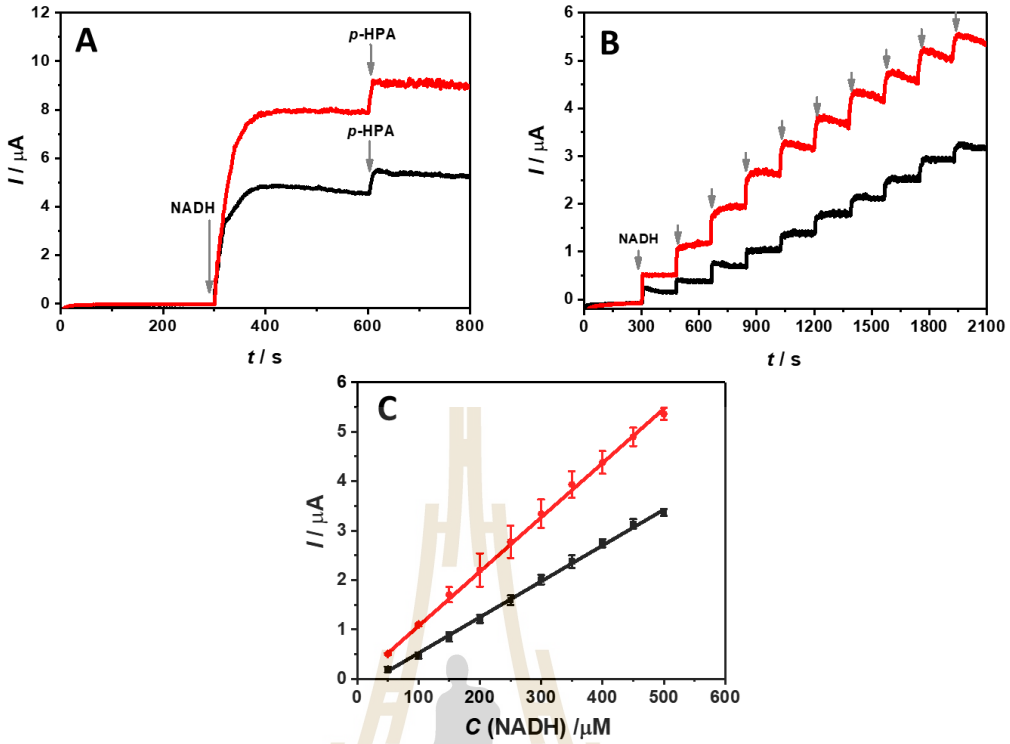

Figure 6.24 The effect of allosteric activator *p*–HPA on the amperometric detection of NADH with PVP-Os modified electrodes. (A) Amperograms with different NADH concentrations (black line: 0.5 mM, red line: 1 mM, added at t = 300 s) in the present of *p*-HPA (500 μM, added at t = 600 s). (B) Chronoamperograms of PVP-Os/C1 electrodes for NADH concentrations in the range of 50 – 500 μM in the absence (black curve) and in the presence of 100 μM (red curve); which is addition of NADH stock solution (grey arrows) the concentration of the substrate was increased by 50 μM. (C) *I*/*C* calibration plots for NADH detection in the presence (red filled cycles) and absence (black filled cycle) of 100 μM *p*-HPA. The different of the slope of the red (11 nA μM^{-1}) and black (7 nA μM^{-1}) linear regression lines shows the increase in the biosensor sensitivity though allosteric C1 activation. Error bares are standard deviations of measurement in PBS, 50 mM, pH 7 at the working electrode potential -100 mV vs. Ag/AgCl/ 3 M KCl.

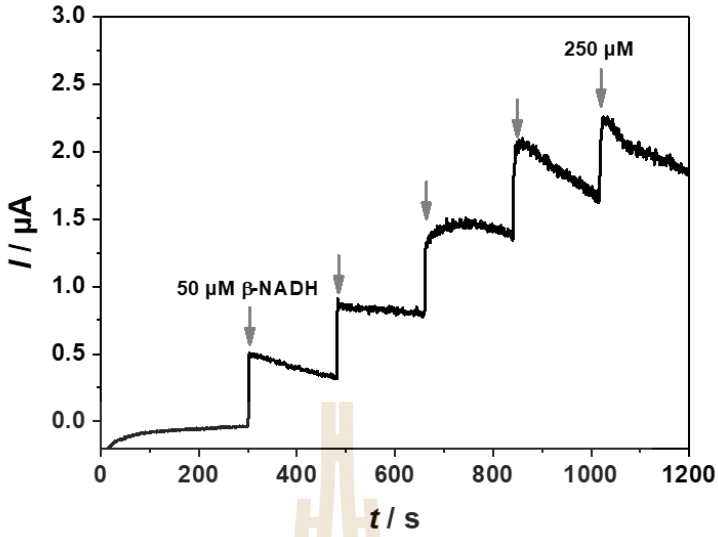

Figure 6.25 Chronoamperometric response of a PVP-Os/C1 NADH, biosensor prepared without crosslinker addition to the polymer/enzyme mixture for the oxidation of analyte in the presence of 50 µM *p*-HPA in the working electrolyte (deaerated PBS, 50 mM, pH 7) Applied potential: -100 mV vs. Ag/AgCl/3 M KCl. Grey arrows indicate the additions of NADH (50 µM intervals), creating an active solution concentration between 50 µM at 300 s and 250 µM after the last addition at t = 1000 s.

NADH-selective C1 biosensors were prepared with different PEGDEG:PVP-Os:C1 ratios and optimal amperometric detection performance was obtained with 5 µL of PBS containing 2.3 mg mL^{-1} PEGDGE, 12 mg mL^{-1} PVP-Os and 7.3 mg mL^{-1} C1, dropped and dried on well-polished graphite precursor electrode disks. Representative amperometric recordings in the presence (Figure 6.26A, red blue and green traces) and absence (Figure 6.26, black trace) of *p*-HPA revealed stable sensor responses to NADH, even at high concentration. As was seen in the calibration plots of simple PVP-Os/C1 sensors, *p*-HPA also increased the sensitivity of the PEGDGE/PVP-Os/C1 biosensor (Figure 6.26B). Apparently, covalent crosslinking of C1 to PEGDGE

chains improved the stability of C1 fixation without adversary effecting the mobility of the substrate, NADH, or activator, *p*-HPA, within the immobilization layer. Comparison of the calibration plots for the three *p*-HPA concentrations (Figure 6.26B, red trace 50 μM, blue trace 100 μM and green trace 150 μM) shown moderate concentration dependence for allosteric C1 stimulation, with the maximum stimulation reached at an activator concentration of 100 μM, equivalent to a 400-fold molecular excess of *p*-HPA molecules in the electrolyte solution over C1 unit on the electrode.

For practical analytical applications, reagent-less biosensors are preferred. We therefor tried replacement of *p*-HPA in the electrolyte by a pre-incubation procedure that exposed the immobilized C1 to the stimulant ex-situ before NADH analysis: PEGDGE/PVP-Os/C1-modified electrode were immerse in PBS (50 mM, pH 7) containing 100 μM *p*-HPA, at room temperature for 10 or 30 min. Original current recordings for amperometric NADH measurements with PEGDGE/PVP-Os/C1 biosensor of the two conditions are shown in Figure 6.26C, and the corresponding calibration plots are depicted in Figure 6.26D. The anodic current steps on incremental additions of NADH are approximately dependent of pre-incubation time, but are significantly greater than those from biosensor untreated with *p*-HPA (see in Figure 6.26A, black trace as example). Obviously, capture allosteric activator molecules by binding sites in C1 occurred during the few min of pre-incubation and, as indicated by lack of decay in the sensor response, the C1/*p*-HPA adducts were active throughout the 35 min chronoamperometric measurement.

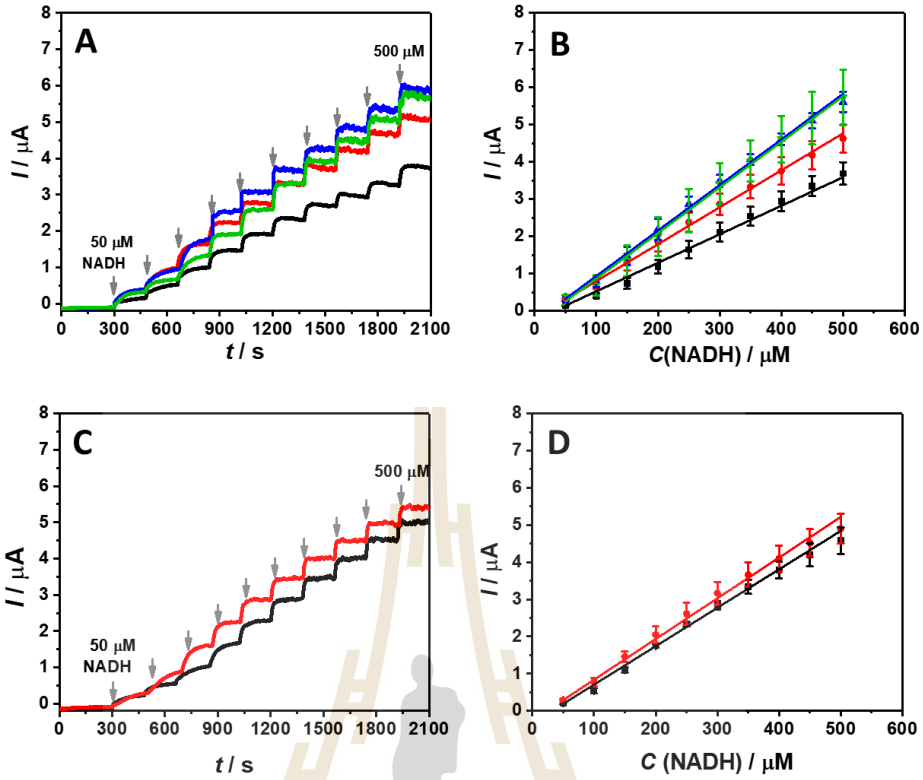

Figure 6.26 (A) Chronoamperograms for analyte concentrations between 50 to 500 µM (grey arrows indicate increment NADH additions of 50 µM) in the presence (red trace: 50 µM, blue trace: 100 µM and green trace: 150 µM) and absence (black trace) of *p*-HPA. (B) Calibration plots computed from the recording in (A), data points are average values of four independent measurements. (C) Chronoamperograms for cross-linked PEGDGE/PVP-Os/C1 films incubate in a PBS solution (50 mM, pH 7) containing 100 µM *p*-HPA (black trace: 10 min incubation and red trace: 30 min incubation). Grey arrows indicate the timing of the individual additions of 50 µM NADH increments. (D) Calibration graphs obtained for pre-incubated PEGDGE/PVP-Os/C1-based NADH sensors; current values were extracted from traces in (C). Values are the means of three independent measurements. For (B) and (D), the error bars represent the calculated standard deviation of the four-fold (B) and triplicate (C) trials in PBS (50 mM, pH 7) at a working electrode potential -100 mV vs. Ag/AgCl/3 M KCl.

Table 6.4 summarizes the sensitivity of the PEGDGE/PVP-Os/C1-based NADH biosensor in the various analytical protocols used in this study. The value was 12.1 nA μM^{-1} when the electrode were continuously exposed to 100 µM allosteric activator. Pre-incubation in a PBS (50 mM, pH 7) with that concentration of *p*-HPA, however, was about 15% less efficient in increasing the sensitivity; however, since the response was stable on the time scale of the performance tests it seems that a reagentless NADH biosensor incubation assay with allosteric signal amplification is possible.

Table 6.4 Sensitivity of PEGDGE/PVP-Os/C1-based NADH biosensors: Effect of in *situ* exposure or pre-incubation with the C1 activator *p*-HPA. Values are means of at least three independent measurements in 50 mM PBS, pH 7 at a working electrode potential of -100 mM vs. Ag/AgCl/3 M KCl and NADH levels in the range 50-500 µM.

Conditions	Sensitivity / nA μM^{-1}
Without *p*-HPA	8.25 ± 0.89
50 µM *p*-HPA in solution	9.70 ± 1.10
100 µM *p*-HPA in solution	12.08 ± 0.64
150 µM *p*-HPA in solution	12.58 ± 1.19
Incubation in *p*-HPA solution for 10 min	10.13 ± 1.08
Incubation in *p*-HPA solution for 30 min	10.45 ± 0.97

6.2.4 Amperometric quantification of NADH with C1/PEGDGE/PVP-Os biosensors under allosteric enzyme activation control

The suitability of the developed PEGDGE/PVP-Os/C1 biosensing assay with allosteric enzyme activation for quantitative of NADH analysis was finally evaluated by assay of model samples with a nominal analyte concentration of 50 μM. The recovery rate was determined by five-fold supplementation of standard measurements in PBS (50 mM, pH 7) with addition of 100 μM *p*-HPA for allosteric activation of C1. Figure 6.27A, a representative example, is one of five original amperometric recordings, showing four stepped current increases on addition of NADH to the measurement buffer.

Figure 6.27B is a standard addition plot constructed from the data in Figure 6.27A. In this particular case, the NADH sample concentration determines was 51.7 μM, equivalent to a recovery rate of 103.3%, for the 50 μM sample. The average recovery rate for the five NADH quantifications was, 105.1 ± 4.5% (52.5 ± 2.1 μM: see Table 6.5 for the individual values), which demonstrated that allosterically activated C1 in a PEGDGE/PVP-Os matrix worked efficiently and reproducibly for accurate quantification of NADH. Apparently, the redox wiring of C1 to and its stable biocompatible entrapment on the transducer electrode were both accomplished through the strategy of using a specially tailored redox polymer/crosslinker composite as immobilization matrix; accordingly, a good NADH sensing quality could be verified.

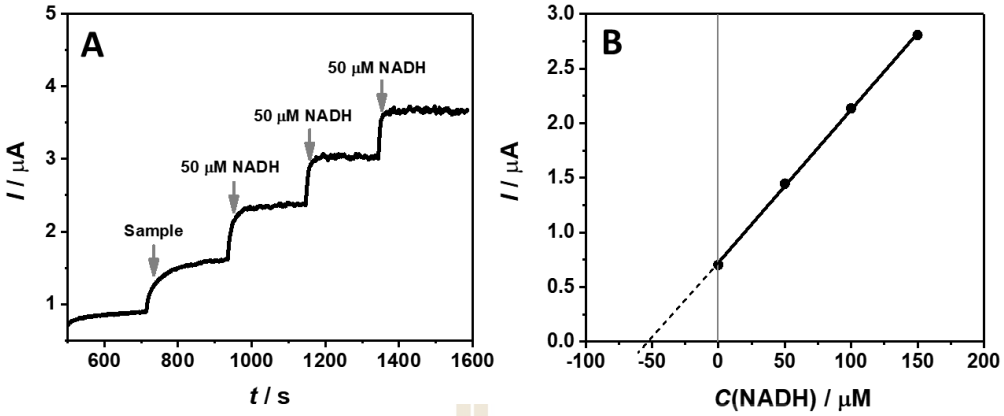

Figure 6.27 Detection of NADH with a PEGDGE/PVP-Os/C1 electrode use in the standard addition mode. (A) Representative chronoamperograms for with an initial addition of 50 μM NADH ("sample") and three subsequence of 50 μM additions. The electrolyte was 50 mM BPS, pH 7 and the working electrode potential of -100 mV vs. Ag/AgCl/3 M KCl. (B) Standard addition plot constructed with the data of the *I*/*t* curve in (A) and evaluation of the test concentration (51.7 μM), and the recovery (103.3%) from the linear regression line.

Table 6.5 Detection of NADH by means of the method of standard addition. Solution level was adjusted to a nominal NADH concentration of 50 µM, followed by the subsequent addition of three NADH standard additions. The initial adjusted "sample" NADH concentration was then estimated from *I*-*C* plots at $I = 0$ via linear regression of the individual data points. Working electrolyte and potential for the trial were deaerated 50 mM PBS, pH 7 and -100 mV vs. Ag/AgCl, 3M KCl, respectively.

experiment	c(NADH) / µM		R^2 of linear regression	recovery rate
	adjusted	found		
1	50	51.67	0.9994	103.34
2	50	55.82	0.9969	110.72
3	50	54.82	0.9960	109.64
4	50	50.20	0.9998	100.40
5	50	51.86	0.9999	103.72
6	50	51.33	0.9970	102.46
mean values		52.52 ± 2.08		105.05 ± 4.15

6.3 Application of C1/redox polymer-modified electrodes for the quantification of the urinary disease biomarker *p*-HPA

6.3.1 Adaptation of PEGDGE/PVP-Os/C1-modified electrodes for successful *p*-HPA amperometry

As introduced in introductory section, a major thesis objective was the accomplishment of a highly efficient but easy to do C1-based biosensing for the quantification of human disease biomarker *p*-HPA. The desired analytical scheme was expected to take advantage of an enhancement of the rates of C1 driven NADH biocatalysis to NAD^+ by the distinct accelerating impact of allosteric C1 effector *p*-HPA

(refer to Figure 6.28A). In previous sections evidence has already been provided that PEGDGE/PVP-Os/C1-based biosensors worked well for the detection and quantification of NADH via amperometric mode, with sensor current signals amplified in favorable manner though allosteric C1 stimulation by *p*-HPA (Figure 6.28B, scheme I). Here the optimal amperometric detection performance of drop-casted films of PEGDGE/PVP-Os/C1 on graphite or glassy carbon disk electrodes was adapted to electrochemical quantification of allosteric C1 activator *p*-HPA, the molecular metabolic biomarker for various human disease (Figure 6.28B, scheme II).

The signal-enhancing effect of the presence of allosteric activator *p*-HPA on the amperometric determination of NADH with C1-based biosensors was already evidenced earlier in Figure 6.26 and the measurements for three concentrations *p*-HPA, namely 50, 100 and 150 μM, exposed a clear concentration-dependence for allosteric C1 activation. For the optimized C1/Os(III) biosensors, the fixed NADH adjustments in solution were expected to be of critical importance for the quality of *p*-HPA analysis and a set of trials was dedicated for the optimization of this parameter.

PEGDGE/PVP-Os/C-modified graphite electrodes were thus immersed at room temperature into PBS (50 mM, pH 7) spiked with different concentrations of NADH (red arrow in Figure 6.29; A: 50 μM, B: 200 μM and C: 500 μM, at 300 s). Original current recordings of amperometric measurements of NADH (1st region, at 300 s) and *p*-HPA (2nd region, at 600 s) at a potential of -100 mV vs. Ag/AgCl/3 M KCl are shown in Figure 6.29. The anodic current due to Os(III) recycling increased upon addition of NADH (at 300 s) and the catalytic oxidation signals of NADH were slightly decreased in response to the additions of *p*-HPA solution. Probably, electrostatic forces between the negatively charged allosteric

activator *p*-HPA and positively charged backbone in PVP-Os affect adversely the desired manifestation of allosteric current amplification.

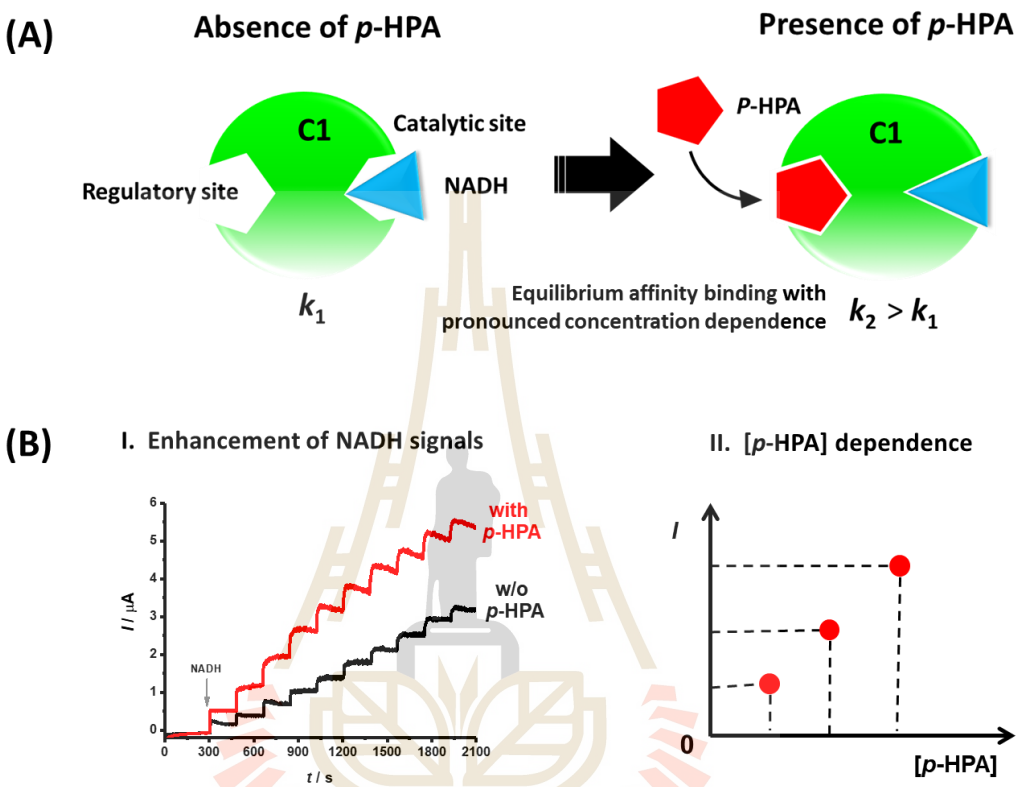

Figure 6.28 (A) Schematic representation of the working principle of the proposed novel allosteric C1 enzyme biosensor in the absence and presence of allosteric activator *p*-HPA molecules, the C1/NADH conversion is accelerated. The concentration dependence of the activator *p*-HPA can be detected by measuring the rise in catalytic oxidation signals of NADH, induced by the addition of the effector. (B) Based on characteristics of C1allostery, two analytical applications are determined: (I) Amperometric quantification of NADH by using PEGDGE/PVP-Os/C1 biosensing assay with allosteric enzyme activation (was completed) and (II) Adaptation of PEGDGE/PVP-Os/C1 biosensing assay for quantification of allosteric activator *p*-HPA, as a molecular disease biomarker.

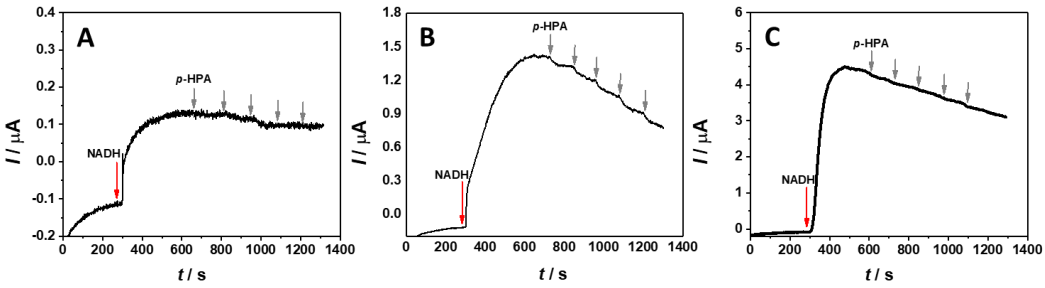

Figure 6.29 Chronoamperograms recorded at a PEGDGE/PVP-Os/C1-based biosensor during exposure to different *p*-HPA concentrations (grey arrows from 0.5 to 2.5 µM, at 600 s) in the presence of NADH (red arrow; A: 50 µM, B: 200 µM and C: 500 µM, at 300 s), trials in 50 mM PBS, pH 7 at working electrode potential of -100 mM vs. Ag/AgCl/ 3 M KCl.

6.3.2 Stabilization of C1/Os(III) biosensor for *p*-HPA electroanalysis via anionic polymer backbone

Typically, PEGDGE/PVP-Os/C1 modification were unstable sensor films on the electrode surface and not suitable for the reliable detection of *p*-HPA (Figure 6.30A). On the other hand, the use of a stabilization matrix, e.g. an anionic P(SS-GMA-BA)-Os polymer backbone, improved the sensor stability as the negatively charge of such polymer apparently influenced behavioral properties of the allosteric activator *p*-HPA within the films (refer to Figure 6.30B).

To enhance the stability of P(SS-GMA-BA)-Os/C1-based biosensors for quantification of *p*-HPA, bifunctional 2,2'-(ethylenedioxy) diethylamine (EDEA) was added as an additional cross-linking agent to the immobilization layer. EDEA contains two electrophilic functional groups, namely amine and epoxide entities. The amine group of EDEA could link with the epoxide function on the polymer backbone

P(SS-GMA-BA)-Os. The epoxide groups on EDEA could, on the other hand, readily react at room temperature with amino functional groups on the allosteric C1. Therefore, covalently bonding of EDEA to P(SS-GMA-BA)-Os and C1 under immobilization matrix was expected and supposed to lead to a more stable fixation of the sensor films on the graphite electrodes. All further experiments used the EDEA/P(SS-GMA-BA)-Os/C1 configurations that had the allosteric C1 entities covalently entrapped into an Os complex-loaded and negatively charged redox polymer network.

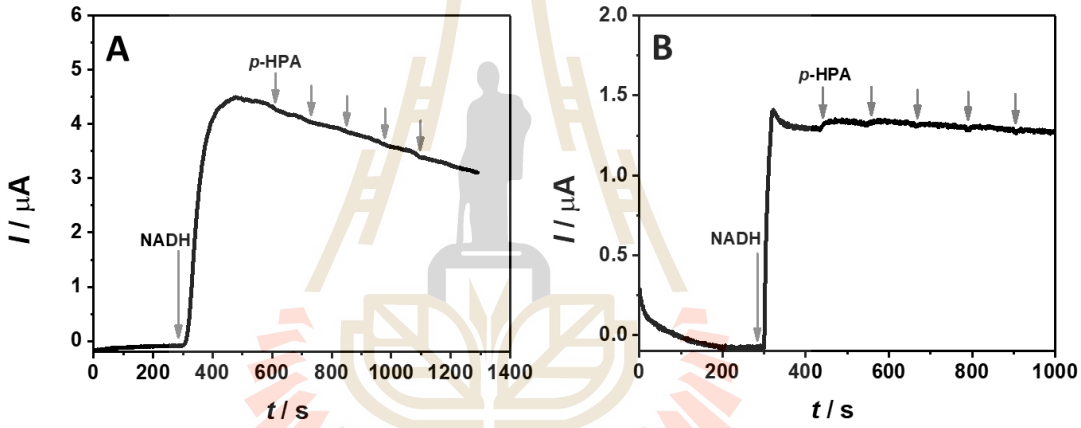

Figure 6.30 NADH amperometry with C1/Os biosensor that used (A) a cationic polymer backbone PEGDGE/PVP-Os/C1 and (B) anionic polymer backbone P(SS-GMA-BA)-Os/C1 for graphite electrode modification. *p*-HPA additions used concentrations between 1 and 5 µM in the presence of 500 µM substrate-NADH.

Calibrations trials of allosteric activator *p*-HPA in the amperometric mode were then carried out with EDEA/P(SS-GMA-BA)-Os/C1 sensor (refer to Figure 6.31). The biosensing was performed by supplementation with analyte using increments of 0.25 at the beginning and then 0.5 µM later, to reach ultimately the 5 µM final

solution level. The *I-t* trace in Figure 6.31B, is the zoom of the current trace in Figure 6.31A and displays better the increases of current signal due to allosteric enzyme activation. The concentration dependence of activator *p*-HPA in the presence of 500 μM NADH (optimal concentration), is confirmed in the calibration plot in Figure 6.31 and by the observation of linear behavior from 0.25-1.5 μM (refer to Figure 6.31D). A careful look at the calibration plot in Figure 6.31C (data points are the average values for four independent experiments), revealed that the measured currents slightly decreased at analyte levels above 3 μM. This gave motivation to improve sensor design further by optimizing the mass ratio of crosslinker, redox polymer and active C1 enzyme.

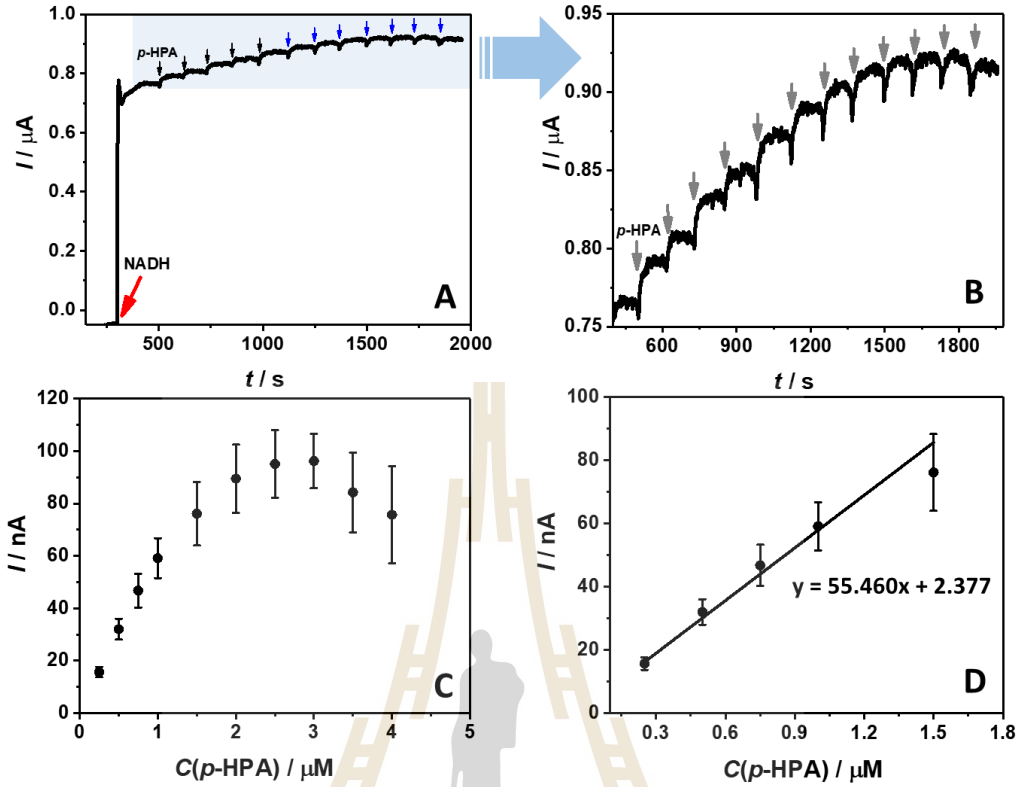

Figure 6.31 Performance characteristic of amperometric EDEA/P(SS-GMA-BA)-Os/C1-based *p*-HPA biosensors. (A) Chronoamperogram of analyte concentrations between 0.25 to 5 µM (black and blue arrows are indicate incremental *p*-HPA addition of 0.25 µM and 0.5 µM, respectively) in the presence of 500 µM substrate-NADH (red arrow, added at 300 s). (B) Chronoamperogram is zoom-in from (A). (C) Calibration plot computed from the recordings in (B); data points are the average values for four independent experiments. (D) Linear regression plot is fitted from the data in (C). The error bars represent the calculated standard deviation of the four-fold trials in 50 µM PBS, pH 7 at a working electrode potential of -100 mV vs. Ag/AgCl/ 3 M KCl.

6.3.3 Optimization of the mass ratio of crosslinker, redox polymer and active C1 enzyme in EDEA:P(SS-GMA-BA)-Os:C1 sensors

p-HPA measuring C1/Os(III) biosensors were prepared with different ratios of EDEA crosslinker:P(SS-GMA-BA-Os(III) redox polymer/:enzyme C1. An optimal amperometric detection performance was actually obtained with the application of 5 µL of a solution of the three sensor components with overall concentrations of 2.5 mg mL^{-1} EDEA, 7.2 mg mL^{-1} P(SS-GMA-BA)-Os and 10.95 mg mL^{-1} C1, dropped and dried on polished graphite electrode disks. Representative original current recordings of amperometric NADH measurements with EDEA/P(SS-GMA-BA)-Os/C1 biosensors of the optimized conditions are shown in Figure 6.32A. Zooms of the *I-t* trace in Figure 6.31A are shown in Figure 6.31B and visualized is nicely that the addition of *p*-HPA to the buffer which already contained 500 µM NADH led to elevations of the current in concentration-dependent manner. The corresponding calibration plot is depicted in Figure 6.32C. The anodic current signals of NADH with incremental the additions of *p*-HPA are significantly greater than those from biosensors with un-optimized of EDEA:P(SS-GMA-BA)-Os:C1 ratio (refer to Figure 6.31C). The linear regression line (Figure 6.32D) is result of a fit the data in Figure 4.32C; observed was a good linear response behavior from 0.25-1.5 µM. The error bars represent the calculated standard deviation of the four-fold trials in 50 µM PBS, pH 7 at a working electrode potential of -100 mV vs. Ag/AgCl/ 3 M KCl.

Obvious was from a look to the amperometric recordings of Figure 6.32B that the noise level of the current measurements was somewhat poor. Encouraged by a previous report by Lankelma and Popper (1976) with the suggestion that electrode noise source relates to electrode roughness a replacement of the graphite precursor

electrode by glassy carbon disk sensors was considered as strategy for noise elimination and recording improvement (Acworth, 1997; Matson *et al.*, 1984).

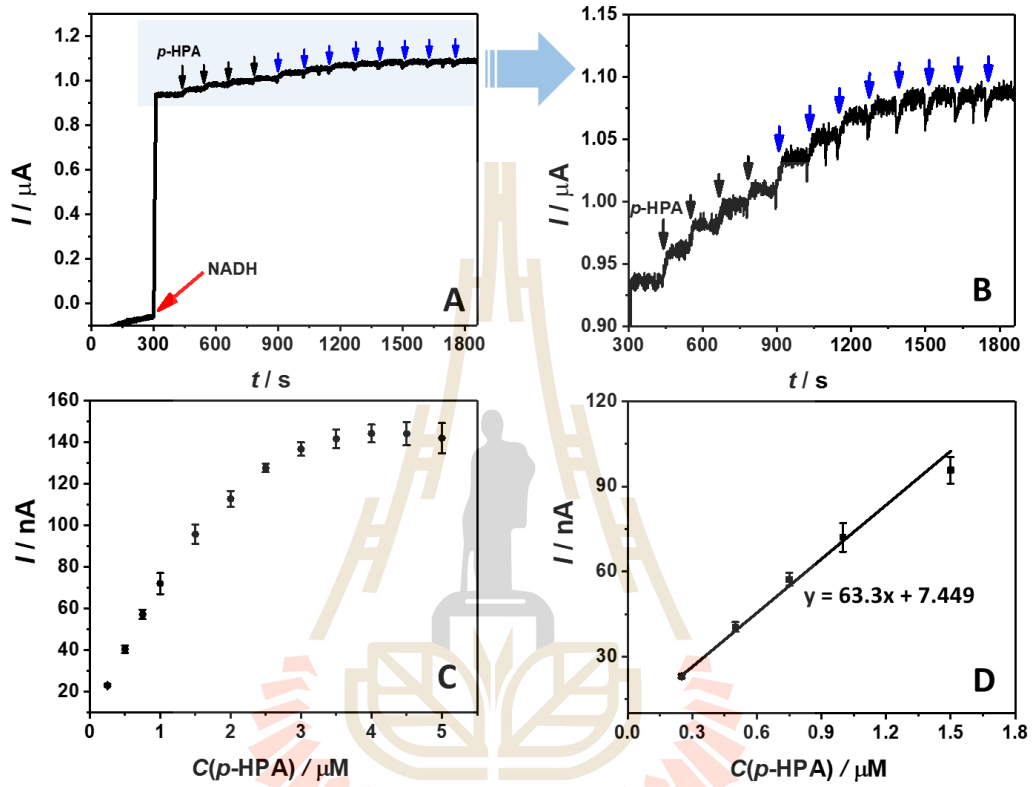

Figure 6.32 Optimization of an amperometric EDEA/P(SS-GMA-BA)-Os/C1-modified graphite electrode. (A) Chronoamperogram of analyte concentrations between 0.25 to 5 μM (black and blue arrows are indicated the incremental of *p*-HPA addition of 0.25 μM and 0.5 μM, respectively) in the presence of 500 μM substrate-NADH (red arrow, added at 300 s). (B) Chronoamperogram is zoom-in from (A). (C) Calibration plot computed from the recordings in (B); data points are the average values for four independent experiments. (D) Linear regression plot is fitted from the data in (C). The error bars represent the calculated standard deviation of the four-fold trials in 50 μM PBS, pH 7 at a working electrode potential of -100 mV vs. Ag/AgCl/ 3 M KCl.

6.3.4 Response testing of EDEA/P(SS-GMA-BA)-Os/C1-modified glassy carbon electrodes

Smooth since well-polished glassy carbon electrodes were modified with the functional EDEA/P(SS-GMA-BA)/C1 layer and then testes for their response behavior in amperometric *p*-HPA quantification trials. Actually, the catalytic oxidation currents of NADH on EDEA/P(SS-GMA-BA)/C1 modified glassy carbon electrode got significantly increased when the level of *p*-HPA was raised from 0.25 µM to 10 µM (refer to Figure 6.33A and zoomed *I-t* trace in Figure 6.33B; grey arrows: 0.25 µM, black arrows: 0.5 µM and blue arrows: 1.0 µM *p*-HPA). The corresponding calibration plot is depicted in Figure 6.33C. The linear regression line in Figure 6.323D is a fit of the data in Figure 6.33C; linearity of the *p*-HPA response stretched from 0.25-1.5 µM. The error bars represent the calculated standard deviation of the four-fold trials in 50 mM PBS, pH 7 at a working electrode potential of -100 mV vs. Ag/AgCl/ 3 M KCl.

Compared to the performance of EDEA/P(SS-GMA-BA)-Os/C1-modified graphite electrode modified (refer to Figure 6.34A), the *p*-HPA calibration trials with EDEA/P(SS-GMA-BA)-Os/C1-modified glassy carbon electrode (refer to Figure 6.34B) showed improved noise properties, a good reproducibility and also a suitable long term stability, respectively. Accordingly, the glassy carbon version of the proposed C1/Os(III) biosensors were chosen as standard for all further work with respect to *p*-HPA biomarker quantification, e.g. for calibrations in amperometric mode and *p*-HPA concentration between 0.25 and 10 µM in presence of 500 µM of the C1 substrate NADH.

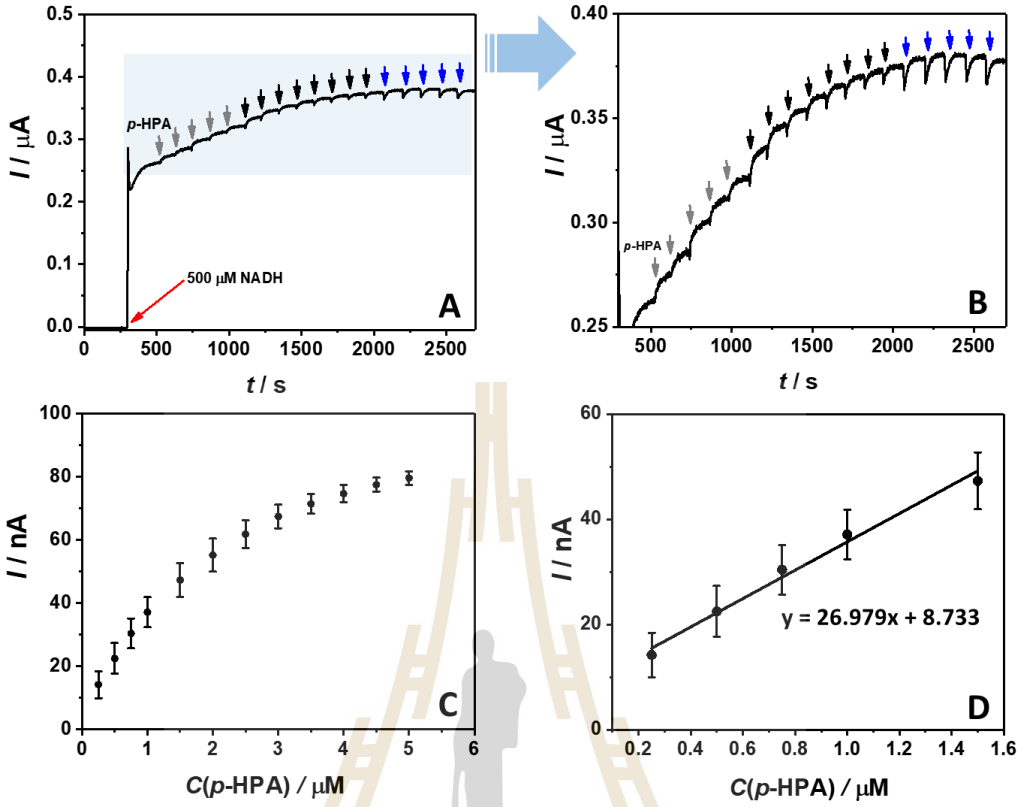

Figure 6.33 Optimization of an amperometric EDEA/P(SS-GMA-BA)-Os/C1-modified glassy carbon electrode. (A) Chronoamperogram of analyte concentrations between 0.25 to 10 μM (grey, black and blue arrows are indicating the incremental of *p*-HPA additions of 0.25 μM, 0.5 μM and 1.0 μM, respectively) in the presence of 500 μM substrate-NADH (red arrow, added at 300 s). (B) This chronoamperogram is a zoom-in from the trace in (A). (C) Calibration plot computed from the recordings in (B); data points are the average values for four independent experiments. (D) Linear regression plot is fitted from the data in (C). The error bars represent the calculated standard deviation of the four-fold trials in 50 μM PBS, pH 7 at a working electrode potential of -100 mV vs. Ag/AgCl/ 3 M KCl.

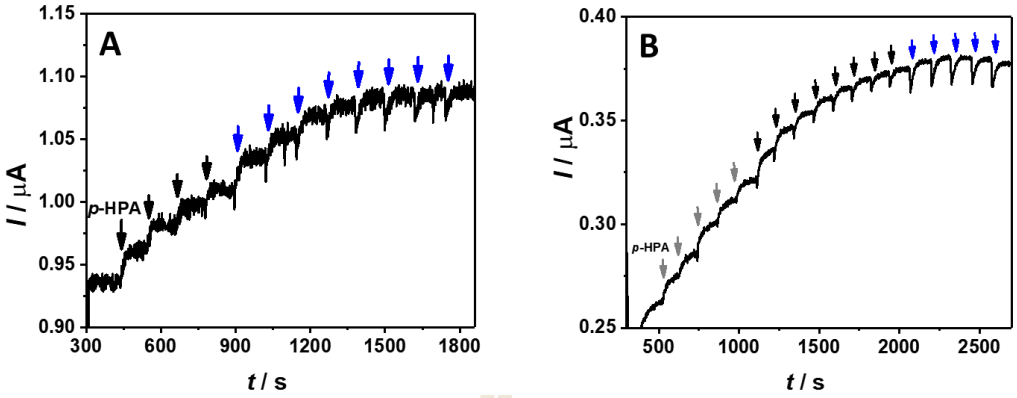

Figure 6.34 *I*/*t* traces of EDEA/P(SS-GMA-BA)-Os/C1modified (A) graphite electrodes and (B) glassy carbon electrode for *p*-HPA concentrations in the range of 0.25 – 10.0 μM (black and blue arrows are indicating the incremental of *p*-HPA additions of 0.25 μM, 0.5 μM and 1.0 μM, respectively) in the presence of 500 μM substrate-NADH in the absence (black curve) and in the presence of 100 μM (red curve); which is addition of NADH stock solution (grey arrows) the concentration of the substrate was increased by 50 μM. (C), at working potential of -100 mV vs. Ag/AgCl/3 M KCl). (B) The linear regression plots for the data in (A).

6.3.5 Cyclic voltammetry characterization of bare and C1/Os(III)-modified glassy carbon electrodes

Bare and modified glassy carbon electrodes were characterized by cyclic voltammetry in a PBS (50 mM, pH 7) containing 2 mM NADH. Measurements were carried out by cycling the potential between -0.4 to 0.2 V vs. Ag/AgCl/3 M KCl at a scan rate of 2 mV/s. Gentle oxidation of NADH at bare glassy carbon electrode was restricted to potentials above 100 mV vs Ag/AgCl/ 3 M KCl (Figure 6.35), indicating only a week oxidation of NADH directly at the glassy carbon electrode

surface. Evaluated was also the contribution direct electron transfer (DET) from the enzyme to the electrode to electrode current, with C1 embedded in the pristine polymer backbone P(SS-GMA-BA) in the absence and presence of 2 mM NADH. Cyclic voltammograms showed only a weak anodic current at potentials above -300 mV vs. Ag/AgCl/3 M KCl, indicating that no considerable electron transfer occurred between the redox-active C1 and the glassy carbon electrode (Figure 6.36A, blue trace).

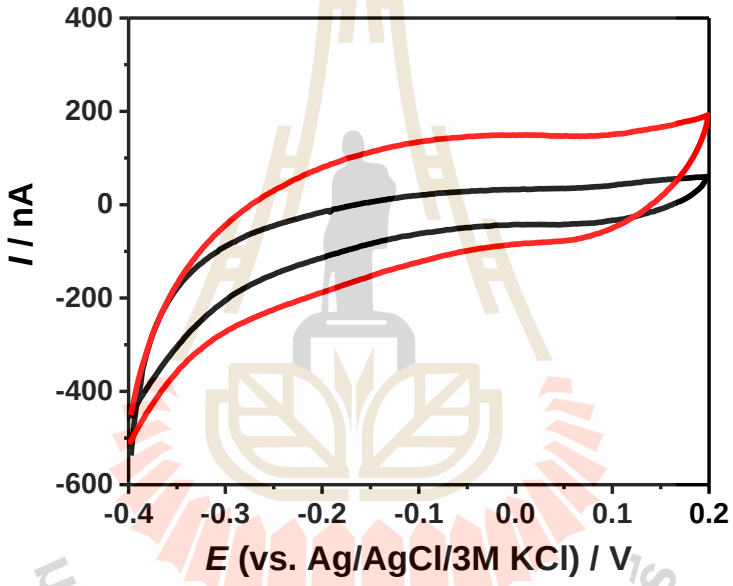

Figure 6.35 Cyclic voltammograms of a bare glassy carbon electrode in the absence (black trace) and presence of 2 mM NADH (red trace). Working electrolyte: deaerated, 50 mM PBS, pH 7, scan rate: 2 mV s^{-1}. Considerable anodic current due to the oxidation of NADH at the electrode surface were observed at potential above -0.1 V vs Ag/AgCl/3 M KCl.

The use of hydrophilic P(SS-GMA-BA) polymer backbone without bound Os-complexes, increase the signal stability but did not lead to catalytic currents.

Cyclic voltammograms of glassy carbon electrode modified with P(SS-GMA-BA)-Os/C1 films showed a well-defined catalytic response upon addition of the substrate NADH (Figure 6.36B). To avoid artefact caused by interfering O_2 all experiment with polymer/enzyme films were conducted in argon saturated electrolytes and argon atmosphere, since the low potential Os-complex catalyzes the oxygen reduction and O_2 represents the natural electron acceptor for the isolated C1 unit.

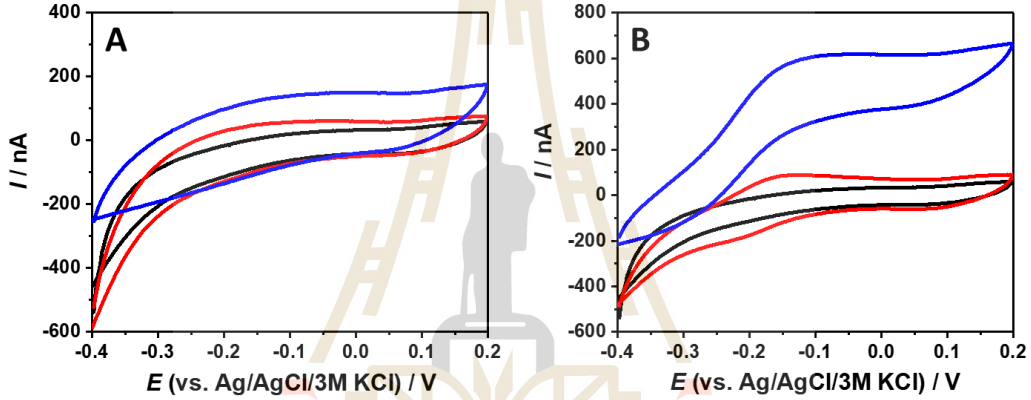

Figure 6.36 Cyclic voltammograms recorded on bare and modified electrodes in 50 mM PBS with and without NADH. The oxidation of NADH with C1 recycling via direct electron transfer (absence of polymer bound Os (III) mediator). Black line: background current recorded with the bare glassy carbon electrode in the absence of NADH; red line: C1 embedded in the pristine polymer backbone P(SS-GMA-BA) in the absence of NADH, blue line: C1 embedded in the pristine polymer backbone P(SS-GMA-BA), 2 mM NADH. Working electrolyte: deaerated 50 mM PBS, pH 7, and scan rate 2 mV/s.

6.3.6 Amperometric quantification of *p*-HPA at EDEA/P(SS-GMA-BA)-Os/C1-modified glassy carbon electrode

The accomplishment of redox polymer/allosteric enzyme-based biosensing for *p*-HPA suggested the realization of urine sample analysis. However, in test trials the novel electrochemical *p*-HPA biomarker assay was first applied to the assessment of model samples with a nominal analyte concentration of 0.25 μM. To investigate the accuracy of the *p*-HPA biosensor, the recovery performance was determined by seven-fold repetitions of standard addition measurements in 5 mL PBS (50 mM, pH 7) contained saturation of 500 μM NADH.

Figure 6.37A, offered as a representative example, is one of seven original amperometric recordings, showing four stepped currents increase on addition of *p*-HPA to the measuring buffer (5 mL). Figure 6.37B is a standard addition plot constructed from the data in Figure 6.37A. In this particular case, the *p*-HPA sample concentration determined was 49.65 μM (*200-fold dilutions factor), equivalent to a recovery rate of 99.30% for the 50 μM sample. The average recovery rates for the seven *p*-HPA quantification was 95 ± 4 (0.24 ± 0.01 μM; see Table 6.6 for the individual values) with demonstrated that allosteric activator *p*-HPA in a EDEA/P(SS GMA-BA)-Os mixture worked efficiently and reproducibly for accurate quantification of *p*-HPA.

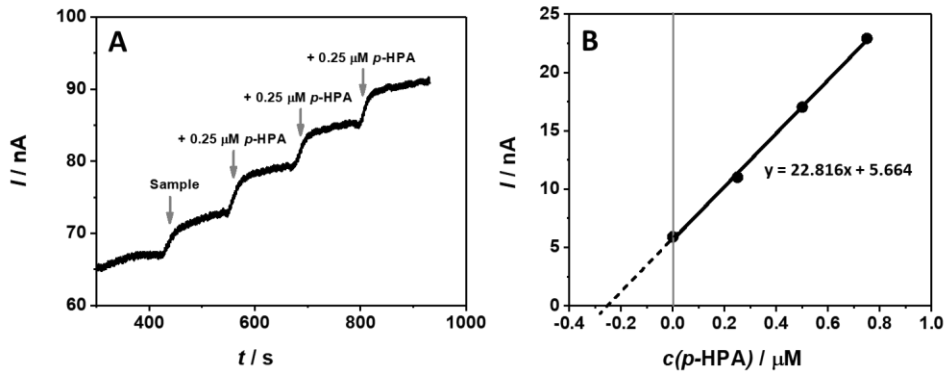

Figure 6.37 Detection of *p*-HPA with a EDEA/P(SS-GMA-BA)-Os/C1 electrode use in the standard addition mode. (A) Representative chronoamperogram for an initial addition of 0.25 µM *p*-HPA ("sample") and three subsequent 0.25 µM additions. The electrolyte was 50 mM BPS, pH 7, and the working electrode potential of -100 mV vs. Ag/AgCl/3 M KCl. (B) Standard addition plot constructed with the data of the *I*/*t* curve in (A) and evaluation of the test concentration (0.248 µM), and the recovery (99.2%) from the linear regression line.

From the standard addition of background current in chronoamperometric experiments (eight blank measurements) and with the linear regression of the *I*-*c* curves (sensitivity; see Figure 6.33) the limit of detection (LOD) in the presence 500 µM NADH was estimated to be about 0.38 µM.

Of note, reused electrodes showed a lower current response than freshly prepared sensors. Thus, we conclude that the developed sensor is suitable for single use only and freshly prepared items should be employed for quantification trials. Nevertheless, the electrodes show good recovery rates and demonstrated high reproducibility.

Table 6.6 Detection of *p*-HPA by means of the method of standard addition. Solution level was adjusted to a nominal *p*-HPA concentration of 0.25 µM (in 5 mL), followed by the subsequent addition of three *p*-HPA standard additions. The initial adjusted "sample" *p*-HPA concentration was then estimated from *I*-*C* plots at $I = 0$ via linear regression of the individual data points. Working electrolyte and potential for the trial were deaerated 50 mM PBS, pH 7 and -100 mV vs. Ag/AgCl, 3M KCl, respectively.

experiment	*c*(p-HPA) / µM		R^2 of linear regression	recovery rate
	adjusted	found		
1	0.250	0.248	0.9987	99.20
2	0.250	0.228	0.9989	91.20
3	0.250	0.247	0.9867	98.80
4	0.250	0.230	0.9999	92.00
5	0.250	0.233	0.9961	93,20
6	0.250	0.231	0.9994	92.40
7	0.250	0.236	0.9981	94.40
mean values	0.24 ± 0.01			95 ± 4

6.3.7 Use of allosteric C1/Os(III) biosensors for amperometric quantification of *p*-HPA in artificial urine sample measured in phosphate buffer electrolyte

The performance of the accomplished analytical scheme with the reductase-C1 operational component of an Os (III) redox polymer films on a sensor surface was tested for the quantification of *p*-HPA in artificial urine samples. Trials were carried out with home-made artificial urine (AU) medium (pH 6.6), that was prepared following a recipe published by Brooks and Keevil (1997). Insights in the

ability to measure the target analyte properly in artificial urine was important because of the many common biological interferences that may be there in human urine and might interfere catalytic signals during *p*-HPA experiments. AU is an accepted replacement for human urine and routinely used a simple “close to real matrix” for model experiments, before finally the move to, for instance, clinical patient urine (which requires ethical approvals) is approached (Brooks and Keevil, 1997).

The recovery rate was determined by adding 25 μL of *p*-HPA stock solution into artificial urine to generate an AU sample which was then spiked into measurement buffer for the amperometric measurement. Eight-fold repetitions of the standard addition quantifications in PBS (50 mM, pH 7) were carried out in the presence of 500 μM NADH as substrate partner of the immobilized C1 on the biosensor surface. Figure 6.38A, as a representative example, is one of the eight original amperometric recordings, showing four stepped currents increases after the addition of the *p*-HPA-containing AU sample to the measuring buffer. Figure 6.38B is a standard addition plot constructed from the data in figure 6.38A. It was found that the calculated extrapolation of the regression line to zero current estimated *p*-HPA concentration of 0.262 μM, considering the previous 200-fold dilution of the spike home-made artificial urine sample into PBS (50 mM, pH 7). In this particular case, the spike *p*-HPA sample concentration determined was 52.40 μM, with acceptable recovery rate of 104.80% for the 50 μM sample. The average recovery rate for eight *p*-HPA quantification with independence electrodes preparations was 101 ± 5 (50.13 ± 2.75, see Table 6.7 for the individual values).

Bare AU was added at completion of the standard addition experiment to the measuring buffer and the recording of current was continued (refer

to Figure 6.39, blue arrows). The absence of significant current elevations verified that the many components in the artificial urine medium did not cause the biosensor to respond and thus confirmed interference-free *p*-HPA detection, at least in artificial urine.

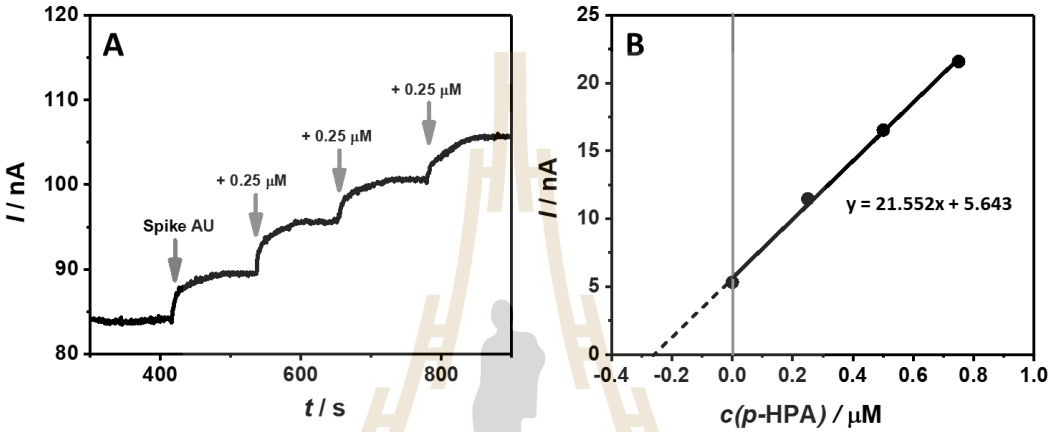

Figure 6.38 Detection of *p*-HPA in spiked artificial urine with a EDEA/P(SS-GMA-BA)-Os/C1 electrode worked with in the standard addition mode. (A) Representative chronoamperogram for with an initial addition of 25 µL known sample solution and three subsequent 0.25 µM standard additions. The measuring electrolyte was 50 mM BPS, pH 7 and the working electrode potential of -100 mV vs. Ag/AgCl/3 M KCl. (B) Standard addition plot constructed with the data of the *I*/*t* curve in (A) and evaluation of the test concentration (0.262 µM), and the recovery (104.80%) from the linear regression line.

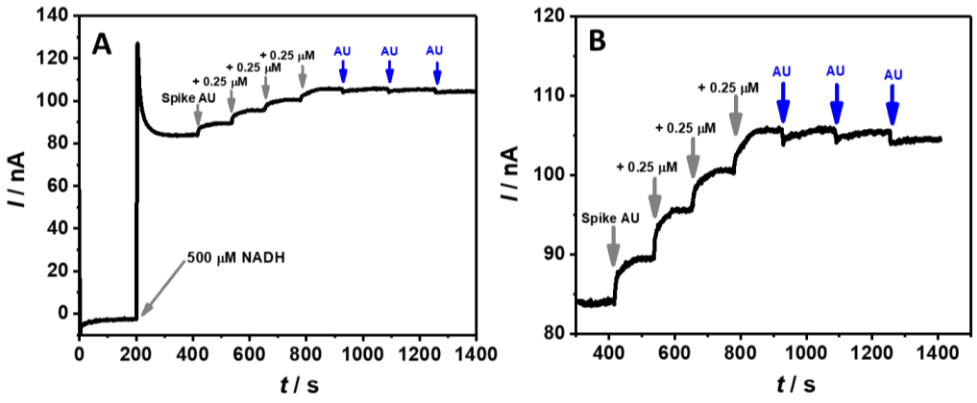

Figure 6.39 (A) Representative chronoamperogram for with an initial addition of 25 µL spike home-made artificial urine sample solution, three subsequence of 0.25 µM additions (gray arrows) *p*-HPA standard stock solution and three subsequence of 25 µL additions (blue arrows) of bare artificial urine solution. The electrolyte was 50 mM BPS, pH 7 and the working electrode potential of -100 mV vs. Ag/AgCl/3 M KCl. (B) *I*/*t* curve is zoomed-in from (A).

The reproducibility of the modified electrode was analyzed comparing the response current of eight different sensor electrodes to 0.25 µM of *p*-HPA. All the sensor exhibited similar response current and variation of only 5.49% was observed. This indicates that the fabrication process optimized is very reliable and uniform, which is a good basis for the development of a new strategy for an electrochemical determination of *p*-HPA for disease biomarkers, via combination of an allosteric redox enzyme with a redox polymer.

Table 6.7 Detection of *p*-HPA by means of the method of standard addition. Solution level was spiking to *p*-HPA concentration of 50 µM, followed by the subsequent addition of three *p*-HPA standard additions. The initial adjusted "sample" *p*-HPA concentration was then estimated from *I*-*c* plots at $I = 0$ via linear regression of the individual data points. Working electrolyte and potential for the trial were deaerated 50 mM PBS, pH 7 and -100 mV vs. Ag/AgCl, 3M KCl, respectively.

Experiment	*c*(p-HPA) / µM		R^2 of linear regression	recovery rate
	adjusted	found		
1	0.250	0.232	0.9987	92.8
2	0.250	0.262	0.9976	104.8
3	0.250	0.245	0.9993	98.0
4	0.250	0.246	0.9991	98.4
5	0.250	0.255	0.9999	102.0
6	0.250	0.239	0.9999	95.6
7	0.250	0.266	0.9981	106.4
8	0.250	0.266	0.9963	106.4
mean values	0.25 ± 0.01			101 ± 5

6.3.8 Use of allosteric C1/Os(III) biosensors for amperometric quantification of *p*-HPA in artificial urine sample measured in artificial urine

Since *p*-HPA is an important urinary disease biomarker we tested the suitability of the proposed sensor scheme for quantification of the target analyte in artificial urine samples, by the standard addition procedure (for the composition of the artificial urine see Table 6.8 and/or (Zhou *et al.*, 2011)).

Table 6.8 Detection of *p*-HPA by the standard addition method in 50 mM phosphate buffer (PB, pH 7) or artificial urine (AU, pH 7 and 8) containing added *p*-HPA. The solution concentration of *p*-HPA was adjusted to a nominal 0.250 µM, with three subsequent standard additions. The initial adjusted sample concentration was estimated from *I*-*c* plots at $I = 0$ A by linear regression through the individual data points. Sensitivities were estimated from the slope of the *I*-*c* plots. Note that the concentrations were adjusted to be within the linear detection range of the sensor. Applied potential for all experiments was -100 mV vs. Ag/AgCl, 3M KCl.

entry	working electrolyte	p-HPA in	*c*(*p*-HPA) / µM		recovery rate / %	sensitivity / nA µM^{-1}
			adjusted	found		
1	PB, pH 7	PB, pH 7	0.25	(0.24 ± 0.01)	(95 ± 4)	(26 ± 5)
2	PB, pH 7	AU, pH 7	0.25	(0.25 ± 0.01)	(101 ± 5)	(24 ± 7)
3	AU, pH 7	AU, pH 7	0.25	(0.26 ± 0.02)	(103 ± 7)	(20 ± 5)
4	AU, pH 8	AU, pH 8	0.25	(0.26 ± 0.01)	(106 ± 2)	(20 ± 7)

With this result and aiming for a point-of-care device that could be used directly for measurements in the sample matrix, i.e. in urine, we examined the applicability of the developed sensor to direct quantification of *p*-HPA in artificial urine, without using any background electrolyte or buffer system for dilution. Artificial urine contains salts such as NaCl (90 mM) and NH_4Cl (25 mM) in rather high concentrations, so the addition of an external supporting electrolyte is unnecessary. Moreover, the low-potential polymer-bound Os-complex based electron mediator that ensures an operational potential of -100 mV vs. Ag/AgCl/3 M KCl should exclude unwanted side-reactions such as the co-oxidation of uric acid (0.4 mM) or other redox-active components of the sample solution.

Figure 6.40A depicts the chronoamperometric response during a standard addition trial conducted in artificial urine (pH 7) as supporting electrolyte. The analyte sample (nominal concentration = 0.25 µM) was first added to the solution, followed by three standard additions that increased the *p*-HPA concentration in steps of 0.25 µM. Quantitative analysis (Figure 6.40B) estimated the sample concentration at 0.266 µM, corresponding to a recovery of 106.40%. Mean values for the estimated concentration, recovery and sensitivity over four independent standard additions (Table S4) were 0.26 ± 0.02 µM, 103 ± 7% and 20 ± 5 nA μM^{-1}, respectively (Table 6.8, entry 3). The slightly lower sensitivity might be due to the effects of the artificial urine on the polymer matrix. The limit of detection in the artificial urine was estimated to be 0.164 µM, which is somewhat higher than in pure phosphate buffer, indicating some matrix effects. However, our results unambiguously demonstrate that quantification of *p*-HPA in artificial urine with the proposed sensor scheme is possible in a reproducible and reliable manner.

Evidently, the high selectivity of the C1-reductase component of *p*-HPA hydroxylase ensures a straightforward measurement protocol for the quantification of the urinary disease biomarker *p*-HPA that circumvents complex sample pre-treatments such as derivatisation (NMR) or separation (HPLC). In the medical diagnostic literature the *p*-HPA content of urine is generally reported relative to the creatinine content, as µg *p*-HPA per g creatinine, since creatinine excretion is relatively constant and unaffected by changes in metabolism (Hoffmann *et al.*, 1989; Zafar *et al.*, 2011). The detection limit referenced to creatinine was estimated to be 31 µg $(g\ creatinine)^{-1}$, which is within the range of the *p*-HPA content of normal urine (21-52 µg $(g\ creatinine)^{-1}$, measured by GC-MS (Shanaiah *et al.*, 2007)) and comparable to

detection ranges with other more complex techniques such as NMR (Shin *et al.*, 2015).

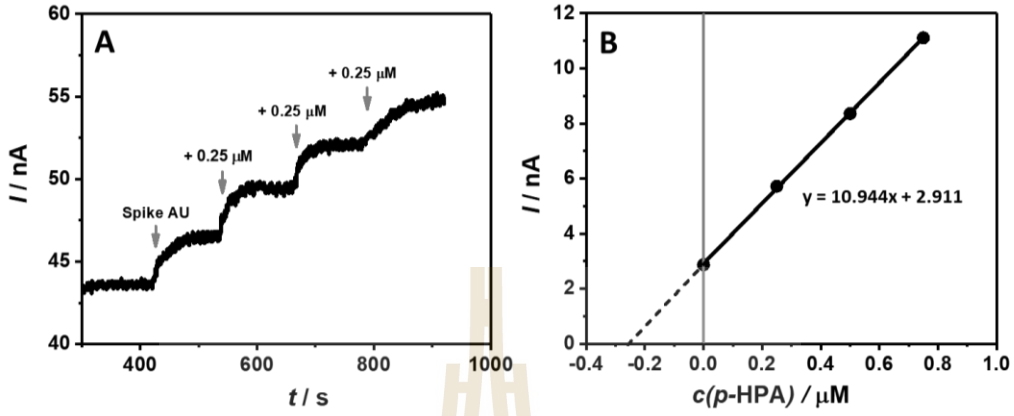

Figure 6.40 Representative chronoamperogram for with an initial addition of 25 µL spike home-made artificial urine sample solution, three subsequence of 0.25 µM additions (gray arrows) *p*-HPA standard stock solution and three subsequence of 25 µL additions (blue arrows) of bare artificial urine solution (A). The electrolyte was artificial urine, pH 7 and the working electrode potential of -100 mV vs. Ag/AgCl/3 M KCl. (B) *I*/*t* curve is zoomed-in from (A)

6.3.9 Effect of the pH value on biosensor performance

Since the pH value of urine may vary, depending on the human subject's state of health, nutrition, fluid uptake or ingestion of drugs (Brooks and Keevil, 1997), and the C1-componet shows a rather constant activity within a pH range of 6.0 to 8.0 (see Experimental Section), we further evaluated the operational pH-window of the proposed sensor by carrying out *p*-HPA quantification at various pH values, i.e. under slightly basic (pH 8) and acidic conditions (pH 6.6). As can be seen in Figure 6.41A, chronoamperometric *p*-HPA measurements in artificial urine at pH 8 (adjusted by adding 6 M NaOH) show a reasonably stable current output in the absence

and presence of the analyte p-HPA (note that measurements at pH 8 in 50 mM phosphate buffer show the same trend, Figure 6.42A). Mean values from four independent standard addition experiments (Table 6.9) determined from the corresponding *I*-*c* plots (Figure 6.41B) were (0.26 ± 0.01) µM and (106 ± 2) %, for the concentration and the corresponding recovery, respectively. The sensitivity for the biosensor operation at pH 8 was estimated to be (20 ± 7) nA µM-1. Apparently, both values are slightly smaller than the values obtained in phosphate buffer of the same pH, indicating a small influence of the measuring environment on sensor performance. However, since the standard deviations for the different conditions are overlapping, the effect is insignificant.

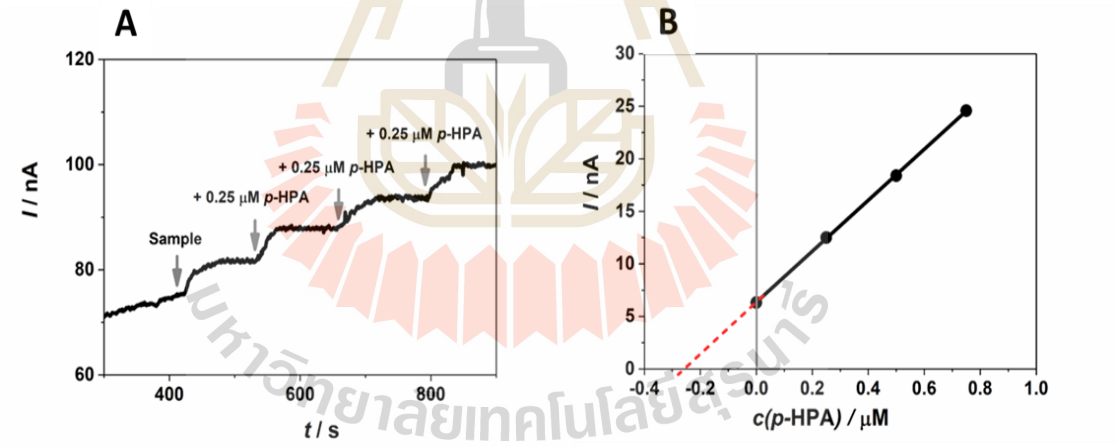

Figure 6.41 (A) Representative chronoamperogram for with an initial addition of 25 µL spike home-made artificial urine sample solution, three subsequence of 0.25 µM additions (gray arrows) *p*-HPA standard stock solution and three subsequence of 25 µL additions (blue arrows) of bare artificial urine solution. The electrolyte was artificial urine, pH 8 and the working electrode potential of -100 mV vs. Ag/AgCl/3 M KCl. (B) *I*/*t* curve is zoomed-in from (A).

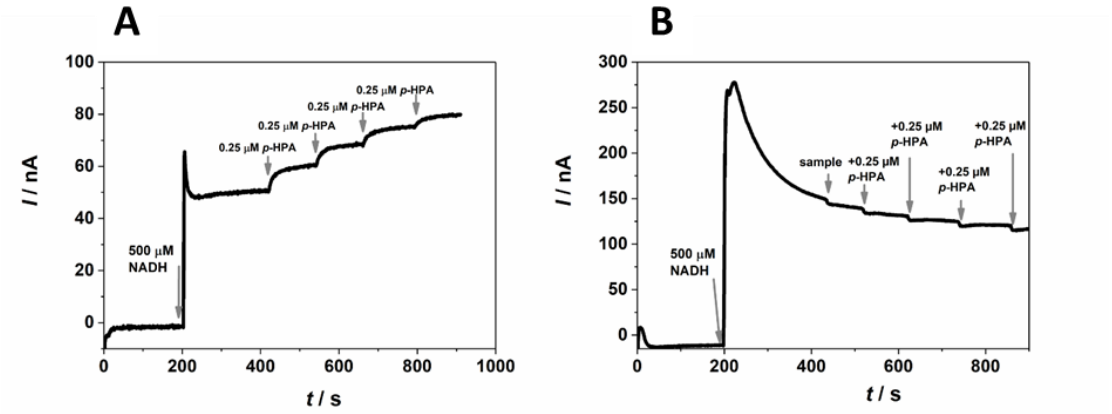

Figure 6.42 Chronoamperometric response measured for a P(SS-GMA-BA)-Os/EDEA/C1-modified glassy carbon electrode in 50 mM PBS at pH 8 (A) and in artificial urine at pH 6.6 (B). Applied potential: -100 mV vs Ag/AgCl/3 M KCl.

In contrast, standard addition measurements in artificial urine at pH 6.6 (adjusted by adding appropriate aliquots of 6 M aqueous HCl) were unsuccessful, as a continuous decrease of the current response was observed even before electrolyte supplementation with the analyte (Figure 6.42B). Thus, quantification in urine of this acidity was not possible with the proposed detection scheme. Moreover, biosensor operation in 50 mM phosphate buffer of pH 6.6 did not show any significant current response. Loss of function at the lower pH value is likely to be due to a decrease of C1-hpah activity in the immobilized/polymer-embedded state (note that the decrease in solution is only little, see Experimental Section) and, though to lesser extent, to a reduced hydrophilicity of the polymer film due to partial protonation of the sulfonate groups. However, in this electrolyte the initial current is significantly lower than that obtained in artificial urine. We therefore conclude that not only effects on the polymer matrix are responsible for the poor current response at this pH value, but that the low pH value itself causes this effect.

Table 6.9 Detection of *p*-HPA by means of the standard addition method measured in artificial urine at pH 8 spiked with samples of *p*-HPA dissolved in artificial urine (pH 8). Solution level was adjusted to a nominal *p*-HPA concentration of 0.250 µM, followed by the subsequent addition of three *p*-HPA standard additions. The initial adjusted sample concentration was estimated from *I*-*c* plots at I = 0 A via linear regression of the individual data points. Working electrolyte: deaerated artificial urine, pH 8; applied potential: -100 mV vs. Ag/AgCl, 3M KCl.

Experiment	*c*(p-HPA) / µM		R^2 of linear regression	recovery rate
	adjusted	found		
1	0.250	0.268	0.9987	107.2
2	0.250	0.257	0.9989	102.8
3	0.250	0.262	0.9999	104.8
4	0.250	0.269	0.9999	107.6
mean values		0.26 ± 0.01		106 ± 2

CHAPTER VII

CONCLUSION

The work within this PhD study aimed at the development of an advanced amperometric biosensing of phenolic urinary human disease biomarker *p*-HPA based on utilization of an allosteric bacterial reductase, the C1 of A. *Acinetobacter baumannii* that has NADH as substrate and is up-tuned in biocatalytic activity by the target analyte. Utilization of enzyme allostery for simple electrochemical biosensing in general and human disease biomarker electroanalysis in particular has not been described in literature and the thesis project objectives had thus a high level of innovative touch.

In a first part of thesis efforts C1 was worked with as dissolved species and substrate conversion and allosteric effector activity amplification took place as response to interaction in the measuring solution, which was a phosphate buffer as electrolyte. Enzymatically produced H_2O_2 was detected and quantified through a low-potential cathodic amperometry at Prussian blue-modified screen-printed electrode platforms. The methodology allowed with good enough sensitivity and response stability the electrochemical visualization of C1-driven turnover of NADH into NAD^+, both in absence of *p*-HPA at unstimulated rate and in presence of *p*-HPA at allosterically increased speed of enzymic reaction. Amperometric *p*-HPA calibrations based on the detection principles were successful and delivered an electrochemical version of affinity binding curves for the C1 interaction with best effector *p*-HPA and some other phenol derivatives with lesser allosteric power. The electrochemically derived ranking

of the strength of the allosteric power of the tested phenols was well in line with the one from published biochemical studies and also with the results from own alternative affinity inspections via Isothermal Calorimetry, ITC. The move to applications of the methodology for quantitative *p*-HPA has not been attempted in this thesis as the more important focus was placed on a transfer of the gained insights in C1/*p*-HPA electroanalysis to the fabrication of a reagent less amperometric biosensor with the enzyme immobilized on polarized electrode disks. However, the data that was compiled here is clearly pointing out the potential of an amperometric H_2O_2 screen at PB-SPEs for the C1-assisted determination of *p*-HPA in clinical samples.

The second and third thesis part dealt thoroughly with the realization of C1-based amperometric biosensor for quantitative NADH and *p*-HPA analysis. Considered was the immobilization of the chosen reductase as biological recognition element into an Osmium (III)-based redox polymer film on graphite or glassy carbon electrode disks. In the targeted biosensor configuration, chains of complexed Os (III) centers along elongated and tangled matrix polymer strings make electrical connection between the immobilized redox protein and a graphite electrode disc, transducing enzymic oxidation of β-NADH into a biosensor current. Use of a redox polymer with a formal potential that matched the redox switch of the embedded reductase and avoided interfering redox interactions and the formation of a crosslinked redox polymer matrix for stable enzyme entrapment indeed led to biosensing tools that allowed sustainable low-potential and thus interference-free anodic signaling of both NADH and, more important, p-HPA, too. The activity of the chosen reductase remained in the immobilized state to be enhanced on binding of an effector, p-hydroxy-phenylacetic acid (p-HPA), allowing the acceleration of the substrate conversion rate on the sensor surface by in-situ addition or

pre-incubation with *p*-HPA. Acceleration of *β*-NADH oxidation amplified the response of the biosensor, with a 1.5-fold increase in the sensitivity of analyte detection, compared to operation without the allosteric activator. Repetitive quantitative testing of solutions of known β-NADH concentration verified the performance in terms of reliability and analyte recovery and proved the suitability of the methodology as novel and advanced approach for NADH electroanalysis.

The pronounced concentration-dependence of allosteric C1-hpah activation in the presence of a constant concentration of NADH further allowed sensitive quantification of the target, *p*-HPA, and the deliberate adapting choice of an immobilizing redox polymer with suitably low working potential allowed biosensor operation without the risk of co-oxidation of potentially interfering substances, such as uric acid or ascorbic acid. Optimized sensor versions worked well for *p*-HPA determination in the complex milieu of artificial urine, with good recovery rates and reproducibility and sub-micromolar detection limits. This use of the allosteric enzyme C1-hpah for *p*-HPA trace electroanalysis is the first successful example of simple amperometric redox enzyme/redox polymer biosensing in which the analyte acts as an effector, regulating the activity of an embedded signaling biocatalyst. Application of this methodology to chip-based sensor platforms should permit the development of a hand-held device for point-of-care urinary *p*-HPA testing, like the polymer/enzyme blood-glucose meters. A general advantage of the concept of allosterically enabled biosensing is its ability to broaden the range of approachable analytes, through the move from substrate to effector detection.

Proposed for future work is a focus on the application of the above described methodologies for C1-based electroanalysis of the *p*-HPA as disease biomarker in

clinical samples of patients of related illnesses. Also recommended are studies that explore whether the modern techniques of synthetic biology and/or protein/enzyme engineering may help to create C1 mutants that offer higher specificity and higher power of the allosteric interaction with *p*-HPA, and thus a further improved quality of the developed kind of biosensing of the particular effector. And searched for should of course be for other enzyme/effector couples that might be appealing candidates for an integration into the biosensing principles of this thesis for the detection of other biomarkers than *p*-HPA.

REFERENCES

REFERENCES

Abdelwahab, A. A. (2016). Electrochemical Pretreatment of Graphene Composite Cnt Encapsulated Au Nanoparticles for H2o2 Sensor. **Electroanalysis**. 28(8): 1901-1906.

Acworth, I. N. (1997). *Coulometric Electrode Array Detectors for Hplc* (Vol. 6): Vsp.

Adamko, D., Rowe, B. H., Marrie, T., and Sykes, B. D. (2007). Variation of Metabolites in Normal Human Urine. **Metabolomics**. 3(4): 439-451.

Albareda-Sirvent, M., Merkoci, A., and Alegret, S. (2000). Configurations Used in the Design of Screen-Printed Enzymatic Biosensors. A Review. **Sensors and Actuators B: Chemical**. 69(1): 153-163.

An, M., and Gao, Y. (2015). Urinary Biomarkers of Brain Diseases. **Genomics, Proteomics & Bioinformatics**. 13(6): 345-354.

Aoyama, Y., Yamagishi, A., Asagawa, M., Toi, H., and Ogoshi, H. (1988). Molecular Recognition. 2. Molecular Recognition of Amino Acids: Two-Point Fixation of Amino Acids with Bifunctional Metalloporphyrin Receptors. **Journal of the American Chemical Society**. 110(12): 4076-4077.

Bai, Y., Yang, H., Yang, W., Li, Y., and Sun, C. (2007). Gold Nanoparticles-Mesoporous Silica Composite Used as an Enzyme Immobilization Matrix for Amperometric Glucose Biosensor Construction. **Sensors and Actuators B: Chemical**. 124(1): 179-186.

Bhalla, N., Jolly, P., Formisano, N., and Estrela, P. (2016). Introduction to Biosensors.

Essays in biochemistry. 60(1): 1-8.

Blakley, E. (1977). The Catabolism of L-Tyrosine by an Arthrobacter Sp. **Canadian Journal of Microbiology**. 23(9): 1128-1139.

Boyle, J. (2005). Lehninger Principles of Biochemistry: Nelson, D., and Cox, M. **Biochemistry and Molecular Biology Education**. 33(1): 74-75.

Brooks, T., and Keevil, C. (1997). A Simple Artificial Urine for the Growth of Urinary Pathogens. **Letters in Applied Microbiology**. 24(3): 203-206.

Chaiyen, P., Suadee, C., and Wilairat, P. (2001). A Novel Two-Protein Component Flavoprotein Hydroxylase. **European Journal of Biochemistry**. 268(21): 5550-5561.

Chalmers, R., Valman, H., and Liberman, M. (1979). Measurement of 4-Hydroxyphenylacetic Aciduria as a Screening Test for Small-Bowel Disease. **Clinical Chemistry**. 25(10): 1791-1794.

Chalmers, R. A., Healy, M., Lawson, A. M., Hart, J., and Watts, R. (1976). Urinary Organic Acids in Man. Iii. Quantitative Ranges and Patterns of Excretion in a Normal Population. **Clinical Chemistry**. 22(8): 1292-1298.

Chaubey, A., and Malhotra, B. D. (2002). Mediated Biosensors. **Biosensors and Bioelectronics**. 17(6-7): 441-456.

Cinti, S., Arduini, F., Moscone, D., Palleschi, G., and Killard, A. J. (2014). Development of a Hydrogen Peroxide Sensor Based on Screen-Printed Electrodes Modified with Inkjet-Printed Prussian Blue Nanoparticles. **Sensors**. 14(8): 14222-14234.

Cox, M. M., and Nelson, D. L. (2008). *Lehninger Principles of Biochemistry*: WH Freeman.

Crumbliss, A. L., Hill, H. A. O., and Page, D. J. (1986). The Electrochemistry of Hexacyanoruthenate at Carbon Electrodes and the Use of Ruthenium Compounds as Mediators in the Glucose/Glucose Oxidase System. **Journal of electroanalytical chemistry and interfacial electrochemistry**. 206(1-2): 327-331.

de Lumley-Woodyear, T., Rocca, P., Lindsay, J., Dror, Y., Freeman, A., and Heller, A. (1995). Polyacrylamide-Based Redox Polymer for Connecting Redox Centers of Enzymes to Electrodes. **Analytical Chemistry**. 67(8): 1332-1338.

de Mattos, I. L., Gorton, L., Laurell, T., Malinauskas, A., and Karyakin, A. A. (2000). Development of Biosensors Based on Hexacyanoferrates. **Talanta**. 52(5): 791-799.

de Mattos, I. L., Gorton, L., and Ruzgas, T. (2003). Sensor and Biosensor Based on Prussian Blue Modified Gold and Platinum Screen Printed Electrodes. **Biosensors and Bioelectronics**. 18(2): 193-200.

Dell'Erba, I., and Williams, R. (2006). Homopolymerization of Epoxy Monomers Initiated by 4-(Dimethylamino) Pyridine. **Polymer Engineering & Science**. 46(3): 351-359.

Di Cera, E. (2009). Kinetics of Allosteric Activation. **Methods in Enzymology**. 466: 259-271.

Dierckx, S., Van Puyvelde, S., Venken, L., Eberle, W., and Vanderleyden, J. (2015). Design and Construction of a Whole Cell Bacterial 4-Hydroxyphenylacetic Acid and 2-Phenylacetic Acid Bioassay. **Frontiers in Bioengineering and Biotechnology**. 3: 88.

Dong, J., Zhao, H., Qiao, F., Liu, P., Wang, X., and Ai, S. (2013). Quantum Dot Immobilized Acetylcholinesterase for the Determination of Organophosphate Pesticides Using Graphene-Chitosan Nanocomposite Modified Electrode. **Analytical Methods**. 5(11): 2866-2872.

Doyle, M. L. (1997). Characterization of Binding Interactions by Isothermal Titration Calorimetry. **Current Opinion in Biotechnology**. 8(1): 31-35.

Ellis, D., Eckhoff, M., and Neff, V. (1981). Electrochromism in the Mixed-Valence Hexacyanides. 1. Voltammetric and Spectral Studies of the Oxidation and Reduction of Thin Films of Prussian Blue. **The Journal of Physical Chemistry**. 85(9): 1225-1231.

Falconer, R. J. (2016). Applications of Isothermal Titration Calorimetry–the Research and Technical Developments from 2011 to 2015. **Journal of Molecular Recognition**. 29(10): 504-515.

Fava, M., and Kendler, K. S. (2000). Major Depressive Disorder. **Neuron**. 28(2): 335-341.

Flynn, J. H., and Wall, L. A. (1966). A Quick, Direct Method for the Determination of Activation Energy from Thermogravimetric Data. **Journal of Polymer Science Part C: Polymer Letters**. 4(5): 323-328.

Freyer, M. W., and Lewis, E. A. (2008). Isothermal Titration Calorimetry: Experimental Design, Data Analysis, and Probing Macromolecule/Ligand Binding and Kinetic Interactions. **Methods in Cell Biology**. 84: 79-113.

Garcıa-Jareno, J., Sanmatıas, A., Navarro-Laboulais, J., and Vicente, F. (1998). The Role of Potassium and Hydrogen Ions in the Prussian Blue⇄ Everitt's Salt Process. **Electrochimica Acta**. 44(2): 395-405.

Gerard, M., Chaubey, A., and Malhotra, B. D. (2002). Application of Conducting Polymers to Biosensors. **Biosensors and Bioelectronics**. 17(5): 345-359.

Gracin, S., and Rasmuson, Å. C. (2002). Solubility of Phenylacetic Acid, P-Hydroxyphenylacetic Acid, P-Aminophenylacetic Acid, P-Hydroxybenzoic Acid, and Ibuprofen in Pure Solvents. **Journal of Chemical & Engineering Data**. 47(6): 1379-1383.

Gregg, B. A., and Heller, A. (1991). Redox Polymer Films Containing Enzymes. 1. A Redox-Conducting Epoxy Cement: Synthesis, Characterization, and Electrocatalytic Oxidation of Hydroquinone. **The Journal of Physical Chemistry**. 95(15): 5970-5975.

Guascito, M., Chirizzi, D., Malitesta, C., Mazzotta, E., Siciliano, M., Siciliano, T., Tepore, A., and Turco, A. (2011). Low-Potential Sensitive H 2 O 2 Detection Based on Composite Micro Tubular Te Adsorbed on Platinum Electrode. **Biosensors and Bioelectronics**. 26(8): 3562-3569.

Guo, Z., Johnston, W. A., Stein, V., Kalimuthu, P., Perez-Alcala, S., Bernhardt, P. V., and Alexandrov, K. (2015). Engineering Pqq-Glucose Dehydrogenase into an Allosteric Electrochemical Ca2+ Sensor. **Chemical Communications**. 52(3): 485-488.

Haber, A., Ali, A. A.-Y., Aviram, M., and Gross, Z. (2013). Allosteric Inhibitors of Hmg-Coa Reductase, the Key Enzyme Involved in Cholesterol Biosynthesis. **Chemical Communications**. 49(93): 10917-10919.

Hashim, O. H., and Adnan, N. A. (1994). Coenzyme, Cofactor and Prosthetic Group—Ambiguous Biochemical Jargon. **Biochemistry and Molecular Biology Education**. 22(2): 93-94.

Heller, A. (1990). Electrical Wiring of Redox Enzymes. **Accounts of Chemical Research**. 23(5): 128-134.

Heller, A. (2006). Electron-Conducting Redox Hydrogels: Design, Characteristics and Synthesis. **Current Opinion in Chemical Biology**. 10(6): 664-672.

Heller, A., and Feldman, B. (2008). Electrochemical Glucose Sensors and Their Applications in Diabetes Management. **Chemical Reviews**. 108(7): 2482-2505.

Henderson, K. L., Francis, D. H., Lewis, E. A., and Emerson, J. P. (2016). Thermodynamics of Substrate Binding to the Metal Site in Homoprotocatechuate 2, 3-Dioxygenase: Using Itc under Anaerobic Conditions to Study Enzyme–Substrate Interactions. **Biochimica et Biophysica Acta (BBA)-General Subjects**. 1860(5): 910-916.

Herren, F., Fischer, P., Ludi, A., and Hälg, W. (1980). Neutron Diffraction Study of Prussian Blue, Fe4 [Fe (Cn) 6] 3. Xh2o. Location of Water Molecules and Long-Range Magnetic Order. **Inorganic Chemistry**. 19(4): 956-959.

Hoehn, T., Janssen, S., Mani, A. R., Brauers, G., Moore, K. P., Schadewaldt, P., and Mayatepek, E. (2008). Urinary Excretion of the Nitrotyrosine Metabolite 3-Nitro-4-Hydroxyphenylacetic Acid in Preterm and Term Infants. **Neonatology**. 93(2): 73-76.

Hoffmann, G., Aramaki, S., Blum-Hoffmann, E., Nyhan, W. L., and Sweetman, L. (1989). Quantitative Analysis for Organic Acids in Biological Samples: Batch Isolation Followed by Gas Chromatographic-Mass Spectrometric Analysis. **Clinical Chemistry**. 35(4): 587-595.

Hušek, P., Švagera, Z., Hanzlíková, D., Řimnáčová, L., Zahradníčková, H., Opekarová, I., and Šimek, P. (2016). Profiling of Urinary Amino-Carboxylic Metabolites by

in-Situ Heptafluorobutyl Chloroformate Mediated Sample Preparation and Gas Chromatography–Mass Spectrometry. **Journal of Chromatography A**. 1443: 211-232.

Itaya, K., Ataka, T., and Toshima, S. (1982). Spectroelectrochemistry and Electrochemical Preparation Method of Prussian Blue Modified Electrodes. **Journal of the American Chemical Society**. 104(18): 4767-4772.

Jaikaew, W., Patanakul, R., and Schulte, A. (2016). Electrical Cable-Based Copper Disk Electrodes as Oxidase Biosensor Platforms with Cathodic H2o2 Readout. **Electroanalysis**.

Jung, J., Jung, Y., Bang, E. J., Cho, S.-i., Jang, Y.-J., Kwak, J.-M., Park, S., and Hwang, G.-S. (2014). Noninvasive Diagnosis and Evaluation of Curative Surgery for Gastric Cancer by Using Nmr-Based Metabolomic Profiling. **Annals of Surgical Oncology**. 21(4): 736-742.

Karyakin, A. A. (2001). Prussian Blue and Its Analogues: Electrochemistry and Analytical Applications. **Electroanalysis**. 13(10): 813-819.

Kishore, G., Sugumaran, M., and Vaidyanathan, C. (1976). Metabolism of Dl-(+/-)-Phenylalanine by Aspergillus Niger. **Journal of Bacteriology**. 128(1): 182-191.

Kobayashi, K., Koide, Y., and Shohmori, T. (1982). Determination of P-Hydroxyphenylacetic Acid in Cerebrospinal Fluid by High-Performance Liquid Chromatography with Electrochemical Detection. **Clinica Chimica Acta**. 123(1-2): 161-168.

Lankelma, J., and Poppe, H. (1976). Design and Characterization of a Coulometric Detector with a Glassy Carbon Electrode for High-Performance Liquid Chromatography. **Journal of Chromatography A**. 125(2): 375-388.

Leavitt, S., and Freire, E. (2001). Direct Measurement of Protein Binding Energetics by Isothermal Titration Calorimetry. **Current Opinion in Structural Biology**. 11(5): 560-566.

Lee, C.-H., Lin, T.-S., and Mou, C.-Y. (2009). Mesoporous Materials for Encapsulating Enzymes. **Nano Today**. 4(2): 165-179.

Lord, R. S., and Bralley, J. A. (2008). Clinical Applications of Urinary Organic Acids. Part 2. Dysbiosis Markers. **Alternative Medicine Review**. 13(4): 292-306.

Luan, H., Liu, L.-F., Tang, Z., Zhang, M., Chua, K.-K., Song, J.-X., Mok, V. C., Li, M., and Cai, Z. (2015). Comprehensive Urinary Metabolomic Profiling and Identification of Potential Noninvasive Marker for Idiopathic Parkinson's Disease. **Scientific Reports**. 5(13): 1-11.

Mano, N., Mao, F., and Heller, A. (2003). Characteristics of a Miniature Compartment-Less Glucose− O2 Biofuel Cell and Its Operation in a Living Plant. **Journal of the American Chemical Society**. 125(21): 6588-6594.

Mao, F., Mano, N., and Heller, A. (2003). Long Tethers Binding Redox Centers to Polymer Backbones Enhance Electron Transport in Enzyme "Wiring" Hydrogels. **Journal of the American Chemical Society**. 125(16): 4951-4957.

Martinez, J. C., Murciano-Calles, J., Cobos, E. S., Iglesias-Bexiga, M., Luque, I., and Ruiz-Sanz, J. (2013). *Applications of Calorimetry in a Wide Context-Differential Scanning Calorimetry, Isothermal Titration Calorimetry and Microcalorimetry*: Amal Ali Elkordy.

Mast, N., Anderson, K. W., Johnson, K. M., Phan, T. T., Guengerich, F. P., and Pikuleva, I. A. (2017). In Vitro Cytochrome P450 46a1 (Cyp46a1) Activation by Neuroactive Compounds. **Journal of Biological Chemistry**. 292(31): 12934-

12946.

Matson, W. R., Langlais, P., Volicer, L., Gamache, P., Bird, E., and Mark, K. (1984). N-Electrode Three-Dimensional Liquid Chromatography with Electrochemical Detection for Determination of Neurotransmitters. **Clinical Chemistry**. 30(9): 1477-1488.

Miah, M. R., and Ohsaka, T. (2006). Cathodic Detection of H2o2 Using Iodide-Modified Gold Electrode in Alkaline Media. **Analytical Chemistry**. 78(4): 1200-1205.

Mor, J.-R., and Guarnaccia, R. (1977). Assay of Glucose Using an Electrochemical Enzymatic Sensor. **Analytical Biochemistry**. 79(1-2): 319-328.

Muthurasu, A., and Ganesh, V. (2014). Horseradish Peroxidase Enzyme Immobilized Graphene Quantum Dots as Electrochemical Biosensors. **Applied Biochemistry and Biotechnology**. 174(3): 945-959.

Nardini, M., and Ghiselli, A. (2004). Determination of Free and Bound Phenolic Acids in Beer. **Food Chemistry**. 84(1): 137-143.

Niraj, G., Varshney, H., Pandey, S., and Singh, S. (2012). Sensors for Diabetes. Glucose Biosensors by Using Different Newer Techniques: A Review. **International Journal of Theoretical and Applied**. 6: 28-37.

Ohara, T. (1995). Osmium Bipyridyl Redox Polymers Used in Enzyme Electrodes. **Platinum Metals Review**. 39(2): 54-62.

Ojanperä, I., Kolmonen, M., and Pelander, A. (2012). Current Use of High-Resolution Mass Spectrometry in Drug Screening Relevant to Clinical and Forensic Toxicology and Doping Control. **Analytical and Bioanalytical Chemistry**. 403(5): 1203-1220.

Ollila, F., Pentikäinen, O. T., Forss, S., Johnson, M. S., and Slotte, J. P. (2001). Characterization of Bile Salt/Cyclodextrin Interactions Using Isothermal Titration Calorimetry. **Langmuir**. 17(22): 7107-7111.

Papadopoulos, G., and Boskou, D. (1991). Antioxidant Effect of Natural Phenols on Olive Oil. **Journal of the American Oil Chemists Society**. 68(9): 669-671.

Phongsak, T., Sucharitakul, J., Thotsaporn, K., Oonanant, W., Yuvaniyama, J., Svasti, J., Ballou, D. P., and Chaiyen, P. (2012). The C-Terminal Domain of 4-Hydroxyphenylacetate 3-Hydroxylase from *Acinetobacter Baumannii* Is an Autoinhibitory Domain. **Journal of Biological Chemistry**. 287(31): 26213-26222.

Pinyou, P., Ruff, A., Pöller, S., Ma, S., Ludwig, R., and Schuhmann, W. (2016). Design of an Os Complex-Modified Hydrogel with Optimized Redox Potential for Biosensors and Biofuel Cells. **Chemistry-A European Journal**. 22(15): 5319-5326.

Pometto, A., and Crawford, D. (1985). L-Phenylalanine and L-Tyrosine Catabolism by Selected Streptomyces Species. **Applied and Environmental Microbiology**. 49(3): 727-729.

Prévoteau, A., and Mano, N. (2012). Oxygen Reduction on Redox Mediators May Affect Glucose Biosensors Based on “Wired” Enzymes. **Electrochimica Acta**. 68: 128-133.

Rahman, M. A., Park, D.-S., and Shim, Y.-B. (2004). A Performance Comparison of Choline Biosensors: Anodic or Cathodic Detections of H 2 O 2 Generated by Enzyme Immobilized on a Conducting Polymer. **Biosensors and Bioelectronics**. 19(12): 1565-1571.

Rajarathnam, K., and Rösgen, J. (2014). Isothermal Titration Calorimetry of Membrane Proteins—Progress and Challenges. **Biochimica et Biophysica Acta (BBA)-Biomembranes**. 1838(1): 69-77.

Ricci, F., Moscone, D., and Palleschi, G. (2007). Mediated Enzyme Screen-Printed Electrode Probes for Clinical, Environmental and Food Analysis. **Comprehensive analytical chemistry**. 49: 559-584.

Ricci, F., and Palleschi, G. (2005). Sensor and Biosensor Preparation, Optimisation and Applications of Prussian Blue Modified Electrodes. **Biosensors and Bioelectronics**. 21(3): 389-407.

Ruangchan, N., Tongsook, C., Sucharitakul, J., and Chaiyen, P. (2011). Ph-Dependent Studies Reveal an Efficient Hydroxylation Mechanism of the Oxygenase Component of P-Hydroxyphenylacetate 3-Hydroxylase. **Journal of Biological Chemistry**. 286(1): 223-233.

Ruff, A. (2017). Redox Polymers in Bioelectrochemistry: Common Playgrounds and Novel Concepts. **Current Opinion in Electrochemistry**.

Saboury, A. (2006). A Review on the Ligand Binding Studies by Isothermal Titration Calorimetry. **Journal of The Iranian Chemical Society**. 3(1): 1-21.

Schuhmann, W. (2002). Amperometric Enzyme Biosensors Based on Optimised Electron-Transfer Pathways and Non-Manual Immobilisation Procedures. **Reviews in Molecular Biotechnology**. 82(4): 425-441.

Shanaiah, N., Desilva, M. A., Gowda, G. N., Raftery, M. A., Hainline, B. E., and Raftery, D. (2007). Class Selection of Amino Acid Metabolites in Body Fluids Using Chemical Derivatization and Their Enhanced 13c Nmr. **Proceedings of The National Academy of Sciences**. 104(28): 11540-11544.

Shin, M., Kaplan, S. V., Raider, K. D., and Johnson, M. A. (2015). Simultaneous Measurement and Quantitation of 4-Hydroxyphenylacetic Acid and Dopamine with Fast-Scan Cyclic Voltammetry. **Analyst**. 140(9): 3039-3047.

Siangproh, W., Dungchai, W., Rattanarat, P., and Chailapakul, O. (2011). Nanoparticle-Based Electrochemical Detection in Conventional and Miniaturized Systems and Their Bioanalytical Applications: A Review. **Analytica Chimica Acta**. 690(1): 10-25.

Song, C., Zhang, S., and Huang, H. (2015). Choosing a Suitable Method for the Identification of Replication Origins in Microbial Genomes. **Frontiers in Microbiology**. 6: 1049.

Stec, D. F., Wang, S., Stothers, C., Avance, J., Denson, D., Harris, R., and Voziyan, P. (2015). Alterations of Urinary Metabolite Profile in Model Diabetic Nephropathy. **Biochemical Biophysical Research Communication**. 456(2): 610-614.

Sucharitakul, J., Chaiyen, P., Entsch, B., and Ballou, D. P. (2005). The Reductase of P-Hydroxyphenylacetate 3-Hydroxylase from Acinetobacter Baumannii Requires P-Hydroxyphenylacetate for Effective Catalysis. **Biochemistry**. 44(30): 10434-10442.

Sucharitakul, J., Chaiyen, P., Entsch, B., and Ballou, D. P. (2006). Kinetic Mechanisms of the Oxygenase from a Two-Component Enzyme, P-Hydroxyphenylacetate 3-Hydroxylase from Acinetobacter Baumannii. **Journal of Biological Chemistry**. 281(25): 17044-17053.

Sucharitakul, J., Phongsak, T., Entsch, B., Svasti, J., Chaiyen, P., and Ballou, D. P. (2007). Kinetics of a Two-Component P-Hydroxyphenylacetate Hydroxylase

Explain How Reduced Flavin Is Transferred from the Reductase to the Oxygenase. **Biochemistry**. 46(29): 8611-8623.

Sucharitakul, J., Tinikul, R., and Chaiyen, P. (2014). Mechanisms of Reduced Flavin Transfer in the Two-Component Flavin-Dependent Monooxygenases. **Archives of Biochemistry and Biophysics**. 555: 33-46.

Swain, J. F., and Gierasch, L. M. (2006). The Changing Landscape of Protein Allostery. **Current Opinion in Structural Biology**. 16(1): 102-108.

Tanaka, K., West-Dull, A., Hine, D. G., Lynn, T. B., and Lowe, T. (1980). Gas-Chromatographic Method of Analysis for Urinary Organic Acids. Ii. Description of the Procedure, and Its Application to Diagnosis of Patients with Organic Acidurias. **Clinical Chemistry**. 26(13): 1847-1853.

Taylor, C., Kenausis, G., Katakis, I., and Heller, A. (1995). "Wiring" of Glucose Oxidase within a Hydrogel Made with Polyvinyl Imidazole Complexed with [(Os-4, 4′-Dimethoxy-2, 2′-Bipyridine) Cl]$^{+/2+}$ 1. **Journal of Electroanalytical Chemistry**. 396(1-2): 511-515.

Thotsaporn, K., Sucharitakul, J., Wongratana, J., Suadee, C., and Chaiyen, P. (2004). Cloning and Expression of P-Hydroxyphenylacetate 3-Hydroxylase from Acinetobacter Baumannii: Evidence of the Divergence of Enzymes in the Class of Two-Protein Component Aromatic Hydroxylases. **Biochimica et Biophysica Acta (BBA)-Gene Structure and Expression**. 1680(1): 60-66.

Ticha, L. A., Baker, P. G., Abbo, H. S., Titinchi, S. J., and Iwuoha, E. I. (2014). Self-Assembled Monolayer of Cyclopentadienyl Ruthenium Thiolate Schiff Base-on-Gold, for Amperometric Detection of H2o2. **International Journal of Electrochemical Science**. 9: 7335-7350.

Tongsook, C., Sucharitakul, J., Thotsaporn, K., and Chaiyen, P. (2011). Interactions with the Substrate Phenolic Group Are Essential for Hydroxylation by the Oxygenase Component of P-Hydroxyphenylacetate 3-Hydroxylase. **Journal of Biological Chemistry**. 286(52): 44491-44502.

Vasylieva, N., Barnych, B., Meiller, A., Maucler, C., Pollegioni, L., Lin, J.-S., Barbier, D., and Marinesco, S. (2011). Covalent Enzyme Immobilization by Poly (Ethylene Glycol) Diglycidyl Ether (Pegde) for Microelectrode Biosensor Preparation. **Biosensors and Bioelectronics**. 26(10): 3993-4000.

Villaverde, A. (2003). Allosteric Enzymes as Biosensors for Molecular Diagnosis. **Federation of European Biochemical Societies Letters**. 554(1-2): 169-172.

Wang, J. (2008). Electrochemical Glucose Biosensors. **Chemical Reviews**. 108(2): 814-825.

Wang, Y., and Hasebe, Y. (2011). Carbon-Felt-Based Bioelectrocatalytic Flow-Detectors: Role of Ultrasound Irradiation During the Adsorption of Horseradish Peroxidase and Thionine for a Highly Sensitive Amperometric Determination of H2o2. **Analytical Sciences**. 27(6): 605-605.

Wijma, H. J., MacPherson, I., Alexandre, M., Diederix, R. E., Canters, G. W., Murphy, M. E., and Verbeet, M. P. (2006). A Rearranging Ligand Enables Allosteric Control of Catalytic Activity in Copper-Containing Nitrite Reductase. **Journal of Molecular Biology**. 358(4): 1081-1093.

Williams, D. L., Doig, A. R., and Korosi, A. (1970). Electrochemical-Enzymatic Analysis of Blood Glucose and Lactate. **Analytical Chemistry**. 42(1): 118-121.

Williamson, G., and Clifford, M. N. (2010). Colonic Metabolites of Berry Polyphenols: The Missing Link to Biological Activity? **British Journal of Nutrition**.

104(S3): S48-S66.

Wollenberger, U., and Scheller, F. W. (1993). Enzyme Activation for Activator and Enzyme Activity Measurement. **Biosensors and Bioelectronics**. 8(6): 291-297.

Woods, A. G., Wetie, A. G. N., Sokolowska, I., Russell, S., Ryan, J. P., Michel, T. M., Thome, J., and Darie, C. C. (2013). Mass Spectrometry as a Tool for Studying Autism Spectrum Disorder. **Journal of Molecular Psychiatry**. 1(1): 6.

Xue, G., Ishida, H., and Koenig, J. (1986). An Investigation of the Polymerization of Pyridine with Epoxy Compounds. **Polymer**. 27(7): 1134-1137.

Zafar, M. N., Wang, X., Sygmund, C., Ludwig, R., Leech, D., and Gorton, L. (2011). Electron-Transfer Studies with a New Flavin Adenine Dinucleotide Dependent Glucose Dehydrogenase and Osmium Polymers of Different Redox Potentials. **Analytical Chemistry**. 84(1): 334-341.

Zamora-Ros, R., Rabassa, M., Cherubini, A., Urpi-Sarda, M., Llorach, R., Bandinelli, S., Ferrucci, L., and Andres-Lacueva, C. (2011). Comparison of 24-H Volume and Creatinine-Corrected Total Urinary Polyphenol as a Biomarker of Total Dietary Polyphenols in the Invecchiare Inchianti Study. **Analytica Chimica Acta**. 704(1): 110-115.

Zamora-Ros, R., Touillaud, M., Rothwell, J. A., Romieu, I., and Scalbert, A. (2014). Measuring Exposure to the Polyphenol Metabolome in Observational Epidemiologic Studies: Current Tools and Applications and Their Limits. **The American Journal of Clinical Nutrition**. ajcn. 077743.

Zhou, C., Wang, J., Li, L., Wang, R., and Hong, M. (2011). A Palladium Chelating Complex of Ionic Water-Soluble Nitrogen-Containing Ligand: The Efficient Precatalyst for Suzuki–Miyaura Reaction in Water. **Green Chemistry**. 13(8):

2100-2106.

Zhu, L., and Anslyn, E. V. (2006). Signal Amplification by Allosteric Catalysis. **Angewandte Chemie International Edition**. 45(8): 1190-1196.

Zorn, J. A., and Wells, J. A. (2010). Turning Enzymes on with Small Molecules. **Nature Chemical Biology**. 6(3): 179-188.

APPENDICES

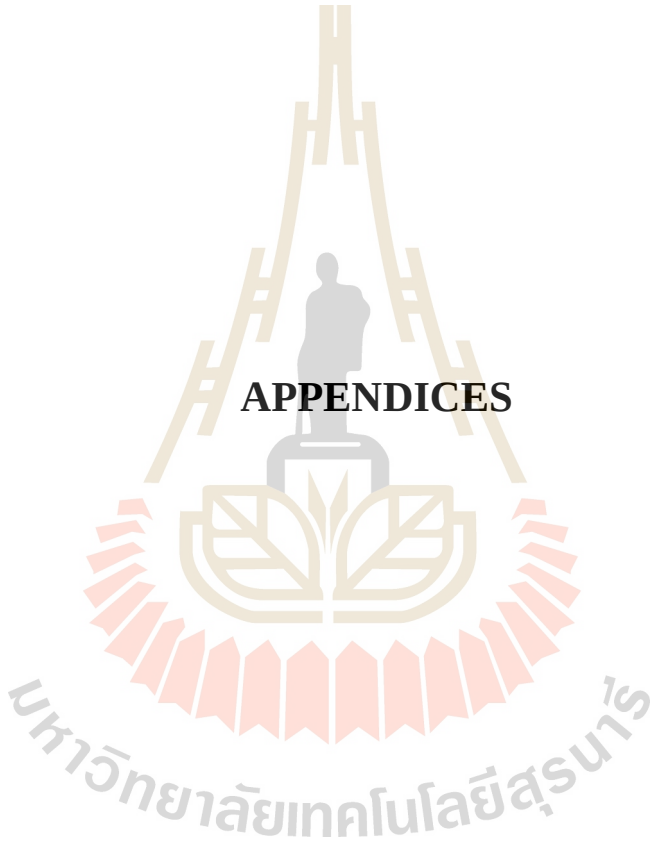

APPENDIX A

REDOX POLYMERS SYNTHESIS

1. Synthesis of the low potential Os-complex based redox mediator 5.

A detailed description of all redox polymers as well as characterization of the compounds is provided in the following information. The synthe sis of the hexanoic acid modified poly(4-vinylptridine) backbone (PVP-C_6-acid) for the covalent binding of the Os-complex base mediator was described earlier (Ruff, 2017), as was the preparation of 2,2′-biimidazole (compound 3, Figure A.1) and ligand N-(6-aminohexyl)-N′-methyl-2,2′-biimidazole (compound 4, Figure A.1) (Alsaoub *et al*., 2017; Mao *et al*., 2003). The preparation of the polymer backbone P(SS-GMA-BA) was adapted from protocols described in (Lopez *et al*., 2017).

2. Synthesis of N,N′-dimethyl-2,2′-biimidazole, BiImMe2

The synthesis of $[Os(BiImMe_2)_2Cl_2](PF_6)$ was adapted from protocols described in (Prévoteau and Mano, 2012), however, K_2OsCl_6 was used as the Os-source instead of $(NH_4)_2OsCl_6$. The bidentate ligand N,N′-dimethyl-2,2′-biimidazole, $BiImMe_2$ (215 mg, 1.33 mmol) and K_2OsCl_6 (312 mg, 0.65 mmol) were suspended in deaerated ethylene glycol (7 mL) under an argon atmosphere. The slurry was heated in a closed vessel to 140°C and stirred for 3 d. After cooling down to room temperature the dark red solution was filtered over a short column filled with celite. The column was eluted with ≈10 mL of ethanol. The red ethylene glycol/ethanol mixture was poured into

diethyl ether and formed red precipitate was separated by filtration and re-dissolved in methanol. The solution was then quenched with water (50 mL) containing 0.31 g $Na_2S_2O_4$. The solution was cooled to 4 °C and stirred overnight in the fridge. Formed red precipitate was removed by filtration. To the methanol/water solution 0.35 g NH_4PF_6 and 10 mL of water were added which leads to the immediate formation of a precipitate. The slurry was cooled for 1.5 h to 4 °C and the precipitate was separated by means of centrifuge and washed with tiny amounts of water. The red solid was dried under reduced pressure overnight. Yield: 247 mg (52%). E = -0.68 V vs. Ag/AgCl/3 M KCl; complex was drop cast onto a glassy carbon electrode from acetone, and inspected in 1 M KCl/water via cyclic voltammetry (Figure A.2).

3. Synthesis of the target Os-complex 5

The Os-complex $[Os(BiImMe_2)_2Cl_2](PF_6)$ (199 mg, 0.27 mmol) and ligand 4 (81 mg, 0.33 mmol) were dissolved in deaerated ethylene glycol under and argon atmosphere and heated to 140 °C in a closed vessel. The slurry was stirred at this temperature overnight and then cooled down to room temperature and quenched with 50 mL of water containing 0.78 g NH_4PF_6 to precipitate the product as the PF_6 salt at 0 °C. The dark-green sticky product was separated by suction filtration using a frit washed first with cold water (50 mL) and then with diethyl ether (50 mL) and then collected. The remaining residue in the frit was washed with copious amounts of acetone. The solvent was removed again and the residues combined. The ethylene glycol/water filtrate was filtered again through a fine paper filter and the residue was washed with water and diethyl ether (shown in Figure 6.16). Finally, the combined fractions were dried in vacuum to yield a green powder. Yield: 222 mg (70%),

E = -0.24 V vs. Ag/AgCl/3 M KCl; complex was drop cast onto a glassy carbon electrode from acetone and inspected in 1 M KCl/water via cyclic voltammetry (refer to Figure 6.17A) and UV-vis in DMSO, λ/nm 286 (max) with a broad shoulder centered at ≈343 (refer to Figure 6.17D, black trace).

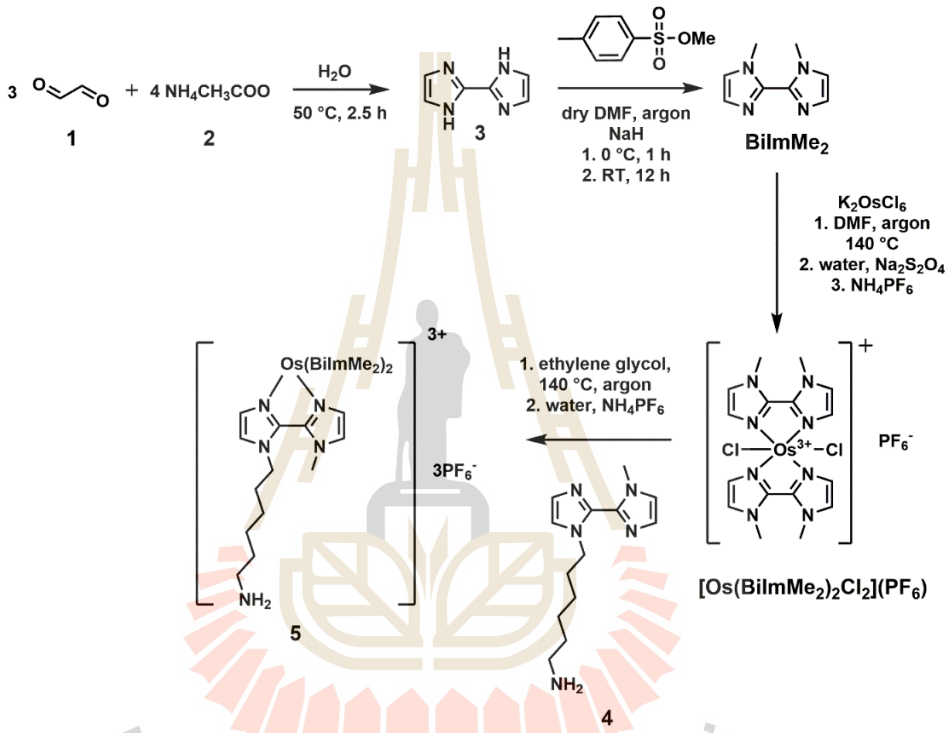

Figure A.1 Multi-step synthesis of the low potential Os-complex 5 bearing a primary amino group that can react with hexanoic acid-modified polymer PVP-C_6-acid via amide formation or P(SS-BA-GMA) with electrophilic epoxide groups on the backbone via a ring opening reaction between the amine and -COC- moieties. The bi-imidazole-based ligand BiImMe2 is a strong electron donor and ensures a low redox potential of the target mediator complex. The synthesis of ligand 4 was described in an earlier publication (Alsaoub *et al.*, 2017). The preparation of complex 5 was adapted from protocols described in refs (Mao *et al.*, 2003; Prévoteau and Mano, 2012), with isolation of the intermediate $[Os(BiImMe_2)_2Cl_2](PF_6)$ ((Prévoteau and Mano, 2012).

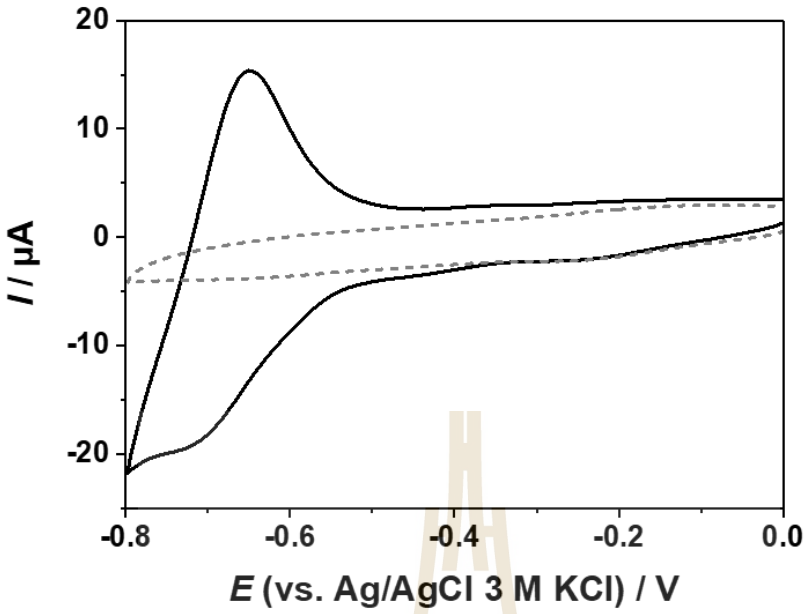

Figure A.2 Cyclic voltammogram in 1 M KCl/water of $[Os(BiImMe_2)_2Cl_2](PF_6)$ (solid line) drop cast onto a glassy carbon electrode; dashed line: bare electrode; scan rate: 100 mV s-1. The mid-point potential of the complex was estimated to be -0.68 V vs. Ag/AgCl/3 M KCl.

4. Synthesis of the positively charged redox polymer PVP-Os

The polymer backbone PVP-C6-acid (57 mg polymer, this corresponds to 18.24 mg/61 µmol hexanoic acid modified pyridine units) was suspended in ≈3 mL of dry dimethyl formamide under and argon atmosphere. Then, TSTU (20.3 mg, 70 µmol) and DIPEA (N,N-diisopropylethylamine, 8.2 mg, 11 µL, 63 µmol) were successively added to this solution. The reaction mixture was stirred for ≈6 h at room temperature to ensure the activation of all hexanoic acid moieties. Afterwards, Os-complex 5 (100.5 mg, 90 µmol) was added in small portions within 5 min together with 1 mL of dimethyl formamide. The dark-green solution was stirred for 23 h at room temperature. The polymer was precipitated by adding 40 mL of ethyl acetate and separated by

centrifugation. The crude product was washed with 20 mL of ethyl acetate and shortly dried under reduced pressure to yield the crude polymer as dark-green sticky material. For purification, small aliquots of the polymer were dissolved in minimal amounts of DMSO and were diluted with water and 3 M KCl/water by stirring overnight (tiny amounts of aqueous HCl can be used to enhance the solubility of the polymer in water). The polymer suspension was then dialyzed using membrane filters with a molecular weight cutoff of 5 kDa (Vivaspin500, Sartorius) first against aqueous KCl to ensure the complete exchange of all PF6- anions against hydrophilic Cl- anions and then against pure water to remove excess Cl (shown in Figure A.3). The polymer was obtained as green aqueous solutions in a concentration of 46.5 mg mL^{-1}. E = -0.19 V vs. Ag/AgCl/3 M KCl; polymer was drop cast onto a graphite electrode from water and inspected in PBS, 50 mM, pH 7 via cyclic voltammetry (refer to Figure 6.17B) and UV-vis (DMSO), λ/nm 285 (max) with a broad shoulder centered at ≈345, (refer to result in Figure 6.17D, blue trace).

5. Synthesis of the negatively charged redox polymers P(SS-BA-GMA)-Os

The preparation of the polymer backbone P(SS-BA-GMA) was based on protocols reported in Lopez *et al*. (2017). Under argon atmosphere, the co-monomers sodium 4-vinylbenzenesulfonate (SS, 1 g, 4.85 mmol), glycidyl methacrylate (GMA, 414 mg, 2.91 mmol) and butyl acrylate (BA, 249 mg, 1.94 mmol) were dissolved in a mixture of 10 mL of isopropyl alcohol and 7 mL of water. The mixture was deaerated by argon bubbling, then the radical initiator AIBN (= 2,2′-Azobis(2-methylpropionitrile), 2.5 mg, 0.015 mmol) were added and the mixture was heated to 70 °C in a closed vessel. The clear solution was cooled down to room temperature and

the product was precipitated by adding 30 mL of tetrahydrofuran. The colorless precipitate was separated by centrifugation and washed with 3 mL of isopropyl alcohol and dried under reduced pressure to yield a colorless product. Finally, the polymer was dissolved in 15 mL of pure water (120 mg mL-1). ^{1}H-NMR (200.^{13} MHz, D_2O): δ/ppm 7.61 and 7.06 (both s, aromatic protons, SS), 3.40, 2.85 and 2.60 (broad, epoxide protons, GMA), 1.63 (very broad, -CH_2- backbone and butyl chain), 0.6 and 0.8 (broad, CH_3 groups, GMA and BA). Due to overlapping signals, the exact composition of the polymer could not be calculated. For all calculations and follow up reactions the

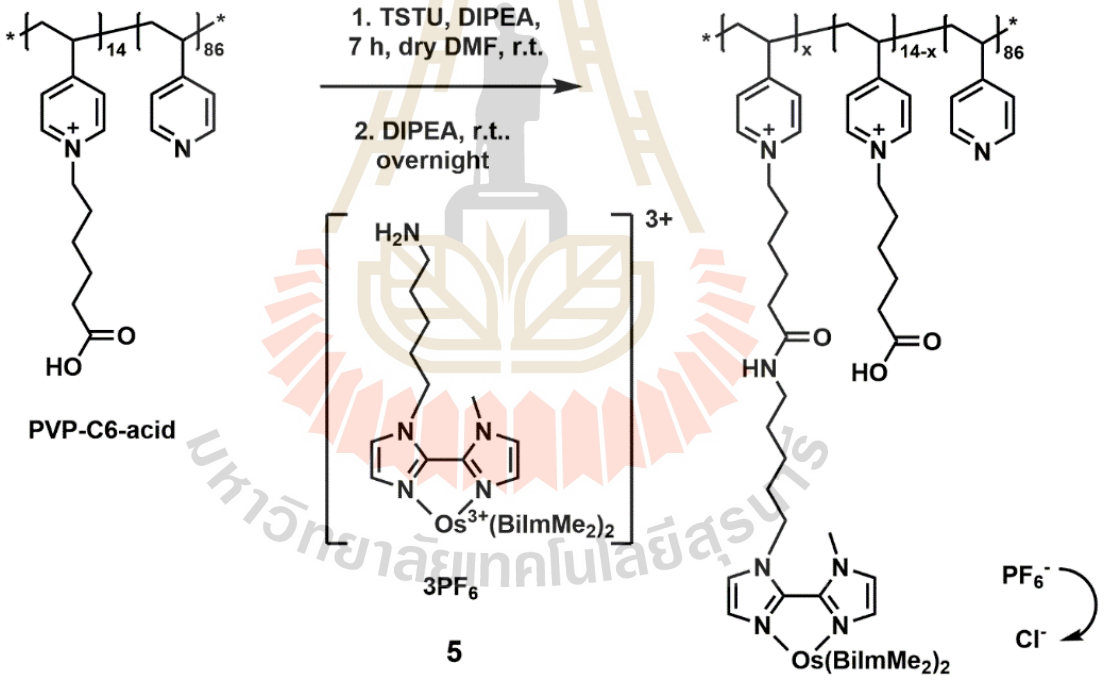

Figure A.3 Synthesis of the positively charged Os-complex modified polymer PVP-Os by coupling complex 5 to the activated acid within PVP-C_6-acid according to Mao *et al.*, 2003. The hydrophobic PF_6^- counter ions were exchanged against the more hydrophilic Cl^- anions by dialysis against aqueous KCl solution. The polymer was obtained after dialysis against water as dark green aqueous solution.

nominal composition of 50 mol% (SS), 30 mol% (GMA) and 20 mol% (BA) was used. Under an argon atmosphere, 42.05 mg (0.04 mmol) of Os-complex 5 was dissolved in a mixture of 1 mL of DMSO and 1 mL of water (Milli-Q). To this solution 15 µL of an aqueous NaOH solution (1 M) and 641 µL of an aqueous P(SS-GMA-BA) solution (39 mg mL-1, corresponds to 25 mg of polymer and to 44 µmol of epoxide groups) were added. The reaction mixture was heated to 50 °C in a closed vessel and stirred overnight. The brown slurry was cooled down to room temperature and diluted with 2.5 mL of DMSO, 7.5 mL of pure water and 100 µL of 1 M KCl/water. The mixture was then dialyzed by means of membrane filters (Vivaspin 500, Sartorius, molecular weight cutoff of 5 kDa) and ultracentrifugation against (i) aqueous KCl (1 M) and (ii) against pure water to ensure a complete exchange of the PF6- anions and to remove excess Cl- anions, respectively (shown in Figure A.4). The concentered final dark-brown solution contained the target polymer in a concentration of 16 mg mL^{-1}. E = -0.22 V, vs. Ag/AgCl/3 M KCl, drop cast onto a graphite electrode from water, electrolyte: PBS, 50 mM, pH 7 (Figure 6.17C). UV-vis (DMSO): λ/nm 287 (max) with a broad shoulder centered at ≈342 (Figure 6.17D, red trace).

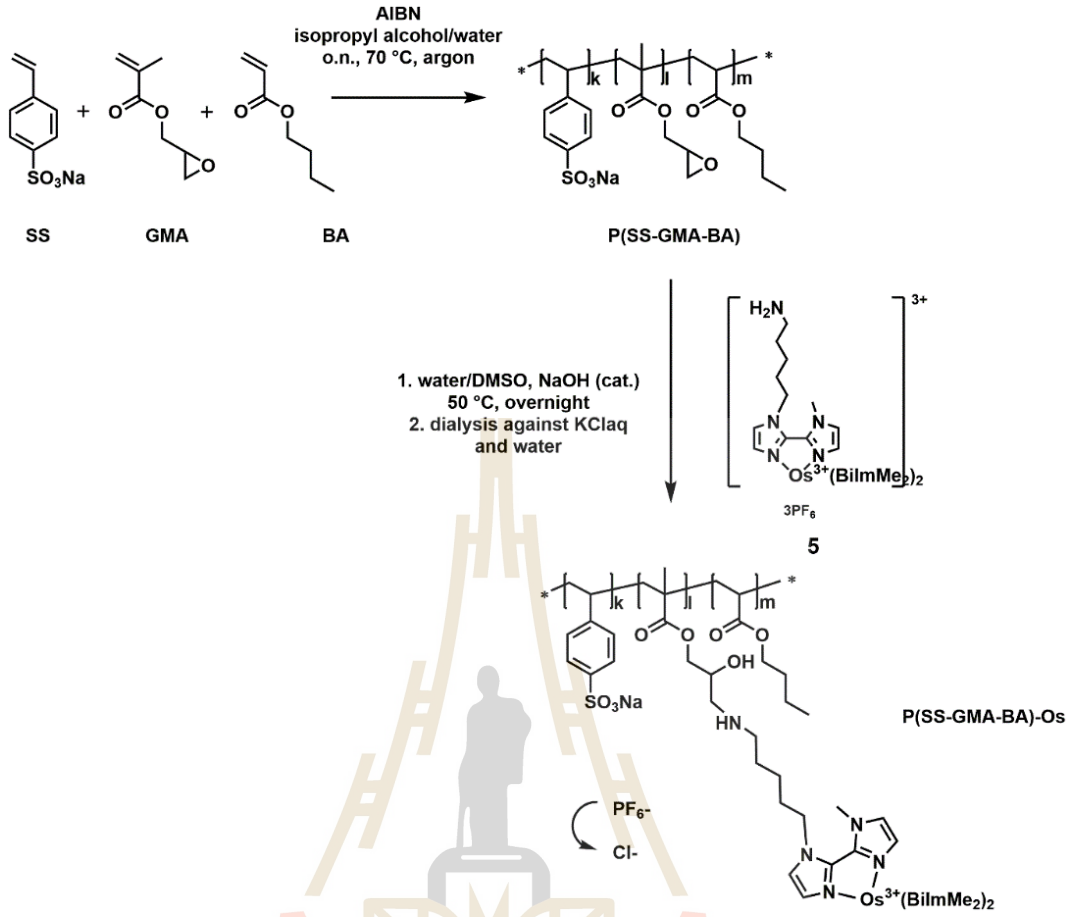

Figure A.4 Synthesis of the polymer backbone P(SS-GMA-BA) and the modification of it with complex **5** via a ring opening reaction between the nucleophilic primary amine within 5 and the electrophilic epoxide functions within the backbone; formation of P(SS-GMA-BA)-Os. Note that the secondary amine that is formed in the ring opening reaction is more nucleophilic than the primary amine in the precursor **5** and can thus readily react with another epoxide function; however, this reaction is assumed to be slow due to the sterical hindrance related to the bulky polymer chain. For clarity reasons, only the product from the reaction between the primary amine and a single epoxide group is shown. The hydrophobic PF_6^- counter ions were exchanged by means of dialysis against aqueous KCl followed by pure water (removal of excess Cl^-). The product was obtained as brown aqueous solution (16 mg mL^{-1}).

APPENDIX B
PREPARATION OF SOLUTIONS AND REAGENTS

1. Reagents for characterization and use of PB-modified SPEs for C1/*p*-HPA electrode

1.1 A stock sodium phosphate buffer solution of 0.2 M of NaH_2PO_4 and Na_2HPO_4 (pH 7.0) for supporting electrolyte.

4.68 g of NaH_2PO_4 was dissolved in DI water and transferred in to 500 mL volumetric flask (A), 16.37 g of Na_2HPO_4 was dissolved in DI water and transfer in to 500 mL volumetric flask (B) and 3.7278 g of KCl was added. Third of them were mixed up to the volume 1000 mL (A + B). The solution was adjusting pH up to 7 levels by HCl solution and store at room temperature.

1.2 A stock tris-base buffer solution of 1 M of $C_4H_{11}NO_3$ for dissolving NADH substrate.

1.21 g of $C_4H_{11}NO_3$ was dissolved in DI-water and transferred in to 10 mL volumetric flask. The solution was made up to the volume with Di-water and store at room temperature.

1.3 A stock of 10 mM NADH in 50 mM phosphate buffer solution (pH 7).

0.071 mg of NADH was dissolved in PBS (50 mM, pH 7) and transferred in to 10 mL volumetric flask. The solution was made up to the volume with PBS (50 mM, pH 7), then checking the concentration via spectrometer at 340 nm and store at 4°C until 2 until used (up to 2 weeks).

1.4 A stock of 10 mM *p*-HPA ($C_8H_8O_3$) in 50 mM phosphate buffer solution (pH 7).

0.015 mg of *p*-$C_8H_8O_3$ was dissolved in PBS (50 mM, pH 7) and transferred in to 10 mL volumetric flask. The solution was made up to the volume with PBS (50 mM, pH 7), then checking the concentration via spectrometer at 277 nm and store at 4 °C until used.

1.5 A stock of 10 mM *m*-HPA ($C_8H_8O_3$) in 50 mM phosphate buffer solution (pH 7).

0.015 mg of *m*-$C_8H_8O_3$ was dissolved in PBS (50 mM, pH 7) and transferred in to 10 mL volumetric flask. The solution was made up to the volume with PBS (50 mM, pH 7), then store at 4 °C until used.

1.6 A stock of 10 mM *o*-HPA ($C_8H_8O_3$) in 50 mM phosphate buffer solution (pH 7).

0.015 mg of *o*-$C_8H_8O_3$ was dissolved in PBS (50 mM, pH 7) and transferred in to 10 mL volumetric flask. The solution was made up to the volume with PBS (50 mM, pH 7), then store at 4 °C until used.

1.7 A stock of 10 mM $C_9H_{10}O_3$ in 50 mM phosphate buffer solution (pH 7).

0.017 mg of $C_9H_{10}O_3$ was dissolved in PBS (50 mM, pH 7) and transferred in to 10 mL volumetric flask. The solution was made up to the volume with PBS (50 mM, pH 7), then store at 4 °C until used.

1.8 A stock of 10 mM $C_9H_{10}O_4$ in 50 mM phosphate buffer solution (pH 7).

0.018 mg of $C_9H_{10}O_4$ was dissolved in PBS (50 mM, pH 7) and transferred in to 10 mL volumetric flask. The solution was made up to the volume with

PBS (50 mM, pH 7), then store at 4 °C until used.

1.9 A stock solution of 7,299.8 unit/200 µL superoxide dismutase in 200 µL phosphate buffer solution pH 7.0.

1.90 mg of SOD was freshly dissolved in 200 µL PBS (50 mM, pH 7) and then store at 4 °C.

1.10 A stock solution of 10 mM hydrogen peroxide in water.

10 µL of H_2O_2 (30%) was freshly diluted in Di-water and transferred in to 10 mL volumetric flask. The solution was made up to the volume DI-water, then store at 4 °C.

2 Reagents for ITC characterization and inspection of C1/*p*-HPA binding affinity

2.1 Separating C1 molecules in a solution by dialysis (a dialyzed against phosphate buffer solution of 50 mM, pH 7).

A typical dialysis procedure for C1 is as follows: (i) prepare the membrane according to instructions (ii) load the C1 into dialysis tubing, cassette or device (molecular weight cut-off is 10 kDa) (iii) place C1 into an external chamber of dialysis buffer (with gentle stirring of the buffer) (iv) dialyze for 2 hours (at room temperature or 4 C) (v) change the dialysis buffer and dialyze for another 2 hours and (vi) change the dialysis buffer and dialyze for overnight. After dialysis, C1 was stored at -40 °C and dialyzed against buffer was stored at 4 °C until use.

2.2 A stock of 10 mM *p*-HPA ($C_8H_8O_3$) in dialyzed agent buffer solution (pH 7).

0.015 mg of *p*-$C_8H_8O_3$ was dissolved in dialyzed agent buffer (50 mM, pH 7) and transferred in to 10 mL volumetric flask. The solution was made up to the volume with PBS (50 mM, pH 7), then checking the concentration via spectrometer at 277 nm and store at 4 °C until used.

2.3 A stock of 10 mM *m*-HPA ($C_8H_8O_3$) in dialyzed agent buffer solution (pH 7).

0.015 mg of *m*-$C_8H_8O_3$ was dissolved in dialyzed agent buffer (50 mM, pH 7) and transferred in to 10 mL volumetric flask. The solution was made up to the volume with dialyzed agent buffer (50 mM, pH 7), then store at 4 °C until used.

2.4 A stock of 10 mM *o*-HPA ($C_8H_8O_3$) in dialyzed agent buffer solution (pH 7).

0.015 mg of *o*-$C_8H_8O_3$ was dissolved in dialyzed agent buffer (50 mM, pH 7) and transferred in to 10 mL volumetric flask. The solution was made up to the volume with dialyzed agent buffer (50 mM, pH 7), then store at 4 °C until used.

2.5 A stock of 10 mM $C_9H_{10}O_3$ in dialyzed agent buffer solution (pH 7).

0.017 mg of $C_9H_{10}O_3$ was dissolved in dialyzed agent buffer (50 mM, pH 7) and transferred in to 10 mL volumetric flask. The solution was made up to the volume with dialyzed agent buffer (50 mM, pH 7), then store at 4 °C until used.

2.6 A stock of 10 mM $C_9H_{10}O_4$ in dialyzed agent buffer solution (pH 7).

0.018 mg of $C_9H_{10}O_4$ was dissolved in dialyzed agent buffer (50 mM, pH 7) and transferred in to 10 mL volumetric flask. The solution was made up to the volume with dialyzed agent buffer (50 mM, pH 7), then store at 4 °C until used.

2.7 A stock 1 mM FMN ($C_{17}H_{21}N_4O_9P$) in dialyzed agent buffer solution

(pH 7).

45.63 mg of $C_{17}H_{21}N_4O_9P$ was dissolved in dialyzed agent buffer (50 mM, pH 7) and transferred in to 1 mL plastic tube. The solution was made up to the volume with dialyzed agent buffer (50 mM, pH 7), then store at -20 or 4 °C.

3 Reagents for synthesis of the redox polymers PVP-Os and P(SS-GMA-BA)-Os

Synthesis of N,N′-dimethyl-2,2′-biimidazole, BiImMe$_2$

3.1 The bidentate ligand N,N′-dimethyl-2,2′-biimidazole, BiImMe$_2$ 1.33 mmol and K_2OsCl_6 0.65 mmol in ethylene glycol.

215 mg of N,N′-dimethyl-2,2′-biimidazole, BiImMe$_2$ and 312 mg of K_2OsCl_6 were suspended in deaerated ethylene glycol (7 mL) under an argon atmosphere.

3.2 A stock 1.78 mmol $Na_2S_2O_4$ in water.

0.31 g of $Na_2S_2O_4$ was dissolved in water and then store at 4°C until used.

3.3 A stock 4.68 mmol NH_4PF_6 in water.

0.35 g of NH_4PF_6 was dissolved in water.

Synthesis of the target Os-complex 5

3.4 The Os-complex $[Os(BiImMe2)_2Cl_2](PF_6)$ 0.27 mmol and ligand 4 0.33 mmol in ethylene glycol.

199 mg of Os-complex $[Os(BiImMe2)_2Cl_2](PF_6)$ and ligand 4 81 mg were dissolved in deaerated ethylene glycol under and argon atmosphere and heated to-

140 °C in a closed vessel.

3.5 A stock 0.17 mmol NH_4PF_6 in water.

0.78 g of NH_4PF_6 was dissolved in water.

Synthesis of the positively charged redox polymer PVP-Os

3.6 The polymer backbone PVP-C_6-acid, corresponds to 61 µmol hexanoic acid modified pyridine units in dry dimethyl formamide under argon atmosphere.

57 mg of polymer backbone PVP-C_6-acid (this corresponds to 18.24 mg hexanoic acid modified pyridine units) was suspended in ≈3 mL of dry dimethyl formamide under and argon atmosphere.

3.7 A stock 70 µmol TSTU (N,N,N′,N′-Tetramethyl-O-(N-succinimidyl)uronium tetrafluoroborate in water.

20.3 mg of $C_9H_{16}BF_4N_3O_3$ was dissolved in water.

3.8 A stock 63 µmol DIPEA (N,N-diisopropylethylamine) in water.

8.2 mg of C8H19N was dissolved in water.

Synthesis of the negatively charged redox polymers P(SS-BA-GMA)-Os

3.9 The co-monomers sodium 4-vinylbenzenesulfonate (SS, 4.85 mmol), glycidyl methacrylate (GMA, 2.91 mmol) and butyl acrylate (BA, 1.94 mmol) in isopropyl alcohol.

1 g of $C_8H_7NaO_3S$ (SS), 414 mg of C7H10O3 (GMA) and 249 mg of $C_7H_{12}O_2$ (BA) were dissolved in a mixture of 10 mL of isopropyl alcohol and 7 mL of water.

3.10 A stock 0.015 mmol AIBN (2,2′-Azobis(2-methylpropionitrile) in water.

2.5 mg of $C_8H_{12}N_4$ was dissolved in water.

4 Reagents for fabrication of an amperometric biosensor assay with HPAH-C1 immobilization

4.1 A stock solution of 11.40 mg mL-1 poly(ethylene glycol) diglycidyl ether in water.

10 µL of PEGDGE (1.14 mg mL-1) was diluted with water in 1.0 mL plastic tube and the solution was made up to volume with water.

4.2 A stock solution of 10.12 mg mL-1 2, 2'-(Ethylenedioxy) diethylamine in water.

10 µL of EDEA (1.012 mg mL-1) was diluted with water in 1.0 mL plastic tube and the solution was made up to volume with water.

APPENDIX C
PUBLICATIONS

Accepted and published:

1. Teanphonkrang, S., Janke, S., Chaiyen, P., Sucharitakul, J., Suginta, W., Khunkaewla, P., Schuhmann, W., Ruff, A., and Schulte, A. (2018). Tuned Amperometric Detection of Reduced β-Nicotinamide Adenine Dinucleotide by Allosteric Modulation of the Reductase Component of the *p*-Hydroxyphenylacetate Hydroxylase Immobilized within a Redox Polymer, *Analytical Chemistry*. 90: 5703-5711.

Submitted for publication:

2. Teanphonkrang, S., Ernst, A., Janke, S., Chaiyen, P., Sucharitakul, J., Suginta, W., Khunkaewla, P., Schuhmann, W., Schulte, A., and Ruff, A. (2019). Amperometric detection of the urinary disease biomarker p-HPA by allosteric modulation of a redox polymer-embedded bacterial reductase. *ACS Sensors*.

In preparation:

3. Teanphonkrang, S., Chaiyen, P., Sucharitakul, J., Suginta, W., Khunkaewla, P., and Schulte, A. From amplified substrate detection to clinical diagnosis: Biosensing with a dissolved enzyme under allosteric control of a urinary biomarker. ACS Catalysis

CURRICULUM VITAE

Name: SOMJAI TEANPHONKRANG

Status: Ph.D.candidate (Chemistry)

Date of Birth: 24th May 1987

Place of Birth: Nakhon Ratchasima, Thailand

Nationality: Thai

Education:

- 2005, High school

  Pakthongchai Phachaniramit School, Nakhon Ratchasima, Thailand

- 2010, B. Sc. (Chemistry)

  Rajamangala University of Technology Isan, Nakhon Ratchasima, Thailand

- 2013, M. Sc. (Chemistry)

  Suranaree University of Technology, Nakhon Ratchasima, Thailand

- Since 2015, Ph.D. student in the School of Chemistry

  Suranaree University of Technology, Nakhon Ratchasima, Thailand

Scholarship

The Royal Golden Jubilee (RGJ) Ph.D. Programme, Thailand, 2015201-8.

Scholarship

Best Oral Presentation, Annual RGJ/TRF Meeting, Pattaya, Thailand, June 2018